Detection and Classification of Transient Disturbances in Power System using Advanced Signal Processing and Machine Learning Techniques

Thesis Submitted by
Ananya Chakraborty
(INDEX NO. D-7/ISLM/90-18)

Doctor of Philosophy (Engineering) Degree of

Jadavpur University

School of Energy Studies
Faculty Council of Interdisciplinary Studies, Law and Management
Jadavpur University
Kolkata-700032
India

2024

1. Title of the thesis

Detection and Classification of Transient Disturbances in Power System using Advanced Signal Processing and Machine Learning Techniques

2. Name, Designation and Institution of the Supervisors

Dr. Ratan Mandal
Professor,
School of Energy Studies
Faculty Council of Interdisciplinary Studies, Law, and Management
Jadavpur University
Kolkata 700032.

Dr. Soumya Chatterjee
Assistant Professor,
Electrical Engineering Department,
National Institute of Technology Durgapur
Durgapur-713209.

3. List of Publications:

- **A. Chakraborty,** S. Chatterjee and R. Mandal, "Power Quality Recognition in Noisy Environment Employing Deep Feature Extraction from Cross Stockwell Spectrum Time-Frequency Images", **Electrical Engineering, Springer, (SCI)**, vol. 106, pp. 443–458, 2024.

- **A. Chakraborty,** S. Chatterjee and R. Mandal, "Time-Frequency Image Representation Aided Deep Feature Extraction-Based Grid connected Solar PV Fault Classification Framework", **Applied Solar Energy, Springer, (Scopus)**, vol. 60. no.2, 2024 (*In press*).

4. List of Presentations in International/National Conferences

- **A. Chakraborty,** S. Chatterjee and R. Mandal, "Autocorrelation Aided Islanding Detection Using Bi-directional Long-short Type Memory Network," Proceedings of **2nd IEEE International Conference on Power Electronics and Energy (ICPEE)**, Bhubaneswar, India, 2023.

- **A. Chakraborty** and R. Mandal "A novel technique employing DWT-based envelope analysis for detection of power system transients", **Proceedings of IEEE International Conference on Energy, Communication, Data Analytics and Soft Computing (ICECDS)**, Chennai, India, 2018.

Certificate from the supervisors

This is to certify that the thesis entitled **"Detection and Classification of Transient Disturbances in Power System using Advanced Signal Processing and Machine Learning Techniques"** submitted by Ms. Ananya Chakraborty, who got her name registered on 27/12/2018 for the award of Ph.D (Energy Studies) degree of Jadavpur University is absolutely based upon her own work under the supervision of Prof. Dr. Ratan Mandal and Dr. Soumya Chatterjee and that neither her thesis nor any part of the thesis has been submitted for any degree/diploma or any other academic award anywhere before.

_____

Signature of the Supervisor and Date
with Official Seal

_____

Signature of the Supervisor and Date
with Official Seal

DECLARATION OF ORIGINALITY

I, Ananya Chakraborty (INDEX NO. D-7/ISLM/90-18) registered on 27/12/2018 do hereby declare that this thesis entitled "***Detection and Classification of Transient Disturbances in Power System using Advanced Signal processing and Machine Learning Techniques***", includes a literature review and original research conducted by the undersigned candidate for a Ph.D degree. I attest that in accordance with the guidelines and conduct, I have accurately referenced and made reference to any materials and conclusions that are not unique to this work. Additionally, I certify that this thesis is in accordance with the "policy on anti-plagiarism, Jadavpur University 2019", and authenticate software found 07% of similarity.

Signature:
Date:

Certified by:

_____

Signature of the Supervisor and Date
with Official Seal

_____

Signature of the Supervisor and Date
with Official Seal

DECLARATION OF ORIGINALITY AND COMPLIANCE OF ACADEMIC ETHICS

I hereby certify that the undersigned candidate completed his doctoral studies in energy science and technology during the academic year 2023-2024 and that this thesis contains both an analysis of literature and original research. The sources from which the data in this document were gathered and presented all followed the standards of academic integrity.

I further confirm that I have correctly referred and cited all data and conclusions that are not original to my work in accordance with these rules and conduct.

Name: Ananya Chakraborty
(INDEX NO. D-7/ISLM/90-18)

Signature:

Date:

Acknowledgment

The author would like to express her sincere gratitude and deep appreciation to her supervisors *Professor Ratan Mandal School of Energy Studies, Jadavpur University* and *Dr. Soumya Chatterjee, Assistant Professor, Electrical Engineering Department, National Institute of Technology, Durgapur,* for their valuable guidance in carrying out the thesis work. The author has been provided with necessary freedom during the course of the research work and at the same time the intense supervision by the supervisors has helped to enhance the quality of the research. Their moral support, amiable and amicable personality, encouragement, and profound knowledge about the subject have made the research work possible. Besides, the author is also grateful to the supervisors for providing necessary mental support during difficult times helping her to become a better individual which led to her overall professional development.

The author would especially like to express her heart-felt gratitude to her husband *Mr. Jitendra Kumar Jaiswal* for supporting her mentally and emotionally and helping her to complete her research work.

The author would like to convey her deep love and respect towards her parents for their never-ending support and encouragement during difficult times. Without their support, the work could never have been completed.

Finally, as it is impossible to mention everybody by name, the author would like to convey her gratitude to all who have contributed in one way or another, in making the work possible.

Dedicated to-
Family

List of Symbols and abbreviations

Symbol	Description
PQ	Power Quality
PV	Photovoltaic
EV	Electric Vehicles
NILM	Non-intrusive load monitoring
WAMS	Wide-area measurement systems
PMU	Phasor measurement unit
DG	Distributed Generation
ANN	Artificial Neural Networks
DT	Decision Trees
PNN	Probabilistic Neural Networks
SVM	Support Vector Machines
BVM	Ball Vector Machines
ELM	Extreme Learning Machines
EL	Ensemble Learning
VMD	Variational mode decomposition
EMD	Empirical mode decomposition
XWT	Cross Wavelet transform
PCA	Principal component analysis
SSA	Stacked sparse autoencoder
TFR	Time frequency representation
SPWVD	Smoothed pseudo-Wigner-Ville distribution
LPPT	Limited power point tracking
MPPT	Maximum power point tracking
WVD	Wigner-Ville Distribution
NB	Naïve Bayesian
TP	True Positive
TN	True Negative
FP	False Positive
FN	False Negative
THD	Total harmonic distortion
XGBost	Extreme gradient boosting machine
Light GBM	Light gradient boosting machine
ANN	Artificial Neural Network
RNN	Recurrent Neural Network
LSTM	Long short-term memory

FFT	Fast Fourier Transform
DTCWT	Dual Tree Complex Wavelet Transform
DWT	Discrete Wavelet Transform
MRA	Multi Resolution Analysis
HT	Hilbert Transform
ANOVA	Analysis of Variance
T-F	Time Frequency
ST	Stockwell Transform
MST	Modified Stockwell Transform
HST	Hyperbolic Stockwell Transform
FST	Fast Stockwell Transform
DOST	District Orthogonal Stockwell Transform
CWT	Continuous Wavelet Transform
XST	Cross Stockwell Transform
CNN	Convolutional Neural Networks
FDR	False Discovery Rate
DL	Deep Learning
TL	Transfer Learning
SNR	Signal to noise ratio
ILSVRC	Image net large scale visual recognition challenge
VGG	Visual geometry group
RF	Random Forest
ML	Machine learning
OSH	Optimum separating hyper plane
SRM	Structural risk minimization
kNN	k-nearest neighbor
MS	Source Model
MT	Target Model
STFT	Short time Fourier transform
MM	Mathematical morphology
PNN	Probabilistic neural networks
EMD	Empirical mode decomposition
Bi_LSTM	Bi-directional long short type memory network
NDZ	Non detection zone
AFD	Active frequency drift
APS	Automatic phase shift
SMS	Slip mode frequency shift
ROCOF	Rate of change of frequency
PCC	Point of common coupling
CB	Circuit breaker
EF	Extracted features

Preface

The present thesis entitled "**Detection and Classification of Transient Disturbances in Power System using Advanced Signal Processing and Machine Learning Techniques**" is submitted for the degree of Doctor of Philosophy (Engineering) at Faculty Council of Interdisciplinary Studies, Law and Management, Jadavpur University, Kolkata. The research work presented here was carried out under supervision of Prof. Ratan Mandal, School of Energy Studies, Jadavpur University and Dr. Soumya Chatterjee, Electrical Engineering Department, National Institute of Technology Durgapur, in between the period of December 2018 to April 2024. To the best of my knowledge, this work is original except where acknowledgement and references are made to previous work. Neither this nor any substantially similar thesis has been or has been submitted for any other degree, diploma or other qualification at any other University.

The present work dealt with detection and classification of various transient events that occur in power systems. For this purpose, several advanced signal processing and machine learning models have been implemented. Transient disturbances are a major concern as they have far-reaching consequences. Moreover, they have severe impact on life of power equipment endangering their proper functionality. If appropriate detection schemes are not designed then these transients can cause insulation degradation, over-heating, malfunction of relays causing catastrophic failure. Considering the aforesaid fact, this present thesis work is aimed to develop accurate methods that can correctly identify and categorize transient events and that too in presence of noise of spurious data. The thesis is aimed to develop novel signal processing and machine learning models for accurate identification of impulsive and oscillatory transients, single and mixed power quality events, islanding and non-islanding events as well as faults in grid connected solar PV systems. Hopefully this work will help future researchers working in the area of power system transient detection to some extent. The aims and objectives of this work are elaborated in ***Chapter 1*** of the thesis.

While working on a PhD is a lonely endeavor, but it is also not possible without others. As I mentioned, My Ph. D work was supervised by Prof. Ratan Mandal, Professor at School of Energy Studies, Jadavpur University and Dr. Soumya Chatterjee, Assistant Professor, Electrical Engineering Department, National Institute of Technology, Durgapur. I am indebted to both of them for their valuable insight into the research work. Their continuous help, encouragement, advice, guidance and unparalleled in-depth knowledge of the present subject make it possible to complete this Ph.D work. In addition, I would like to express my sincere thanks and regards to Prof. Tushar Jash, Professor, School of Energy studies, Jadavpur University, for his continuous encouragement, advice and help in this work. Finally, I would like to convey thanks to all who have contributed in one way or another to make this work possible.

Abstract

Accurate detection of transient disturbances in power systems is key from the point of view of reliability and safety of power system operation. Transient overvoltage and overcurrent occurring in power systems jeopardize the life of power equipment significantly leading to their unwanted and premature failure. If not detected early, they may lead to malfunctioning of relays and circuit breakers which may result in partial or complete shutdown of power substations as well as distribution substations. Moreover, transients degrade the quality of power leading to power quality issues. Accurate and early detection of transient events can prevent catastrophic events and maintain the reliability of power transmission systems. Considering the foresaid fact, the present thesis is aimed at identification as well as segregation of different types of power system transients. For this purpose, advanced signal processing as well as machine learning including the newly developed state of the art deep learning techniques have been implemented for accurate detection and classification of various transient events. It has been observed that the methods presented in this thesis are capable of discerning transient events accurately achieving very high recognition accuracy even in presence of noisy or spurious data. Thus, the proposed methods can be implemented in real-life environments. A brief overview of the present thesis work is given below.

In ***Chapter 2***, the objective was to detect impulsive as well as oscillatory transients occurring in power systems. For this purpose, a method is proposed using non-stationary signal processing tools like discrete wavelet transform-based multi-resolution analysis and Hilbert transform. Finally, SVM classifier has been used for classification of impulsive and oscillatory transients.

In ***Chapter 3,*** a novel PQ detection framework employing cross-spectral analysis using Stockwell transform and deep learning based automated feature extraction is proposed. The proposed framework has been developed in such a way that it can detect single and multiple PQ events correctly even in noisy environmental conditions. The proposed framework has been

validated on simulated PQ signals as well as on real life PQ signals to validate the practicability of the proposed method.

The aim of ***Chapter 4*** is to propose a novel method for detection and classification of islanding and other transient disturbances (non-islanding events) in renewable energy grid connected systems. For this purpose, an autocorrelation-based feature extraction method is proposed. The features were extracted from negative sequence voltage signals. A deep learning algorithm has been designed to classify islanding and non-islanding events using extracted features from auto correlograms for classification of islanding and other disturbances.

In ***Chapter 5,*** a method has been developed for accurate identification of faults in grid connected solar PV systems based on current data obtained from real-life grid connected solar PV system. A novel extended Park's vector modulus-based fault detection algorithm has been developed and smoothed pseudo-Wigner-Ville distribution-based time frequency analysis of different faults and fault free current data has been analyzed in time-frequency frame. In addition, unsupervised machine learning has been developed for accurate identification of faults in grid connected solar PV systems.

Finally, ***Chapter 6***, concludes the thesis by presenting a summarized overview based on findings of the present work and provides some idea regarding the possible future extensions of the proposed research work.

Contents

		Page No.
Chapter 1: Introduction		
1.1	Introduction	1
1.2	Sources of transient disturbances in power systems	2
	1.2.1 Internal Sources	2
	1.2.2 External Sources	3
1.3	Categorization of transients in power systems	4
1.4	Detrimental effect of transients	6
1.5	Effect of transients on power quality (PQ) issues	8
1.6	Transients in grid connected renewable energy sources	9
1.7	Overview of signal processing and machine learning methods	11
	1.7.1 Types of signal processing algorithms	12
	1.7.2 Types of Machine Learning algorithms	14
1.8	Limitations of the existing signal processing and machine learning methods for transient detection	16
1.9	Scope and objective of the thesis	18
1.10	Originality of the thesis	20
1.11	References	22
Chapter 2: A Novel Technique Employing Discrete Wavelet Transform-Based Envelope Analysis for Detection of Power System Transients		
2.1	Introduction	25
2.2	Theoretical background	26
	2.2.1 Discrete wavelet transform	26
	2.2.2 Hilbert transform	27
2.3	Methodology	27
	2.3.1 Synthetic signal generation	27
	2.3.2 Feature extraction from DWT Envelope	28
	2.3.3 ANOVA test of the extracted features	29
	2.3.4 Support vector machines	32
	2.3.5 Performance analysis	32
	2.3.6 Effect of noise	34

2.4 Conclusions 34
2.5 References 36

Chapter 3: Power Quality Recognition in Noisy Environment Employing Deep Feature Extraction from Cross Stockwell Spectrum Time-Frequency Images

3.1 Introduction 38
3.2 Generation of synthetic PQ signals 42
3.3 Methodology 42
3.3.1 Brief theory of Stockwell transform 42
3.3.2 Brief theory of Cross Stockwell transform 44
3.3.3 Convolutional Neural Network 45
3.3.4 Transfer Learning 49
3.3.5 Pre-trained CNN models 49
3.3.6 Machine Learning classifiers 52
3.4 Results and Discussions 54
3.4.1 Analysis of PQ signals using XST 54
3.4.2 Performance metrics 56
3.4.3 CNN training 58
3.4.4 Results of PQ classification 59
3.4.5 Comparison with different number of folds 61
3.4.6 Effect of noise on classification performance 62
3.4.7 Effect of frequency variation on classification performance 63
3.4.8 Classification performance using other time-frequency methods 64
3.4.9 Computational Cost 64
3.4.10 Validation on Real-life PQ signals 65
3.4.11 Comparative study with existing literature 65
3.5 Conclusions 67
3.6 References 69

Chapter 4: Autocorrelation Aided Islanding Detection Using Bi-directional Long Short Type Memory Network

4.1 Introduction 75
4.2 System under study 78
4.3 Methodology 79
4.3.1 Negative sequence computation 79
4.3.2 Autocorrelation sequence computation feature 80

extraction
4.3.3 Feature extraction 80
4.3.4 Bi- directional-long short term memory network 80
4.4 Results and Discussions 83
4.4.1 Autocorrelation of negative sequence voltage signals 83
4.4.2 Training of Bi-LSTM 86
4.4.3 Evaluation of Bi-LSTM 87
4.4.4 Ccomparison with standard machine learning algorithms 88
4.4.5 Performance analysis in presence of noise 89
4.5 Conclusions 90
4.6 References

Chapter 5: Time-Frequency Image Representation Aided Deep Feature Extraction-Based Grid Connected Solar PV Fault Classification Framework

5.1 Introduction 96
5.2 Acquisition of Fault data 100
5.3 Methodology 103
5.3.1 Extended Park's Vector approach 103
5.3.2 Smoothed pseudo-Wigner-Ville distribution 106
5.3.3 Stacked sparse auto encoder 110
5.3.4 Machine learning classifiers 112
5.4 Results and Discussions 112
5.4.1 Performance analysis of Stacked sparse auto encoder (SSA) 112
5.4.2 Statistical test of different classifiers 115
5.4.3 Comparison by varying number of folds 116
5.4.4 Comparison using different methods 116
5.4.5 Comparison with other T-F methods 117
5.5 Conclusions 118
5.6 References 120

Chapter 6: Conclusions and Future Work

6.1 Conclusions 124
6.2 Future Works 128

Appendix: A.1 Mathematical Model of PQ disturbances 130
A.2 Confusion Matrix of PQ classification 131

List of Figures

Figure No.	Caption of the Figure	Page No.
2.1	Typical nature of (a) oscillatory voltage transient and (b) Impulsive voltage transient signal	28
2.2	First four detail coefficients of the oscillatory voltage transient signal D_1-D_4.	30
2.3	Envelope of the First four detail coefficients of the oscillatory voltage transient signal E_1-E_4.	30
3.1	Illustration of the flowchart of the proposed method	41
3.2	Structure of AlexNet	50
3.3	Structure of VGGNet16	51
3.4	Structure of a residual module	52
3.5	Structure of an inception module	53
3.6	Time domain PQ signal (a) S_6 and corresponding T-F images obtained using (b) XST (c) ST for SNR=15dB	55
3.7	Time domain PQ signal (a) S_{22} and corresponding T-F images obtained using (b) XST (c) ST for SNR=15 dB	56
3.8	Variation of classification accuracy with no of folds	61
3.9	Variation of classification accuracy with varying SNR (dB)	62
3.10	Variation of classification accuracy with the change in frequency	63
3.11	T-F image of (a) real life PQ signal obtained using (b) XST (c) ST	66
4.1	Flow chart of proposed framework	77
4.2	Simulated power system model	78
4.3	Simplified structure of RNN.	82
4.4	Structure of BRNN	82
4.5	Structure of Bi-LSTM	83
4.6	Normalized negative sequence voltage of different transient events	84
4.7	Autocorrelation sequences of negative sequence voltages	85
4.8	Training of Bi-LSTM classifier	86
4.9	Variation of accuracy with noise level (SNR)	90

Figure No.	Caption of the Figure	Page No.
5.1	Flow chart of the proposed fault detection method	99
5.2	Schematic of (a) Experimental set-up (b) Actual photograph [25]	101
5.3	Single cycle fault current signals for (a) C_0 (b) C_1(c) C_2 and (d) C_3	103
5.4	Direct (*d*)-axis current signals (I_d) for (a) C_0 (b) C_1(c) C_2 and (d) C_3	105
5.5	Quadrature (*q*)-axis current signals (I_q) for (a) C_0 (b) C_1(c) C_2 and (d) C_3	105
5.6	Time-frequency representation of *d*-axis current signals obtained using SPWVD for class (a) C_0 (b) C_1 (c) C_2 and (d) C_3	108
5.7	Time-frequency representation of *d*-axis current signal obtained using SPWVD for class (a) C_0 (b) C_1 (c) C_2 and (d) C_3	109
5.8	Structure of stacked sparse auto encoder	111
5.9	Training of sparse auto encoder	113
5.10	Post-hoc statistical test (Tukey Kramer) between all the classifiers	115
5.11	Variation in classification accuracies with varying number of folds	116

List of Tables

Table No.	Title of the Table	Page No.
2.1	Extracted features	29
2.2	Variation of extracted features (mean ± standard deviation) with '*p*' values for oscillatory transient	31
2.3	Variation of extracted features (mean ± standard deviation) with '*p*' values for oscillatory transient	31
2.4	Performance analysis using all features for different training testing ratio	33
2.5	Variation of classification accuracy with SNR (dB)	34
3.1	Generated PQ signals	43
3.2	Classification performance of different classifiers	60
3.3	Classification performance using other T-F methods	64
3.4	Classification performance on real-life PQ signals	66
3.5	Comparison with existing methods	67
4.1	Extracted features	81
4.2	Classification Problem	88
4.3	Performance of Bi-LSTM classifier	88
4.4	Classification performance using other ML classifiers	88
5.1	Fault classes and their description	102
5.2	Classification performance of quadrature axis (I_q) current data	114
5.3	Classification performance of quadrature axis (I_q) current data	115
5.4	Comparison using different methods	117
5.5	Comparison with existing literature	118

Synopsis

The present thesis work deals with detection and classification of various transient events that occur in power systems. For this purpose, several advanced signal processing and machine learning models have been implemented. Transient disturbances are a major concern as they have far-reaching consequences. Moreover, they have severe impact on the life of power equipment endangering their proper functionality. If appropriate detection schemes are not designed then these transients can cause insulation degradation, over-heating, malfunction of relays causing catastrophic failure. Considering the aforesaid fact, this present thesis work is aimed to develop accurate methods that can correctly identify and categorize transient events and that too in presence of noise of spurious data. The thesis is aimed to develop novel signal processing and machine learning models for accurate identification of impulsive and oscillatory transients, single and mixed power quality events, islanding and non-islanding events as well as faults in grid connected solar PV systems. Hopefully this work will help future researchers working in the area of power system transient detection to some extent. The aims and objectives of this work are elaborated briefly.

(i) Development of a novel for accurate detection of impulsive and oscillatory transients occurring in power systems. In the present thesis work an efficient method for accurate classification of impulsive and oscillatory transients is developed.

(ii) In real life power systems, different types of transient disturbances can happen which results in poor power quality (PQ). The PQ disturbances can be broadly classified as single as well as multiple PQ disturbances. So accurate detection and classification of PQ disturbances is essential from the point of view of safety of operators as well prevention of malfunction of power apparatus. Detection of single as well as multiple PQ events is a challenging task in a noisy environment. Hence, in this work, a method has been developed to accurately classify single and multiple PQ events in noisy background.

(iii) In grid connected renewable energy sources, detection of islanding and non-islanding is a major issue that still needs to be addressed carefully. Appropriate signal processing and feature extraction methods need to be developed for accurate detection of islanding as well as non-islanding events. In the present thesis work a novel method has been proposed to distinguish between islanding and non-islanding events.

(iv) Accurate detection of faults in grid connected solar PV systems is also a challenging issue. Proper methodologies for accurate fault detection are still lacking and there is still a dearth of accurate fault detection models. In the present thesis work, an accurate fault detection model in grid connected solar PV systems is developed.

Abstract

Accurate detection of transient disturbances in power systems is key from the point of view of reliability and safety of power system operation. Transient overvoltage and overcurrent occurring in power systems jeopardize the life of power equipment significantly leading to their unwanted and premature failure. If not detected early, they may lead to malfunctioning of relays and circuit breakers which may result in partial or complete shutdown of power substations as well as distribution substations. Moreover, transients degrade the quality of power leading to power quality issues. Accurate and early detection of transient events can prevent catastrophic events and maintain the reliability of power transmission systems. Considering the foresaid fact, the present thesis is aimed at identification as well as segregation of different types of power system transients. For this purpose, advanced signal processing as well as machine learning including the newly developed state of the art deep learning techniques have been implemented for accurate detection and classification of various transient events. It has been observed that the methods presented in this thesis are capable of discerning transient events accurately achieving very high recognition accuracy even in presence of noisy or spurious data. Thus, the proposed methods can be implemented in real-life environments. A brief overview of the present thesis work is given below.

In ***Chapter 2***, the objective was to detect impulsive as well as oscillatory transients occurring in power systems. For this purpose, a method is proposed using non-stationary signal processing tools like discrete wavelet transform-based multi-resolution analysis and Hilbert transform. Finally, SVM classifier has been used for classification of impulsive and oscillatory transients.

In ***Chapter 3,*** a novel PQ detection framework employing cross-spectral analysis using Stockwell transform and deep learning based automated feature extraction is proposed. The proposed framework has been developed in such a way that it can detect single and multiple PQ events correctly even in noisy environmental conditions. The proposed framework has been validated on simulated PQ signals as well as on real life PQ signals to validate the practicability of the proposed method.

The aim of ***Chapter 4*** is to propose a novel method for detection and classification of islanding and other transient disturbances (non-islanding events) in renewable energy grid connected systems. For this purpose, an autocorrelation-based feature extraction method is proposed. The features were extracted from negative sequence voltage signals. A deep learning algorithm has been designed to classify islanding and non-islanding events using extracted features from auto correlograms for classification of islanding and other disturbances.

In ***Chapter 5,*** a method has been developed for accurate identification of faults in grid connected solar PV systems based on current data obtained from real-life grid connected

solar PV system. A novel extended Park's vector modulus-based fault detection algorithm has been developed and smoothed pseudo-Wigner-Ville distribution-based time frequency analysis of different faults and fault free current data has been analyzed in time- frequency frame. In addition, unsupervised machine learning has been developed for accurate identification of faults in grid connected solar PV systems.

Finally, ***Chapter 6***, concludes the thesis by presenting a summarized overview based on findings of the present work and provides some idea regarding the possible future extensions of the proposed research work.

Plagiarism declaration

The present thesis is in accordance with the “policy on anti-plagiarism, Jadavpur University 2019”, and authenticate software found 07% of similarity. The snapshot is attached herwith.s

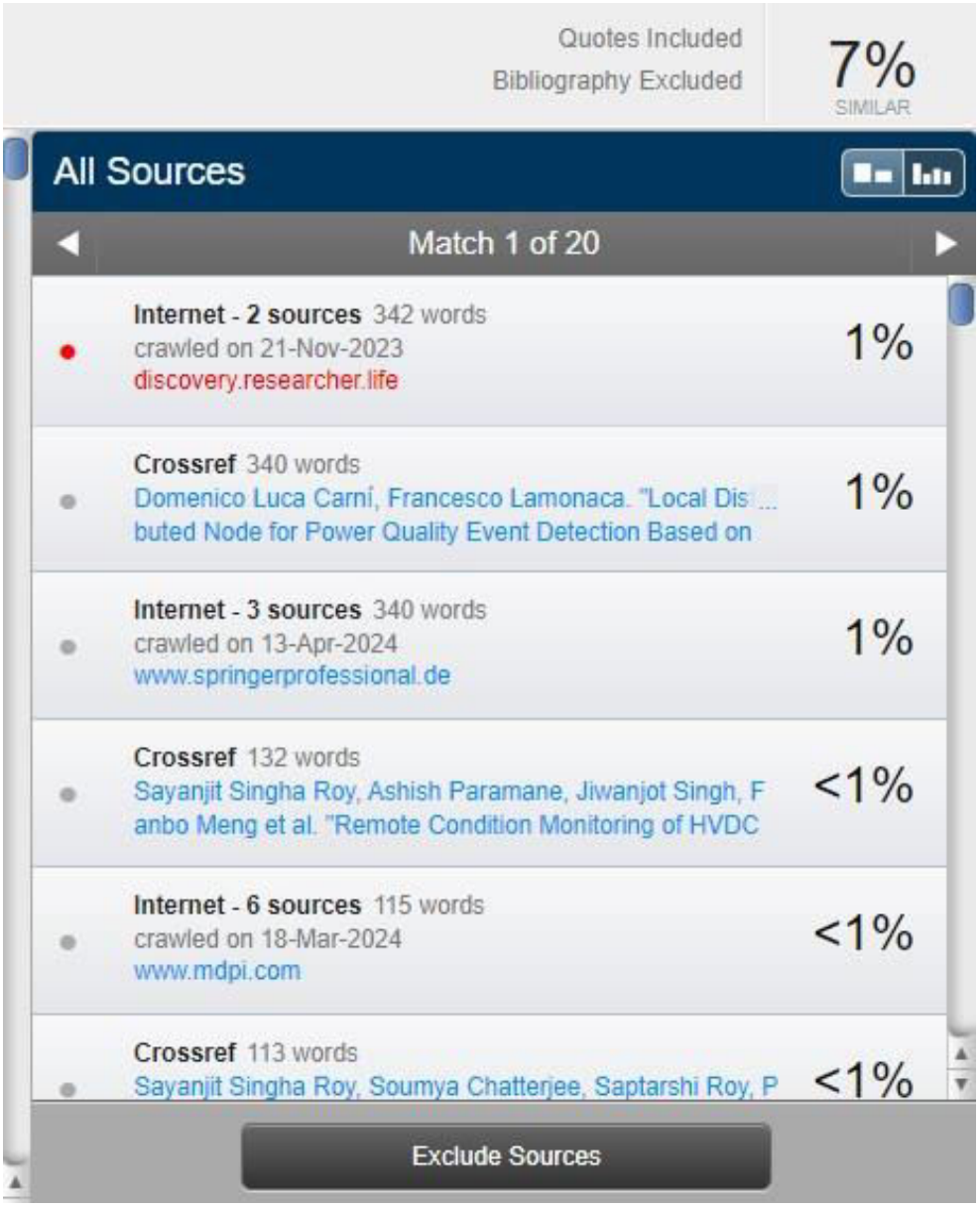

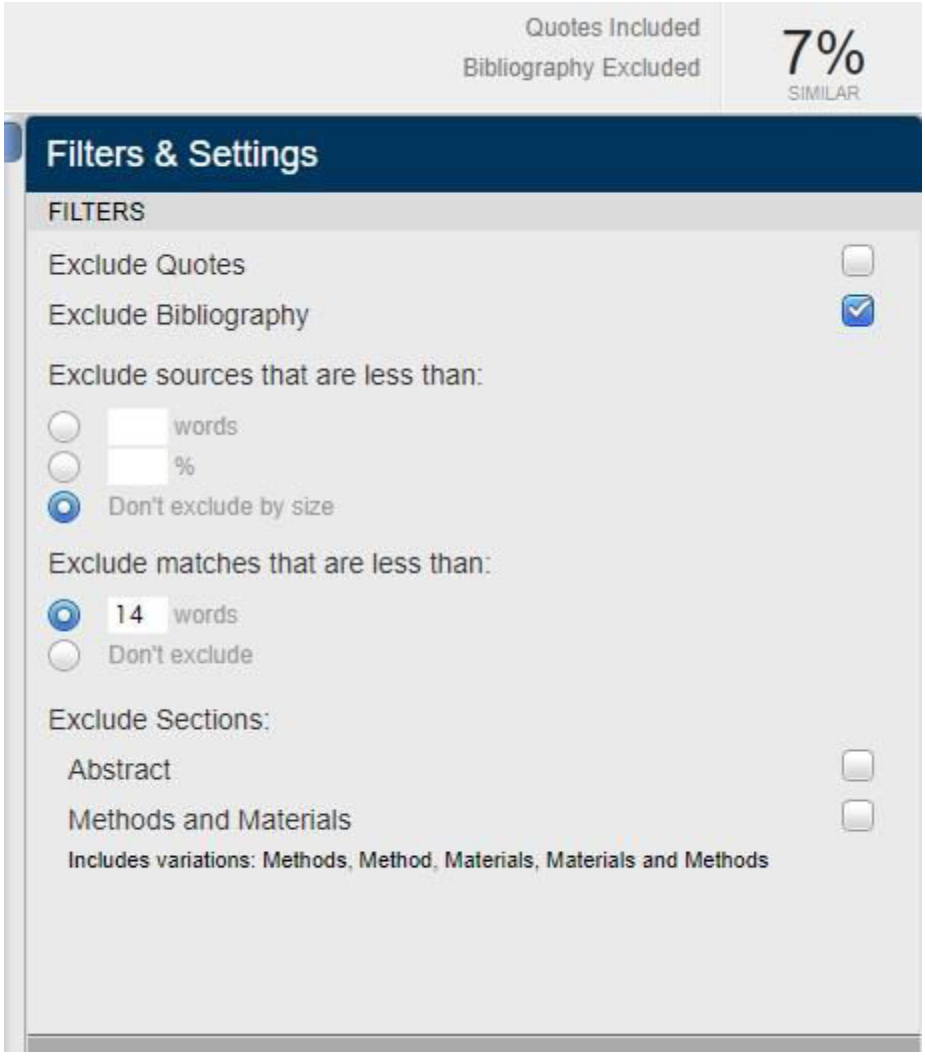
Quotes Included
Bibliography Excluded
7%
SIMILAR
Filters & Settings
FILTERS
Exclude Quotes
Exclude Bibliography
Exclude sources that are less than:
words
%
Don't exclude by size
Exclude matches that are less than:
14
words
Don't exclude
Exclude Sections:
Abstract
Methods and Materials
Includes variations: Methods, Method, Materials, Materials and Methods

Chapter 1

Introduction

1.1 Introduction

Transients in power transmission and distribution systems originate from various sources, exerting detrimental impacts on system equipment and its overall reliability. Although transients are typically short-lived occurrences, in the context of electrical systems, they have significant implications. These momentary surges of energy affect power, data, and communication lines, disrupting the functionality of vital amenities. Characterized by intense voltage and current spikes and substantial current flow lasting anywhere from microseconds to milliseconds, transients drive the system from stability to a temporary disruption, and then return it to its stable state. The eventual return to a stable state is known as the steady-state operating mode. According to the traditional definition, a transient event refers to an abrupt alteration in the system state, triggering a momentary surge of energy for a limited duration [1]. Transients in power systems can be mainly classified as voltage and current transients. Detection of transients is extremely important as they can lead to serious consequences due to overvoltage and overcurrent which can cause critical failure of power system equipment. Although many of the electrical transients have relatively minor magnitudes, they still pose a serious threat to the performance of circuits and protective devices [2]. These transients cause overheating of circuit components and semiconductor devices, leading to malfunctions and failures. Additionally, a significant proportion These electrical transients carry enough energy to potentially compromise the insulation of power system equipment. Adverse transient conditions can inflict significant damage on the power system, protective equipment, and switchgear. The maloperation of relays and circuit breakers can cause serious threat to the protection system. The effects on devices differ depending on their specific characteristics and their position within the power system. As a result, power system engineers must continuously develop strategies to mitigate transient magnitudes and control their effects

on operational equipment. Development of suitable transient detection methods can render reliable operation of power system components thereby preventing unwanted failure of power supply. Thus, in the context of power system reliability, detection and categorization of transient events is an important problem to address.

1.2 Sources of transient disturbances in power systems

Transient disturbances in power transmission and distribution systems stem from two main sources: internal and external factors. Internally, the intricate network of electrical components and devices, both within and outside the system, plays a crucial role in generating transient events.

1.2.1 Internal Sources

Components such as transformers and motors, known for their inductive properties, can instigate voltage transients when their magnetic fields collapse during current flow disruptions [3]. The impact of these transients depends on factors like the system's location, source size, time intervals, and rise time, as well as their effects on neighboring equipment and the electrical configuration. Various internal sources of transient voltages include internal capacitor switching, current interruptions in motors, and switching of power electronics devices involving silicon-controlled rectifiers (SCRs) or thyristors are among the factors contributing to internal transients [4]. Additionally, internal transients can result from electrostatic discharge, arc welding, photocopiers, faulty wiring, circuit breaker malfunctions, contact and relay closures, as well as load start-ups or disconnects [5]. While these internal sources can cause transients, they usually do not lead to significant voltage surges. Research indicates that internal sources seldom raise the system voltage to twice the normal level. Moreover, internal sources of transient voltages, originating from the everyday operation of devices such as low voltage motors, welding stations, electrical furnaces, ovens, and induction heaters within the facility, can also affect nearby equipment. These internal transients, though less widely recognized, can still exert a substantial influence on the overall stability of the electrical system.

1.2.2 External Sources

Transient voltages, originating from both external and internal sources, can substantially affect the seamless operation of an electrical facility. External factors such as lightning strikes, capacitor bank switching, line cable transitions, transformer operations, and current-limiting fuse actions, can create transient voltages that propagate through the facility's electrical system. These transients can lead to disruptions in the normal functioning of equipment and machinery, potentially causing damage and downtime.

Lightning, as one of the most prominent external sources of transients, can induce transient voltages into nearby conductors when it strikes in the vicinity of power lines. While direct lightning strikes are infrequent, the induced electric fields during a discharge can generate substantial induced transients, even without physical contact with the power lines. Apart from lightning, various normal utility operations, like the switching of loads, disconnect, and capacitor banks, can introduce transients into the power lines [6]. Loose connections in the distribution system, often caused by adverse weather conditions such as high winds, can result in power lines colliding or arcing, producing further transients that can disrupt the smooth operation of electrical systems. It is essential to mention that shared transformers can also contribute to transient activities. Given that multiple users are connected at the secondary side of the transformer, any transient activity generated within the shared system can impact the electrical main, affecting the overall functioning of the facility. One prominent trigger for the formation of transients is the occurrence of lightning, although their impact typically manifests indirectly by affecting the power line. This influence generates induced transients by coupling with the power system. Routine utility tasks, such as switching facility loads, toggling on-off disconnects on energized lines, operating capacitor banks, and tap-changing transformers, represent another significant external factor contributing to transient generation [7].

Natural calamities and other environmental factors can lead to the development of transients by causing poor connections within power distribution networks. Energization of power transformers can contribute

transient over voltages [8]. The underlying reason behind transformer transients lies in the collapse of the magnetic field upon energization, leading to transient generation. Arcing arises from malfunctions in the operation of breakers and contractors, often occurring when voltage fluctuations occur abruptly, resulting in disruptive electrical arcs. In addition to the above, faults in electrical systems can lead to momentary voltage sag and voltage swelling. Faults in electrical systems can be broadly categorized into four types: (i) Line to ground fault (LG) (ii) Line to line fault (LL) (iii) Line to line and ground fault (LLLG) (iv) Open circuit fault [9]. All these faults cause substantial increase in overvoltage and overcurrent that may lead to mal operation of protective devices. Understanding, managing and diagnosing these various sources of transient voltages and currents are crucial for maintaining the stability and efficiency of the electrical transmission and distribution network.

1.3 Categorization of transients in power systems

According to the definition outlined in the IEEE 1150-90-2019 standard, Transients can be classified into two main types: impulsive and oscillatory [10]. An impulsive transient is characterized by a sudden, non-power frequency alteration in voltage or current with a unidirectional polarity, such as lightning strikes and electrostatic discharges. The impulsive transients are known as fast front over voltages. In terms of response, impulsive transients typically rise within 0.1 ms and endure for about 1 ms. Conversely, oscillatory transients can exhibit a frequency surge of up to 5 kHz [11]. Analytically, these transients are calculated for benchmarking and troubleshooting purposes, aiding in the understanding and management of transient events within the electrical system. Conversely, oscillatory transients feature a sudden, non-power frequency shift in voltage or current with a bidirectional polarity, like capacitor bank energization or cable switching etc. for a longer duration unlike switching transients [11]. The oscillatory transients are slow front over voltages characterized by transient periods of oscillation that, although brief in comparison to the standard power frequency, can exert significant stress on the various components and

electrical equipment comprising the system. These two transients are mainly witching transients as they are characterized by high frequency components.

Besides, there are two other types of transients such as electromagnetic and electromechanical transients, though closely linked, exhibit some nuanced differences. Electromagnetic transients primarily revolve around fluctuations in voltages and currents, often triggered by the actuation of circuit breakers, malfunctions in power electronic or electronic equipment, faults, or lightning strikes [3]. On the other hand, electromechanical transients arise from imbalances between power generation and consumption, resulting in a shift in the generator's speed relative to its normal rotation. This typically occurs due to disturbances in the system, such as the sudden outage of a neighboring transmission line. Unlike electromagnetic transients, which occur rapidly, electromechanical transients manifest over a more extended period due to the inertia of the two generator shafts. Understanding the intricate nature of these transients is pivotal, particularly in instances where the transient waveform arises from multiple simultaneous switching actions, resulting in the convergence of transients. Moreover, phenomena like current chopping, which occurs when a circuit breaker's current reaches zero before the natural zero crossing, and restrike, which can happen during the de-energization of a capacitor by a gradually moving switch, underscore the complexity and multifaceted nature of these transient events [5].

In addition, any type of power quality disturbances like harmonics, voltage sags, voltage swell, sudden interruption, voltage flicker etc. may also come under the umbrella of power system transients [12]. These power quality disturbances are transient events which are not strictly oscillatory or impulsive transients. Recently, with the integration of renewable energy sources to grid, islanding events also characterize a typical transient event which is difficult to detect. Thus, categorization of transients is difficult in the true sense as different types of power system disturbances can occur whose amplitude, frequency content may vary from pure sinusoid.

The consequences of these afore-mentioned transients can be far-reaching, leading to a range of issues such as over-voltages, which can trigger

flashovers or insulation breakdown, and over-currents that may result in power equipment damage due to electromagnetic forces and excessive heat generation. Sources of power system transients are diverse and encompass lightning strikes on power system elements or the ground, as well as switching activities occurring in network components and end-user equipment. In the next section, the detrimental effects of power system transients are discussed in detail.

1.4 Detrimental effect of transients

Transient-induced equipment damage can manifest in various forms, including dielectric breakdown, electric flashover, fracture, and thermal overloads caused by surpassing specific dV/dt and dI/dt limits. Additionally, transients can render dielectric materials electrically conductive, especially when exposed to high magnitudes of stress. For instance, the physical separation of two conductive mediums at different voltage potentials can cause air, serving as a dielectric, to become conductive resulting in dielectric breakdown. Dielectric breakdown, often identified as electric flashover or arc flash, is associated with the exceeding of electrical stresses. These stresses can convert into mechanical energy, causing fractures in component materials at both microscopic and macroscopic scales. Additionally, transients produce thermal energy, which can degrade the insulation material [12]. On a molecular level, the speed of voltage and current fluctuations induced by transients plays a crucial role in determining the effects these stresses impose on the materials and components.

The impact of transients is primarily felt through disruptions to the accurate functioning of electronic equipment, leading to decreased efficiency and shortened device lifespans. Integrated circuits (ICs) are particularly susceptible, often experiencing burnouts because of the transient-induced voltage and current stress. Transients also trigger excessive heating in motors, affecting their overall performance. They interfere with device timing, causing functional disruptions and generating noise, while also hastening the deterioration of installations.

In technical terms, transients lead to increased hysteresis loss, resulting in higher current injections for the same output, thereby straining the motor further. Additionally, transients can severely compromise the performance of lightning protection systems, causing a decrease in operational capacity and even complete failure [12]. Visible darkening of the anode's ring, induced by transients, signals a decline in system effectiveness. Controlling transient phenomena is crucial for extending the lifespan of these vulnerable devices.

The distribution system is critically affected, as evidenced by the degradation of contact areas in breakers and switches. This deterioration causes faulty breaker behavior, leading to circuit interruptions under false pretenses [13]. Voltage transients can impact electrical equipment in four primary ways: intermittent interruption, chronic degradation, latent failure, and catastrophic failure. Intermittent interruption occurs when transients are injected into data or control networks, leading to data loss or corruption and the malfunctioning of loads or devices. Chronic degradation occurs when repeated transients gradually compromise the integrity and reliability of exposed components, ultimately rendering them inoperable.

Latent failures resemble chronic degradation but stem from significant transient events that damage components without fully impairing their function. Over time, these components become inoperable due to the stresses of normal operation. Catastrophic failures are more immediately identifiable, as the affected component or device stops functioning properly almost instantly. Such events often exceed the component's rated threshold, resulting in permanent open circuits or short circuits.

Devices such as microprocessors and programmable logic controllers (PLCs) are particularly susceptible to damage caused by voltage transients, potentially reducing their reliability and operational lifespan. The shrinking scale of device components due to technological advancements further exacerbates their susceptibility to damage from transients. Consequently, transient voltages can disrupt normal operations, leading to erratic behavior and reduced product quality. In industrial settings, interruptions in continuous

manufacturing processes can result in significant revenue losses due to production downtime.

1.5. Effect of transients on power quality (PQ) issues

The significance of power quality in power systems cannot be overstated, as subpar electricity not only poses hazards but also proves uneconomical for both utilities and consumers. Consequently, a concerted emphasis on enhancing the quality of power supplied to loads is imperative. Scrutinizing the root causes of poor power quality, diverse measuring parameters, established power quality standards, and an array of techniques to bolster power quality represents a crucial starting point. Essentially, power quality reflects the power grid's efficacy in delivering power proficiently to consumers and the capability of equipment to efficiently consume the supplied power [14]. Technically, it involves the assessment, refinement, and examination of sinusoidal waves at specified frequency and voltage levels. The financial and operational aspects of the power system are heavily influenced by power quality, necessitating a certainty that the power consumed by the system adheres to desired standards. Modern consumers exhibit heightened awareness regarding power quality, prompting numerous governments to amend policies and compel heightened sensitivity to any fluctuations in power quality. Manufacturers, utilities, and consumers all share a vested interest in power quality, contributing to the escalating concerns in this domain. Power system transients stand out as a primary catalyst for degradation of power quality [15]. Poor power quality can have detrimental effects on both the utility and consumer ends [15]. Some of the primary consequences within the power system resulting room subpar power quality include:

1. Harmonics contribute to waveform distortion, potentially subjecting equipment to elevated wave form peaks, which in turn can inflict damage. Excessive voltage levels can also force equipment into a saturation state, introducing further disruptions.

2. Harmonics induce over-voltages that cause significant damage to the insulation endangering the life of high voltage apparatus like power transformers, cables etc.

3. Equipment longevity is compromised due to factors like overheating and noise, leading to reduced lifespan. The suboptimal power quality substantially diminishes system efficiency and performance.

4. Power outages or interruptions can result in the loss or corruption of critical data, leading to significant losses.

5. The costs associated with power systems substantially escalate when power quality is lacking.

6. In the event of power failures, consumers can encounter a multitude of issues due to power unavailability, which also impacts utility expenses.

7. Consumer loads suffer from detrimental effects and potential damage stemming from power quality concerns.

8. In certain cases, the power system may need to be oversized to cope with the additional stress imposed by poor power quality, inevitably leading to elevated installation costs.

Thus, considering the detrimental effect of transients on PQ, it is necessary to develop methods that can efficiently detect different type of PQ events accurately so that the reliability of power transmission and malfunctioning of power equipment can be prevented.

1.6. Transients in grid connected renewable energy sources

Over the past decade, electrical power systems have evolved from conventional energy systems to advanced next-generation smart grid systems. Conventional power systems primarily depend on a few centralized, large-

scale power generation sources, predominantly hydropower or fossil fuel-based systems. These systems utilize a vast transmission network to distribute power to consumers through a distribution system. However, the emergence of smart grids and smart energy systems has increasingly captured the attention of researchers. Unlike their conventional counterparts, smart grids facilitate two-way power and information flow, transforming them into active grids. This transformation is attributed to the integration and contribution of various distributed and renewable energy resources. The bidirectional flow of power and communication not only enhances the reliability, security, and efficiency of power systems but also positions the smart grid as the future of power distribution. Its benefits include improved energy efficiency, cost-effectiveness, reduced emissions, lowered costs, and enhanced utility. A pivotal aspect enabling the smart grid's multifaceted operations compared to conventional systems is the plethora of interconnected devices capable of exchanging commands and information to execute energy-related tasks efficiently [16]. This shift from conventional to smart grids has ushered in a myriad of distributed generation (DG) systems, encompassing photovoltaic (PV), wind energy, and electric vehicles (EV) [17]. Essentially, the smart grid amalgamates processes, technologies, and distributed renewable generation systems, augmenting the intelligence and efficiency of the conventional power grid.

However, the integration of diverse DGs introduces several challenges. These encompass load forecasting, fault and failure analysis, demand-side management, non-intrusive load monitoring (NILM) [7], cybersecurity, electricity theft detection, and islanding detection [among others. The increasing prevalence of intermittent and DG systems, coupled with technological advancements, necessitates the development of more accurate and reliable solutions for these challenges. Switching of renewable energy sources to grid results in transients which are often difficult to discern from naturally occurring transients like capacitor switching load switching etc. [17]. Islanding is one such phenomenon where the renewable energy source gets disconnected from the main grid and operates in a standalone mode if there is some disturbance in the main grid. Detection of islanding is a key challenge in distributed generation system. Failure to detect islanding events results in maloperation of relays and circuit breakers resulting in unwanted

tripping of transmission lines. So, detection of islanding and non-islanding events in grid connected renewable energy sources is a key challenge.

In addition to the above, grid connected renewable energy sources need lots of power electronics components for grid integration. Power electronic converters and inverters are the main components which are used to integrate renewable energy sources to the grid. Switching of these power electronic components often results in transients which are difficult to identify. In addition, faults in converters also lead to mal operation of power electronic components which may lead to unwanted islanding, tripping and catastrophic failure. Early and accurate detection of faults in grid connected renewable energy sources is thus a major challenge and suitable methods need to be developed so that accurate measures can be taken, and pre-mature failure can be minimized.

In existing literature several methods have been proposed for detection and classification of transients in power systems in presence or absence of renewable energy sources with or without grid connected mode. In the next section, a brief overview of different signal processing and machine learning methods available for voltage and current signal analysis is presented.

1.7. Overview of signal processing and machine learning methods

Evaluating transient detection and protection in power systems presents a considerable challenge due to the swift reactions and complex infrastructure inherent in these systems. This task is pivotal for operational considerations and is crucial in monitoring stability status and constraints [1]. Nonetheless, conventional power systems, characterized by their low sampling frequencies for measurement devices, make the monitoring of power system transients nearly unfeasible. The emergence of wide-area measurement systems (WAMS) and advanced measurement tools, notably phasor measurement units (PMUs), has furnished the necessary infrastructure for real-time transient security assessment. Local measurement devices may not always cover predefined areas and can experience temporary or permanent failures.

Consequently, designing a comprehensive model has become essential. In existing literature, various signal processing and machine learning methods are available for analyzing power system transients. Signal processing methods involve analyzing measured voltage and current signals in both time and frequency domains to ascertain stable or unstable conditions. The available signal processing methods for analysis of voltage and current signals in power systems can be broadly classified into three types:

1.7.1 Types of signal processing algorithms

Signal processing algorithms allow analysis of voltage and current signals in three domains namely:

1. Time domain analysis

2. Frequency domain analysis

3. Time frequency domain analysis

1.Time domain analysis

In time domain analysis, the voltage and the current signals are analyzed using different time domain signal analysis methods like cross-correlation, autocorrelation, derivative based method etc. [18]. These methods do not allow any frequency information present in a signal. The features can be extracted from the time domain analysis of the signals itself without losing the temporal information.

2. Frequency domain analysis:

In frequency domain analysis, the voltage and current signals are usually converted from time domain to frequency domain to observe the frequency components present in a signal. Popular signal processing methods for converting a signal from time domain to frequency domain include discrete and fast Fourier transform [19], power spectral density estimate etc. [19].

Frequency domain analysis gives only spectral information present in a signal, but the temporal information is lost.

3. Time-frequency domain analysis
In time-frequency domain analysis, the time domain voltage signals are converted from time domain to time-frequency domain. To elucidate further, the time-frequency analysis provides time as well as frequency information of a signal at the same time. Thus, unlike frequency domain, where the frequency information of a signal is lost, time-frequency analysis provides joint time and frequency information at the same time. Some of the popular time-frequency analysis methods like short time Fourier transform (STFT) [20], continuous wavelet transform (CWT) [20], Stockwell transform [20] etc. Time frequency domain method is mainly used to analyze non-stationary signals.

Many analytical techniques demand significant computational resources, relying on intricate physical models and predefined thresholds. In contrast, data-driven methods leverage historical data for decision-making and are suitable for real-time monitoring. These data-driven approaches generally categorize into three types: shallow, deep, and hybrid methods. Currently, power systems are undergoing rapid transformation towards more active, flexible, and intelligent smart grids. This evolution introduces challenges across various domains, including the integration of distributed renewable energy sources, cybersecurity, demand-side management, and decision-making in system planning and operation. The successful implementation of advanced functionalities in the smart grid largely hinges on the robustness of its information and communication infrastructure. Additionally, effectively managing the vast amounts of data generated from multiple sources, such as smart meters, phasor measurement units, and various sensors, is crucial. In recent years, there has been a growing interest and trend in leveraging machine learning-based techniques to address the myriad challenges faced by smart grids. Machine learning is expected to be a major driving force in future smart electric power systems. In the next section, brief overview of different machine learning algorithms is given.

1.7.2 Types of Machine Learning algorithms

Machine learning encompasses four distinct categories of techniques, namely [21]:

1. Supervised Learning

2. Unsupervised Learning

3. Semi-Supervised Learning

4. Reinforcement Learning

1. Supervised learning:

In supervised machine learning, machines are trained using labeled datasets, using this information to predict future outcomes. This training process is based on guidance and supervision, hence the name 'supervised.' The labeled dataset serves as a roadmap for machines, as specific input values are associated with corresponding output values. Subsequently, test datasets are provided post-training to validate the accuracy of predictions. The primary objective of supervised learning techniques is to establish relationships between input and output variables. Supervised machine learning can be classified into two distinct problem types [21]:

• Classification: Classification algorithms are employed when the output variable assumes a binary or multiclass in nature. These algorithms categorize responses into distinct classes such as 'Available' or 'Unavailable,' 'Yes' or 'No,' 'Pink' or 'Blue,' based on the labeled datasets provided during training. This method is extensively used in tasks like spam detection.

• Regression: Unlike classification, regression algorithms address problems where a linear relationship exists between input and output variables. Regression techniques are employed to make predictions in scenarios like weather forecasting and market conditions.

2. Unsupervised Learning

Unlike supervised learning, unsupervised learning operates without guidance or supervision. It uses unlabeled and unclassified datasets for machine training, allowing machines to make autonomous predictions without human intervention. This approach is often employed to categorize or group unorganized data based on their inherent characteristics, similarities, and differences. Machines excel in uncovering hidden patterns and trends within the input data. Unsupervised learning can be again broadly classified into two types:

- Clustering: Machines segment data based on inherent features, similarities, and differences. They identify clusters within complex data to facilitate object classification. This method is commonly used to understand customer segments and purchasing behaviors across diverse geographical contexts.

- Association: Machines detect relationships and connections among variables within extensive datasets. This approach is particularly popular in domains like web usage mining and plagiarism detection in doctoral research.

3. Semi-Supervised Learning

This approach combines the strengths of both supervised and unsupervised learning techniques, using a mix of labeled and unlabeled datasets for training. It leverages all available data, making it cost-effective. Initially, similar data is grouped using an unsupervised learning algorithm, aiding in labeling unlabeled data [21].

4. Reinforcement Learning

Reinforcement learning operates without labeled data, relying on experiences and a trial-and-error approach based on feedback. AI explores data, learns from previous experiences, and enhances its performance.

- Positive Reinforcement Learning
- Negative Reinforcement Learning

Shallow-architecture methods, such as artificial neural networks (ANNs), decision trees (DT) [22], random forests, kernel regression, Lasso regression, probabilistic neural networks (PNN) [22], support vector machines (SVMs) [22], ball vector machines (BVM), extreme learning machines (ELM), and ensemble learning (EL) [22], are established tools in power system security assessment. However, these shallow architectures may struggle to precisely capture the nuances and characteristics of transient behavior, often lacking generality due to their constrained hypothesis space.

Deep learning, an emerging subset of machine learning, has demonstrated success in various engineering applications in recent years, adept at capturing intricate, nonlinear, and highly variable features [23]. In the area of power systems, deep learning has been deployed for tasks including residential load forecasting, induction machine condition monitoring, wind turbine surveillance, controller design for renewable energy systems, power quality evaluation, and power transformer protection, among others [23]. Nonetheless, the application of deep learning in transient security assessment remains a relatively uncharted territory. For instance, a contingency-based security assessment is framed as a CNN-based classification problem with two classes. In another approach, a deep autoencoder is integrated with the Vine Copulas model to bolster transient security evaluation and discern stable from unstable conditions with heightened accuracy. The intrinsic capability of deep networks for automatic feature extraction markedly enhances performance.

1.8 Limitations of the existing signal processing and machine learning methods for transient detection

Although numerous signal processing and machine learning algorithms have been implemented for detection and classification of different power system transients, yet from the practical point of view of transient detection in power systems existing methods have certain limitations. The potential drawbacks of the existing methods are mentioned below.

1. In the context of detection of transient disturbances, there is need to develop an accurate method for analysis of both impulsive and oscillatory transients. Also, selection of suitable features and machine learning algorithms is a major challenge for accurate detection of impulsive and oscillatory transients.

2. For reliable detection and classification of power quality (PQ) disturbances, detection in noisy environment is a challenging issue. In general, analysis of PQ signals in joint in time-frequency plane is done using traditional signal processing algorithms. However, performance of most of the available methods will fail miserably under low signal to noise ratio condition. Another important issue is the feature extraction. Manual feature extraction always imposes the risk of selection of redundant features that may peril and degrade the performance of the classifier. Hence, automated feature extraction from time-frequency analysis of PQ signals in noisy environments is an important problem to address.

3. In grid connected renewable energy sources, detection of islanding and non-islanding is a major issue that still needs to be addressed carefully. Appropriate signal processing and feature extraction methods need to be developed for accurate detection of islanding as well as non-islanding events. Additionally, design of suitable deep learning models for classification of islanding events also needs to be looked at meticulously for accurate segregation of non-islanding events from the islanding ones.

4. In addition to islanding, detection of faults in grid connected systems is also a challenging issue. Proper methodologies for accurate fault detection are still lacking and there is still a dearth of deep learning models for unsupervised fault detection in grid connected renewable energy systems. Unlike supervision classification models where the machine learning models work on a pre-labelled dataset, in unsupervised learning the models are not pre-labeled. Unsupervised machine learning models are becoming very popular owing to their ability to work satisfactorily on unlabeled data. Hence, there is need to develop unsupervised machine learning tools for accurate classification of faults in grid connected renewable energy systems.

Thus, based on the limitations of the existing methods as stated above, the present thesis is aimed to fill some of the research gaps. The aims and scope of the present thesis are enumerated below.

1.9 Scope and objective of the thesis

The main objective of the present thesis is to develop advanced signal processing and machine learning algorithms for transient detection and classification in power systems. In this context, the present thesis is divided into the following chapters which are explained below.

In ***Chapter 2***, a method for accurate detection of impulsive and oscillatory transients occurring in power systems is proposed using non-stationary signal processing tools like discrete wavelet transform-based multi-resolution analysis and Hilbert transform. As stated earlier, impulsive and oscillatory transients are one of the most frequently occurring power system disturbances. So, accurate detection of these two transient disturbances is a challenging task. Moreover, these two transient disturbances are short-time disturbances which are either manifested as sudden voltage spikes or oscillation for finite duration. These voltage waveforms are predominantly non-stationary in nature. So, non-stationary signal analysis is needed for proper analysis of power system transient disturbances. In addition to signal analysis, proper feature extraction is necessary for accurate classification of

impulsive and oscillatory transients. So, in ***Chapter 2***, a new method to detect impulsive and oscillatory transients in power systems is proposed by applying discrete wavelet transform-based envelope analysis and supervised machine learning algorithms.

In ***Chapter 2***, it has been observed that application of discrete wavelet transform based multiresolution analysis and envelope analysis using Hilbert transform has delivered accurate results for detection and classification of oscillatory and impulsive transients. However, only lightning and switching transients were considered in the earlier chapter. In real life power systems, several other types of transient disturbances can happen which results in poor power quality (PQ) issues. The PQ disturbances can be broadly classified as single as well as multiple PQ disturbances. So accurate detection and classification of PQ disturbances is essential from the point of view of safety of operators as well prevention of malfunction of power apparatus. Considering the aforementioned facts, in ***Chapter 3,*** a novel PQ detection framework employing cross-spectral analysis using Stockwell transform and deep learning based automated feature extraction is proposed. The proposed framework has been developed in such a way that it can detect single and multiple PQ events correctly even in noisy environmental conditions. The proposed framework has been validated on simulated PQ signals as well as on real life PQ signals to validate the practicability of the proposed method.

In ***Chapter 3***, a novel framework for detection and classification of PQ disturbances in noisy environment employing cross spectral analysis and deep learning is proposed. However, in the previous chapter, generalized and commonly occurring PQ disturbances in power systems are considered where the effect of transient disturbances occurring due to renewable energy systems connected to grid are not considered. When renewable energy sources are connected to grid, detection of islanding and other transient disturbances becomes a challenging issue. Considering the above facts, in ***Chapter 4***, a novel method employing autocorrelation-based feature extraction method is proposed for detection of islanding and other transient disturbances in renewable energy grid connected systems. A deep learning algorithm has been designed to classify islanding and non-islanding events

using extracted features from auto correlograms for classification of islanding and other disturbances.

In ***Chapter 4***, only detection of islanding and non-islanding events using autocorrelation-based feature extraction and deep learning has been proposed. However, in addition to islanding, detection of faults in grid connected solar PV systems is a challenging issue and if not detected properly may lead to severe maloperation. Hence, ***in Chapter 5,*** a method has been developed for accurate identification of faults in grid connected solar PV systems based on current data obtained from real-life grid connected solar PV system. A novel extended Park's vector modulus-based fault detection algorithm has been developed and smoothed pseudo-Wigner-Ville distribution-based time frequency analysis of different faults and fault free current data has been analyzed in time- frequency frame. Finally, an unsupervised machine learning has been developed for accurate identification of faults in grid connected solar PV systems.

In ***Chapter 6***, deals with the summary and conclusions of the present thesis work. In addition to conclusions, the scope of the future work has been discussed in chapter 6.

In ***Appendix,*** some additional results like mathematical formulae of PQ events and confusion matrix of PQ classification are shown.

1.10 Originality of the thesis

To the best of author's knowledge, the original contributions of the thesis are as follows:

1 Development of a novel discrete wavelet transform based multiresolution analysis and envelope extraction method using Hilbert transform for accurate detection of impulsive and oscillatory transients in power systems.

2 Application of cross Stockwell transform and deep feature extraction employing convolutional neural network for detection and

classification of single and multiple PQ events in noisy environment.

3 Development of a novel islanding detection method for grid connected renewable energy sources employing autocorrelation and bi-directional long-short term memory classifier.

4 Application of smoothed-pseudo-Wigner-Ville distribution-based time-frequency analysis and autoencoder based unsupervised fault classification model for grid connected solar PV systems.

References

[1] P. Hariramakrishnan, S. Sendil Kumar, "Transients detection using Artificial Neural Network based HS-transform", 2nd IEEE International Conference on Power and Embedded Drive Control (ICPEDC), pp.413-420, 2019.

[2] S. Banerjee, P.S. Bhowmik, "A machine learning approach based on decision tree algorithm for classification of transient events in microgrid", Electrical Engineering, 105, 2083–2093,2023.

[3] I. Niazazari, R.J. Hamidi, H. Livani and R. Arghandeh, "Cause identification of electromagnetic transient events using spatiotemporal feature learning", International Journal of Electric Power and Energy Systems, vol. 123:106255, 2020.

[4] N. W. A. Lidula and A. D. Rajapakse, "A Pattern Recognition Approach for Detecting Power Islands Using Transient Signals—Part I: Design and Implementation," IEEE Transactions on Power Delivery, vol. 25, no. 4, pp. 3070-3077, 2010.

[5] E. A. Bhuiyan, et al. "A deep learning through DBN enabled transmission line fault transient classification framework for multimachine microgrid systems" International Transactions on Electrical Energy Systems, vol. 2022, 2022.

[6] D. C. Robertson, O. I. Camps, J. S. Mayer and W. B. Gish, "Wavelets and electromagnetic power system transients," IEEE Transactions on Power Delivery, vol. 11, no. 2, pp. 1050-1058, 1996.

[7] H. H. Chang, H.J. Chang and C.L. Lin, "Novel High-Frequency Transient Techniques in Non-Intrusive Load Monitoring Techniques", IEEE 8th Asia Conference on Power and Electrical Engineering (ACPEE), pp.1533-1538, 2023.

[8] A. Thomas, S. Koshy, R. Sunitha, "Machine Learning Based Detection and Classification of Power System Events", IEEE International Conference on Power, Instrumentation, Control and Computing (PICC), pp.1-6, 2020.

[9] "IEEE Recommended Practice for Monitoring Electric Power Quality," IEEE Std. 1159-1995, vol., no., pp.1-80, 30 Nov. 1995.

[10] S. Banerjee, P.S. Bhowmik, "Multiclass transient event classification in hybrid distribution network based on co-training of fine KNN and ensemble KNN classifier", Smart Science, vol.11, no.4, pp.744, 2023.

[10] F.Z. Md. Fadzil, A. Mousavi and M. Danishvar, "Simulation of Event-Based Technique for Harmonic Failures", IEEE/SICE International Symposium on System Integration (SII), pp.66-72, 2019.

[11] "IEEE Recommended Practice for Monitoring Electric Power Quality," in IEEE Std. 1159-1995, vol., no., pp.1-80, 30 Nov. 1995.

[12] A. Chakraborty and R. Mandal, "A novel technique employing DWT-based envelope analysis for detection of power system transients," 2017 International Conference on Energy, Communication, Data Analytics and Soft Computing (ICECDS), Chennai, India, pp. 346-350, 2017.

[13] A. Greenwood, Electrical Transients in Power Systems, 2nd edition John Wiley & Sons,1991.

[14] P. Khetarpal, M. M. Tripathi, "A critical and comprehensive review on power quality disturbance detection and classification", Sustainable Computing: Informatics and Systems, vol.28, pp.100417, 2020.

[15] A. Chakraborty, S. Chatterjee and R. Mandal, "Power Quality Recognition in Noisy Environment Employing Deep Feature Extraction from Cross Stockwell Spectrum Time-Frequency Images", Electrical Engineering, Springer, Volume 106, pages 443–458, 2024.

[16] N.W.A Lidula, A.D. Rajapakse, “Fast and reliable detection of power islands using transient signals”, IEEE International conference on Industrial and information systems. ICIIS, pp 493–498, 2009.

[17] A. Chakraborty, S. Chatterjee and R. Mandal, "Autocorrelation Aided Islanding Detection Using Bi-directional Long-short Type Memory Network," Proceedings of 2nd IEEE International Conference on Power Electronics and Energy (ICPEE), Bhubaneswar, India, 2023.

[18] S. Dalai, B. Chatterjee, D. Dey, S. Chakravorti and K. Bhattacharya, "Rough-Set-Based Feature Selection and Classification for Power Quality Sensing Device Employing Correlation Techniques," in IEEE Sensors Journal, vol. 13, no. 2, pp. 563-573, Feb. 2013.

[19] S. Dalai, D. Dey, B. Chatterjee, S. Chakravorti and K. Bhattacharya, "Cross-Spectrum Analysis-Based Scheme for Multiple Power Quality Disturbance Sensing Device," in IEEE Sensors Journal, vol. 15, no. 7, pp. 3989-3997, July 2015.

[20] J.E. Caicedo, D. Agudelo-Martínez,E.Rivas-Trujillo, et al. "A systematic review of real-time detection and classification of power quality disturbances", Prot Control Mod Power Syst, vol.8, no.3, 2023.

[21] S. Ray, "A Quick Review of Machine Learning Algorithms," 2019 International Conference on Machine Learning, Big Data, Cloud and Parallel Computing (COMITCon), Faridabad, India, 2019.

[22] R. Kuppusamy, S. Nikolovski, Y. Teekaraman, "Review of Machine Learning Techniques for Power Quality Performance Evaluation in Grid-Connected Systems",Sustainability 2023, 15, 15055.

[23] R. A. Oliveira, M. H.J. Bollen, "Deep learning for power quality", Electric Power Systems Research, Volume 214, Part A, no.1, January 2023, 108887.

Chapter 2

A Novel Technique Employing Discrete Wavelet Transform-Based Envelope Analysis for Detection of Power System Transients

2.1 Introduction

The term 'transient' in power systems can be thought of a phenomenon leading to a sudden alteration in voltage and current waveforms persisting for a very small duration [1]. Occurrence of power system transients are very frequent in power transmission and distribution networks. Although persisting for a very short duration, power system transients can endanger the life of power equipment by imposing severe electrical and thermal stress on power equipment. In the long run, a complete failure of the power equipment may take place leading to a catastrophic failure of the entire power system network. Therefore, detection of power system transients has been a major focal point of research for the past few years. In this context, researchers all over the world have implemented several advanced signal processing and machine learning techniques which have been able to detect and classify different transient phenomenon occurring in power systems with reasonable efficacy.

Since power system transients represent highly nonstationary behavior application of wavelet transform for automated detection of transient disturbances have been reported in many existing literatures. Detection and classification of different transient phenomena occurring in power transformers using combined wavelet transform and neural network have been reported in [2]. Automated detection and classification of power system transients implementing wavelet transform and feed forward artificial neural network has been reported in [3]. Power system transient analysis based on using scalograms and wavelet multi resolution analysis have been reported in [4]. Features based on dual tree complex wavelet transform (DTCWT) and

artificial neural network for detection of power system transients have been reported in [5]. In [6], a sparse representation classifier based on DTCWT based features has been successfully implemented for recognition of different power system transients. It is therefore evident from the existing literatures that, wavelet transform is a very popular feature extraction tool that have been widely used to analyze different types of power system transients. Hence, in the present work, a novel technique based on envelope analysis of discrete wavelet transform (DWT) coefficients has been proposed to detect different type of power system transients. DWT based envelope analysis has been recently proposed as a novel feature extraction technique from non-stationary signals. Application of DWT based envelope analysis have been reported in biomedical engineering for detection of epilepsy in [7] and in mechanical engineering also for condition monitoring in rolling element bearings [8]. In this paper, it has been used for the first time in the area of power systems to detect different transient disturbances.

2.2 Theoretical background

2.2.1 Discrete wavelet transform

Discrete wavelet transform (DWT) is an efficient technique to analyze any nonstationary time series. DWT based multiresolution analysis (MRA) offers localization both in joint time and frequency frame. DWT based MRA offers good frequency resolution for the low frequency components of a signal and good time resolution for the high frequency components of a signal. Moreover, DWT has low computational complexity and easy to implement. The mathematical details of DWT can be found out in many available literatures [2-3] and hence are not discussed in greater details in this paper. Mathematically, DWT of any signal $f(t)$ can be expressed as:

$$DWT(p,q) = \int_{-\infty}^{\infty} f(t) \frac{1}{\sqrt{|2^p|}} \psi\left(\frac{t-2^{pq}}{2^p}\right) dt \tag{2.1}$$

where $\psi$is the mother wavelet and 2^p and 2^{pq} are the translation and dilation parameters, respectively. One of the major issues associated with DWT based analysis is the choice of the mother wavelet. In the present work

'Daubechies-4' mother wavelet is used to decompose the power system transient signals, since, it has been reported in existing literatures that 'Daubechies' wavelet can detect high frequency short time disturbances [9].

2.2.2 Hilbert transform

For envelope detection of any nonlinear & nonstationary signal, Hilbert Transform is a very efficient and popular method. Mathematically, Hilbert transform of a signal *f*(t) is given by:

$$f_H(t) = f(t) \times \frac{1}{\pi\tau} = \int_{-\alpha}^{\alpha} \frac{f(\tau)}{t-\tau} d\tau \tag{2.2}$$

where $f_H(t)$ is the Hilbert transform of $f(t)$. The envelope spectrum $E(t)$ corresponding to each frequency sub bands are calculated by the following equation:

$$E(t) = |f_H(t)| \tag{2.3}$$

In the present work, instead of using envelope spectrum from the signals directly, the envelope of the detail coefficients of different frequency sub bands have been extracted for the purpose of detection of power system transients. The proposed methodology is therefore a modification over the existing method [10] which directly uses envelope extraction from the signal itself.

2.3 Methodology

2.3.1 Synthetic signal generation

In the present study, two common power system transient signals have been generated in MATLAB 2016 (a) environment using numerical models as per IEEE Standard-1159 [11]. The sampling frequency of the signals are kept at 10 kHz. Further, it is reported in [12], that the simulated power system transient signals generated using numerical models closely resemble real time transient disturbances that take place in power system networks. Fig. 2.1(a)

and Fig. 2.1(b) show the typical oscillatory and impulsive power system transient signals used in the present work.

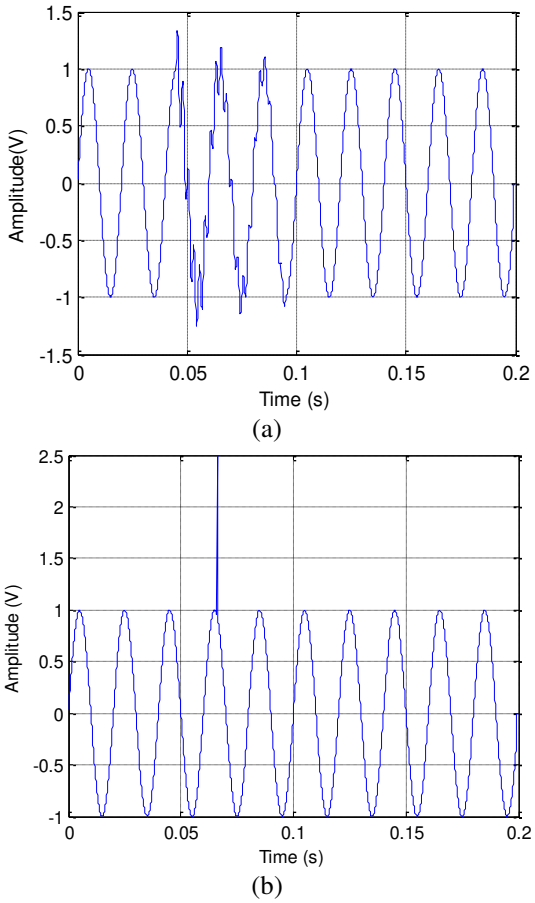

Fig, 2.1 Typical nature of (a) oscillatory voltage transient and (b) Impulsive voltage transient signal

2.3.2 Feature extraction from DWT Envelope

The power system transient signals are at first decomposed using DWT into different frequency sub bands. Since most of the transient phenomenon are

high frequency short time disturbances, hence, the first four detail coefficients D_1-D_4 have been chosen in this work since high frequency information of a signal are mostly retained within the first few detail coefficients. Table 2.1 shows the respective frequency sub bands for the first 4 level of wavelet decomposition.

Table 2.1 Extracted features

Level of Decomposition	Range of Frequency
D_1	5kHz-2.5kHz
D_2	2.5kHz-1.25kHz
D_3	1.25kHz-625Hz
D_4	625Hz-312.5Hz

After extraction of different frequency sub bands using DWT based MRA, HT is applied on each of the first four decomposed sub bands and using equation (3), the envelope spectrum corresponding to each sub band have been obtained. Fig.2.2 shows the first four detail coefficients D_1-D_4 obtained for oscillatory transient signal after wavelet decomposition and the corresponding envelope of each frequency sub bands are shown in Fig.2.3. The choice of features is very important in any classification problem. The selection of suitable features can be done by either hit and trial method or on prior experience. Similar types of features has been found to yield reasonably high degree of classification accuracy in existing literatures [6-7]. Hence, from the envelope spectrum corresponding to each sub band following statistical features have been extracted in the present work for the classification of power system transients.

F_1=Standard deviation of the envelope for each sub band

F_2=Mean of the envelope for each sub band

F_3=Energy of the envelope for each sub band

F_4=Maximum value of the envelope for each sub band

2.3.3 ANOVA test of the extracted features

After extracting the selected features from the DWT envelope spectrum of both type of transient signals, a statistical null hypothesis test known as analysis of variance (ANOVA) test is done to analyze the discriminative

probability of the selected features. Based on the output of the ANOVA test, which yields a '*p*'

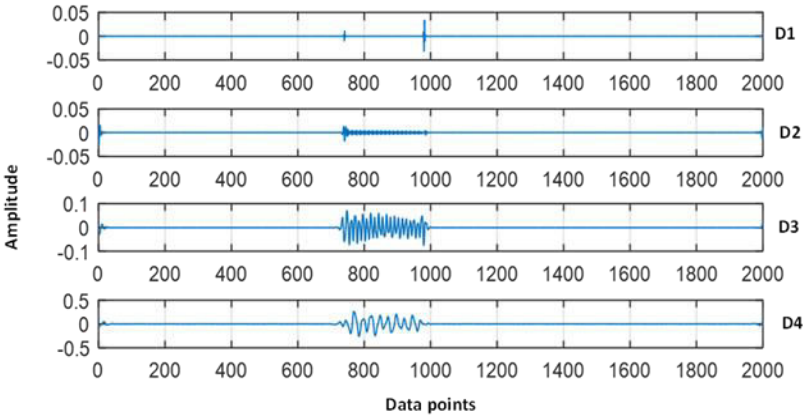

Fig.2.2 First four detail coefficients of the oscillatory voltage transient signal D_1-D_4.

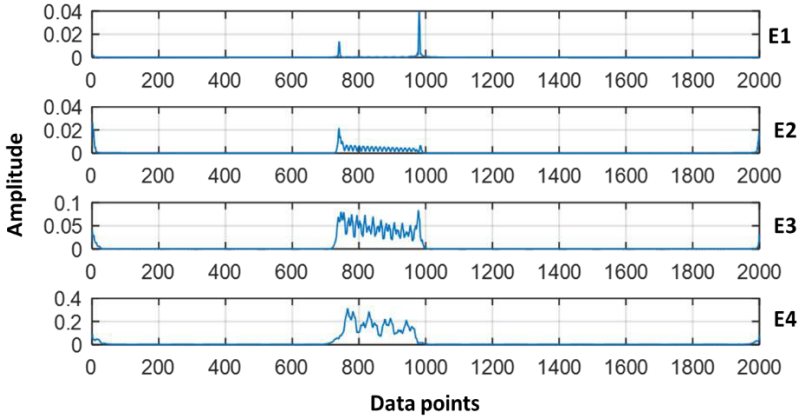

Fig.2.3 Envelope of the First four detail coefficients of the oscillatory voltage transient signal E_1-E_4.

value, the discriminative capability of the features can be assessed. A lower '*p*' value is an indicator of very high discriminative capability [13]. Table 2.2

and Table 2.3 show the variation of the extracted features from the envelope spectrum along with respective '*p*' values computed for each feature corresponding to each sub band for oscillatory and impulsive transients, respectively. It can be observed from the results presented in Table 2.2 and Table 2.3, that the extracted features from the envelope spectrum of each sub

Table 2.2 Variation of extracted features (mean ± standard deviation) with '*p*' values for oscillatory transient

Envelope corresponding to each Sub-band	**Standard Deviation**	**Mean**	**Energy**	**Max**	**'*p*' values**
E_1	0.005 (±0.0006)	0.0008 (±0.0001)	0.024 (±0.002)	0.119 (±0.00003)	4.33×10^{-17}
E_2	0.0087 (±0.0009)	0.002 (±0.0009)	0.014 (±0.003)	0.073 (±0.005)	5.69×10^{-13}
E_3	0.024 (±0.007)	0.006 (±0.002)	0.144 (±0.062)	0.162 (±0.021)	5.80×10^{-11}
E_4	0.029 (±0.009)	0.009 (±0.002)	0.215 (±0.129)	0.197 (±0.055)	4.49×10^{-11}

Table 2.3 Variation of extracted features (mean ± standard deviation) with '*p*' values for impulsive transient

Envelope corresponding to each Sub-band	**Standard Deviation**	**Mean**	**Energy**	**Max**	**'*p*' values**
E_1	0.035 (±0.005)	0.004 (±0.0008)	1.143 (±0.338)	0.849 (±0.112)	2.43×10^{-14}
E_2	0.031 (±0.013)	0.003 (±0.001)	0.769 (±0.693)	0.598 (±0.288)	7.95×10^{-17}
E_3	0.029 (±0.016)	0.004 (±0.002)	0.603 (±0.713)	0.452 (±0.278)	3.48×10^{-15}
E_4	0.023 (±0.009)	0.006 (±0.002)	0.218 (±0.181)	0.244 (±0.117)	8.65×10^{-18}

band for both types of transient signals are significantly different from each other. Besides, from the results of the ANOVA test, it is evident that the selected features have a significant discrimination capability between two classes with '*p*' value < 0.0001, and henceforth can be used as inputs to the classifier for the classification of power system transients.

2.3.4 Support vector machines

Support Vector machines is a very popular machine learning algorithm which has been implemented by researchers in various fields for solving classification problems. SVM is proposed to solve a binary classification problem using the principle of structural risk minimization. Details of SVM can be found in [14]. Here, a brief description of the classifier is given below.

An SVM aims to classify sample points belonging to two different classes by finding an optimum hyperplane which maximizes the margin i.e. separation between the data points with the nearest data points better known as support vectors. Nonlinear SVMs can map the training samples to a high dimensional feature space with the help of several mapping functions known as kernel functions. There are several kernel functions present in an SVM like linear, polynomial, RBF etc. In the present work, initially, the performance is evaluated using all kernel functions of SVM, and it has been observed that RBF kernel yields better performance compared to other kernel functions, based on which the classification accuracies are reported in this work. Moreover, since the present problem is a simple binary classification problem, hence, SVM has been used in the present work.

2.3.5 Performance analysis

The performance of the proposed method based on extracted features from the envelope spectrum from each frequency sub bands and employing SVM classifier have been analyzed in this section. Since, four statistical features are extracted from the first four frequency sub bands, hence the size of the input feature vector is 16×150.The performance of the present work is being assessed in terms of the following statistical testing parameters which are given in equations (2.4) -(2.6). In the following equations, the true positives, true negatives, false positives and false negatives are computed from the

confusion matrix for the classification of power system transient signals. In the present study 150 signals belonging to either class of transients i.e. oscillatory or

Table 2.4 Performance analysis using all features for different training testing ratio

Training data (%)	Testing data (%)	Accuracy (%)	Sensitivity (%)	Specificity (%)
70	30	100	100	100
60	40	100	100	100
50	50	99.1	100	98.8
40	60	98.5	98.7	97.8

impulsive transients have been generated. Out of 150 signals, at first 40% of the signals are selected randomly to be used for training and the rest of 60% for testing purpose. Next the training and the testing ratio has been varied and the performance of the classifier has been evaluated for each case. The performance of the SVM classifier for classification of different power system transients has been reported in Table 2.3.

$$Accuracy = \frac{TruePostive+TrueNegative}{TrueNegative+FalseNegative+TruePositive+FalsePositive} \times 100 \quad (2.4)$$

$$Sensitivity = \frac{TruePositive}{TruePositive+FalseNegative} \times 100 \quad (2.5)$$

$$Specificity = \frac{TrueNegative}{TrueNegative+FalsePositive} \times 100 \quad (2.6)$$

From the results presented in Table 2.4, it can be observed that the classification accuracy of 100% is obtained when the ratio of training data to the testing data is 70:30. Besides classification accuracy, 100% sensitivity and specificity is also obtained in classification of different type of transient signals.Further, it can be observed from Table 2.4, the classification accuracy is found to decrease with the decrease in training to testing data ratio. The maximum reported classification accuracy is 98.5% when the training to testing data ratio is 40:60. However, the classification accuracy achieved in the present work using statistical features derived from DWT based envelope

and SVM classifier is reasonably high, even when the training to testing data ratio is less than 1, which further indicates that the efficacy of the proposed method.

2.3.6 Effect of noise

The performance of the SVM classifier in presence of background noise has been estimated in this section. In real life power systems, signals often get corrupted with noise and interference from the mains. The detection system should therefore be robust against noise. To emulate background noise, white Gaussian noise of different signal to noise ratios starting from 35 dB to 5dB have been mixed with different transient signals. Table 2.5 report the performance of SVM classifier in presence of different noise levels. It can be observed from Table 2.5, that the maximum classification accuracy of 100 % is obtained when the SNR is 35dB. The performance of SVM classifier is found to degrade with the increase in noise level yielding a maximum classification accuracy of 94.5%, in presence of background noise as low as 5 dB, which clearly indicates the robustness of the proposed method.

Table 2.5 Variation of classification accuracy with SNR (dB)

SNR (dB)	**Classification Accuracy (%)**
35	100
25	98.4
15	96.2
5	94.5

2.4 Conclusions

In the present work, a novel method based on DWT based envelope analysis has been proposed for automated detection and classification of power system transients. Signals representing two very common and frequently occurring power system transients namely oscillatory transient and impulsive transient are at first decomposed using DWT into set of different frequency sub bands. Then, by applying HT on the first four decomposed sub bands, the envelope spectrum corresponding to each subbands is obtained by taking the absolute value of the analytic frequency sub bands. From the envelope

spectrum, four set of distinct statistical features have been obtained. The statistical analysis of the extracted features has been done using one way ANOVA to test the discriminative probability of the selected features between different classes. It has been observed that 100% accuracy is obtained in classifying different transient disturbances using the proposed set of statistical features and SVM classifier. Besides, the performance of the proposed method is found to be reasonably satisfactory, when evaluated in the presence of different background noise levels. Hence, it can be inferred that that the proposed method of DWT-based envelope analysis for detection of power system transients can be implemented in real life power transmission and distribution systems for monitoring of various transient disturbances.

References

[1] A. Greenwood, Electrical Transients in Power Systems, 2nd edition John Wiley & Sons,1991.

[2] P. L. Mao, R.K. Agarwal, "A novel approach to the classification of the transient phenomena in power transformers using combined wavelet transform and neural network", IEEE Trans. Power Delivery, vol.16, no.4, pp. 654–660, 2001.

[3] M. A. Beg, M. K. Khedkar, S.R. Paraskar and G.M. Dhole, "Feed-Forward Artificial Neural Network-Discrete Wavelet Transform Approach to Classify Power System Transients", Electric Power Components and Systems, vol.41, No. 6, pp.586-604, 2013.

[4] J.Liu, P. Pillay, and P. Reibeiro, "Wavelet analysis of power systems transients using scalograms and multiresolution analysis," Elect. Power Compon. Syst., Vol. 27, No. 12, pp. 1331–1341, November 1999.

[5] S. Chakraborty, A. Chatterjee, and S. K. Goswami, "A dual tree complex wavelet transform based approach for recognition of power system transients", Expert Systems, Vol.32, No.1, pp. 132-140, 2015.

[6] S. Chakraborty, A. Chatterjee, and S. K. Goswami, "A sparse representation-based approach for recognition of power system transients," Engineering Applications of Artificial Intelligence, vol. 30, pp. 137-144, 2014.

[7] M. Li, W. Chen and T. Zhang, "Classification of epilepsy EEG signals using DWT-based envelope analysis and neural network ensemble", Biomedical Signal Processing and Control, vol. 31, pp. 357-365, 2017.

[8] P. Nguyen, M. Kang, J.M. Kim, B. Ahn, J. Ha and B. Choi, "Robust condition monitoring of rolling element bearings using de-noising and envelope analysis with signal decomposition techniques", Expert Syst. Appl. vol.42, no.22, pp.9024–9032, 2015.

[9] S. Chatterjee, A. Banik, S. Dalai and B. Chatterjee, "Identification of Salt and Salinity Level of 11kV Contaminated Porcelain Disc Insulator using STD-MRA Analysis of Leakage Current," Proceedings of 2nd IEEE International Conference on Condition Assessment Techniques in Electrical Systems (CATCON), Bengaluru, Karnataka, India, 2015.

[10] T. Jayasree, D. Devaraj and R. Sukanesh, "Power quality disturbance classification using Hilbert transform and RBF networks," Neurocomputing, Vol. 73, No. 7–9, pp. 1451–1456, 2010.

[11] IEEE, "Recommended practice for monitoring electric power quality," IEEE 1159, 1995.

[12] R. Kumar, B. Singh, D.T. Shahani, Recognition of Single-stage and Multiple Power Quality Events Using Hilbert–Huang Transform and Probabilistic Neural Network, Electric Power Components and Systems, vol.43, No.6, pp.607-619, 2015.

[13] U.R. Acharya, E.Y.K.Ng, G. Swapna and Y.S.L Michelle, "Classification of normal, neuropathic, and myopathic electromyography signals using nonlinear dynamics method', Journal of Medical Imaging and Health Informatics, Vol. 1, No. 4, pp.375–380,2011.

[14] V. N. Vapnik, The Nature of Statistical Learning Theory, Springer, ISBN:0-387-94559-8, 2000.

Chapter 3

Power Quality Recognition in Noisy Environment Employing Deep Feature Extraction from Cross Stockwell Spectrum Time-Frequency Images

3.1 Introduction

Electric power utilities all over the world are concerned with the quality of electric power since it plays a vital role in maintaining the reliability of transmission and distribution networks [1]. In this context, monitoring of power quality (PQ) at regular intervals is important so that the voltage waveforms do not deviate significantly from pure sinusoid. However, due to operations such as capacitor switching, faults, lighting strike, non-linear load switching etc. the voltage waveforms get seriously distorted [2]. Recently, with the integration of renewable energy sources into the grid using power electronic devices, voltage waveforms most often tend to become non-sinusoidal in nature [3]. These high frequency and distorted waveforms may endanger the life of costly power equipment thereby hindering the smooth operation of power system network. Thus, accurate and fast detection of power quality is important so that appropriate preventive measures can be taken to prevent pre-mature failure of the power equipment.

In this context, researchers have proposed several signal processing and machine learning algorithms for automated detection of PQ signals. Detection and classification of PQ signals using fluctuations of amplitude and decision tree (DT) algorithm has been reported in [4]. Since most of the PQ signals are nonstationary in nature, many signal processing techniques have been proposed for analysis of PQ signal in joint time-frequency (T-F) plane

[5]. Application of discrete wavelet transform (DWT) and wavelet networks for classification of PQ signals have been reported in [6]. Detection and classification of PQ signals using curvelet transform and optimized extreme learning machine has been reported in [7]. Classification of PQ signals using wavelet packet transform and multiclass support vector machines have been reported in [8]. Application of tunable Q-factor wavelet transform and dual multiclass SVM for classification of PQ signals have been reported in [9]. In [10], empirical wavelet transform has been used to classify single and multiple PQ disturbances. In [11], an adaptive window-based fast generalized S-transform has been proposed for analysis of simulated as well as real-time PQ events. Application of hybrid model employing Stockwell transform (ST) and dynamics for classification of PQ events have been reported in [12]. In [13], classification of PQ signals using S-transform and modular neural network has been reported. Application of Stockwell transform (ST) and hidden Markov model for classification of PQ events have been reported in [14]. Thus, it is imperative that ST is a popular signal processing technique mainly used for analysis of PQ signals in joint time-frequency (T-F) plane. The ST spectrogram i.e. T-F plot indicates the variation in instantaneous frequency of a non-stationary signal which can be used to discriminate various types of PQ signals.

Compared to continuous wavelet transform (CWT), ST offers certain advantages. ST is proposed as a phase corrected version of CWT. Thus, ST can preserve instantaneous phase characteristics of the signal [15]. Moreover, the performance of ST does not depend on the selection of the mother wavelet [16]. Considering the aforesaid advantages, various versions of ST like, modified Stockwell transform (MST) [17], hyperbolic Stockwell (HST) [18], fast ST (FST) [19], discrete orthogonal ST (DOST) [20] etc. have been successfully implemented for analysis and feature extraction from PQ signals. Although different versions of ST have been successfully implemented for PQ signal analysis, yet one limitation of the ST based T-F analysis is that the spectrogram images obtained using ST becomes noisy especially when SNR of the input signal is low. This makes it extremely difficult to discern between single and multiple power quality signals based on the information obtained from conventional ST spectrogram. One way to improve the noisy spectrum is to optimize the Gaussian window parameters

of ST [15]. However, the aforesaid technique is computationally complex, and the performance depends on the type of optimization algorithm used. Considering the aforesaid issue, in this work, we propose cross Stockwell transform (XST)-a much simpler modification of ST which can improve the anti-noise performance of ST significantly.

In this chapter, XST is used to analyze single and multiple PQ signals. A distinct advantage of cross spectrum analysis is that it can eliminate the effect of random and uncorrelated noise present in any two cross-correlated signals i.e. if two signals are contaminated with random uncorrelated noise, then the effect of that noise will not be reflected in the cross-correlogram as cross correlation coefficient value for random uncorrelated noise is very small [21]. This eliminates the need of additional denoising of PQ signals in the data-pre-processing stage. Also, real life noisy PQ signals with low SNR can be accurately distinguished. Moreover, as reported in [22], cross spectrum analysis points to those regions in the T-F plane where two signals have highest common power in T-F plane [23]. Thus, XST has better noise rejection capability in T-F plane compared to ST. Considering the advantages of cross-spectrum analysis, XST is proposed in this work for analysis of PQ signals in T-F plane.

In this chapter, single as well as multiple PQ signals representing various transient events are generated using standard mathematical models as described in [24]. After generation of PQ signals, they were transformed into T-F frame using XST. The T-F images represent RGB color images of the transformed PQ signals. Next, instead of manual feature extraction from the T-F images, deep learning was employed for automated feature extraction from T-F images. The advantage of deep learning-based feature extraction is that it is fully automated compared to manual feature extraction method which is unsophisticated and tedious. In this study, convolutional neural network (CNN)-a state of the art deep learning model is used for automated deep feature extraction from T-F images of PQ signals obtained using XST. The outline of the proposed PQ detection model is shown in Fig. 3.1.

To the best of the authors' knowledge, following are the original contributions of the present chapter:

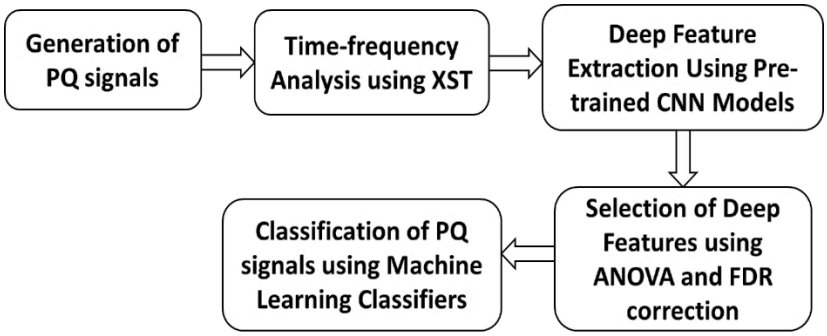

Fig. 3.1 Illustration of the flowchart of the proposed method

(i) Cross Stockwell transform (XST) based novel time-frequency (T-F) analysis of PQ signals is proposed in this work. The cross spectrum is done to improve the noise robustness of T-F images so that classification of single as well as multiple PQ signals can be done accurately in presence of noise.

(ii) Four benchmark deep neural network architectures have been trained for extraction of deep features from cross spectrum images. To reduce training time, a transfer learning strategy has been employed here. The extracted deep features were further subjected to feature selection using one-way analysis of variance (ANOVA) and false discovery rate (FDR) correction.

(iii) Three machine-learning classifiers have been used to classify the PQ signals based on extracted deep features. Extensive studies have been carried out by varying noise-level, fundamental frequency, train-test ratio etc. and by comparing with other T-F methods.

(iv) Finally, the method has been validated on real-life PQ data to verify the practicability of the proposed method.

3.2 Generation of synthetic PQ signals

In this chapter, synthetic PQ signals were generated using the formulae prescribed in IEEE std. 1159-2009. Detailed description of PQ signals is given in Table 3.1. The mathematical formulae used to generate the signals are reported in Appendix in Table A.1 [7, 24]. The synthetic PQ signals were generated using MATLAB 2020 a. Total 22 classes of PQ signals were generated and for each class of PQ signal, 500 signals were generated. To emulate real-life PQ signals, white Gaussian noise of varying SNR from 10 dB to 30 dB. The generated PQ signals are described in Table 3.1. It is to be mentioned here that the generated PQ signals consist of both single as well as multiple PQ events since occurrence of both are very common in power system network. In addition to synthetic signals, several real-life PQ signals were also procured, and the proposed methodology has also been validated on real-life PQ signals to validate the practicability of the proposed PQ detection scheme.

3.3 Methodology

3.3.1 Brief theory of Stockwell transform

Stockwell Transform (ST) was proposed by R.G. Stockwell [25] to study non-stationary geophysical signals. Stockwell introduced ST as the "phase corrected" adaptation of the Continuous Wavelet Transform (CWT) that retains the absolute phase information of the signal. In general, the ST can be seen as a fusion of Gabor transform and CWT. It uses a Gaussian frequency localization window whose width varies in proportion to frequency, thus providing a time-frequency representation with frequency dependent resolution. The basic definition of ST of a signal $h(t)$ is given by [25]:

$$S(\tau, f) = \int_{-\infty}^{\infty} h(t) g(\tau - t) e^{-j2\pi f t} dt \tag{3.1}$$

where τ and f denote the time instant of spectral localization and Fourier frequency, respectively and $g(t)$ is the Gaussian window function. The

Table 3.1: Generated PQ signals

Signal identifier	**PQ signal type**	**Type of PQ signals**
S_1	Sine + noise	Single
S_2	Harmonics + noise	Single
S_3	Sag + noise	Single
S_4	Swell + noise	Single
S_5	Flicker + noise	Single
S_6	Transient + noise	Single
S_7	Interruption + noise	Single
S_8	Notch + noise	Single
S_9	Harmonics + Sag + noise	Multiple
S_{10}	Harmonics + Swell + noise	Multiple
S_{11}	Harmonics + Flicker + noise	Multiple
S_{12}	Harmonics + Interruption + noise	Multiple
S_{13}	Harmonics + Transient + noise	Multiple
S_{14}	Sag + Flicker + noise	Multiple
S_{15}	Swell + Flicker + noise	Multiple
S_{16}	Sag +Transient + noise	Multiple
S_{17}	Swell +Transient + noise	Multiple
S_{18}	Transient + Interruption + noise	Multiple
S_{19}	Harmonics + Interruption + noise	Multiple
S_{20}	Sine + Harmonics+ noise	Multiple
S_{21}	Sine + Interruption+ noise	Multiple
S_{22}	Sine +Transients + Harmonics + noise	Multiple

Gaussian window as a function of frequency (f) and time (t) is defined as:

$$g(t,\sigma) = \frac{|f|}{\sqrt{2\pi}} e^{-\frac{t^2 f^2}{2}} \tag{3.2}$$

The ST can thus be defined as:

$$S(\tau,f) = \int_{-\infty}^{\infty} h(t) \frac{|f|}{\sqrt{2\pi}} e^{-\frac{(\tau-t)^2 f^2}{2}} e^{-i2\pi f t} dt \tag{3.3}$$

Sometimes for ease of analysis and to take advantage of the FFT algorithm already available in programming languages, the S-Transform is presented as operations on the Fourier spectrum $H(f)$ of the time series $h(t)$ as:

$$S(\tau, f) = \int_{-\infty}^{\infty} H(\alpha + f) G(\alpha, f) e^{i2\pi\alpha\tau} d\alpha \;\; ; \; f \neq 0$$

$$S(\tau, f) = \int_{-\infty}^{\infty} H(\alpha + f) e^{-\frac{2\pi^2\alpha^2}{f^2}} e^{i2\pi\alpha\tau} d\alpha \;\; ; \; f \neq 0$$

$$S(\tau, f) = \frac{1}{T} \int_{-\infty}^{\infty} h(t) dt \; ; \; f = 0 \tag{3.4}$$

3.3.2 Brief theory of Cross Stockwell transform

The performance of ST (mentioned earlier section) can be further improved if it can be used to find the degree of correlation between two-time series in both time scale and time-frequency plane. Since ST localizes spectral elements in time, the cross correlation of two spatially separated signals should provide phase synchrony information. The proposed cross S-Transform (XST) uses this property to perform cross spectral analysis on time domain signals. The XST between two-time series $h(t)$ and $y(t)$ is defined as:

$$XST(\tau, f) = ST_h(\tau, f) \times \{ST_y(\tau, f)\}^* \tag{3.5}$$

Where,$\{ST_h(\tau, f)\}$and$\{ST_y(\tau, f)\}$ indicates the S-transform of signals $h(t)$ and $y(t)$, respectively and * denotes the complex conjugate operation. The phase of XST is given by:

$$arg(XST) = \varphi_h(\tau, f) - \varphi_y(\tau, f) \tag{3.6}$$

Where, $\varphi_h(\tau, f)$ and $\varphi_y(\tau, f)$ are the respective phases of $h(t)$ and $y(t)$ with respect to a reference frame. The XST operation yields a complex matrix, the

magnitude of which is known as the cross Stockwell spectrum which gives localization of different frequency components at different instants in a T-F image plot. The steps to obtain the XST for a given time series $h(t)$ and *y*(*t*) are given in the following pseudocode as:

Pseudocode of XST
Step 1: *Find* $H(\alpha)$, *by applying FFT to* $h(t)$ $$h(t) \xrightarrow{FFT} H(\alpha)$$
Step 2: *Find* $G(\alpha, f)$, *by applying FFT to* $g(t, \sigma)$ $$g(t, \sigma) \xrightarrow{fft} G(\alpha, f)$$
Step 3: *Shift* $H(\alpha)$ *to* $H(\alpha + f)$
Step 4: *Multiply* $G(\alpha, f)$ *with the shifted* $H(\alpha)$
Step 5: *Take the inverse FFT of Step 4 to obtain* $ST_h(\tau, f)$
Step 6: *Compute XST two functions h(t) and y(t) by* $ST_h(\tau, f) \times \{ST_y(\tau, f)\}^*$

3.3.3 Convolutional Neural Network

Convolutional Neural Network (CNN) belongs to the family of deep neural networks which has been extensively applied for object detection as well as classification of images [26-27]. When compared against other different feed-forward deep learning (DL) models such as artificial neural network (ANN), CNN boasts the advantage of its end-to-end learning architecture which is particularly suitable for automated feature extraction and classification purpose. Usually, the structure of a CNN consists of three parts: (i) input layer (ii) hidden layers in the middle and finally an (iii) output layer. The hidden network layers consist of several convolution layers, followed by pooling layers, fully connected layers etc. Being sequentially embedded to each other, these deep operating layers extract high-level abstract features from the image inputs using the principle of regularized multi-layer perceptions [27]. Brief description of the hidden layers of CNN is presented below:

1) Convolution Layer

Convolution layers are the basic building blocks of a CNN module which are used to produce the initial high-dimensional feature maps from image inputs. Generally, convolution blocks consist of fixed number of filters, which are also known as kernel functions. The main concept behind the operation of a convolution block is local receptive fields and the shared weights and biases between its hidden units. In this way, instead of processing the entire image, the convolution block recognizes and extracts significant feature information from only a small, localized region of the image using the filters or the kernel functions. Using forward propagation, these filters or the kernels are then convolved transversely around the width and height of the entire input image to obtain the high-dimensional feature data. Mathematically, the 2-D output of the convolution operation on a signal of dimensions (a, b) is represented as:

$$(S * T)(s,t) = \sum_{m,n} S(a,b)\, T(s+a, t+b) \tag{3.7}$$

To help with the convolution procedure, a series of pixel values namely stride (q) is incorporated to tune the movement of the kernel functions. In addition to that, to maintain uniformity in detecting the same local features throughout the whole image, the weights and biases of convolution blocks are also shared between different deep operating layers. This process of sharing information and connecting the sequential convolution blocks reduces the number of hidden parameters utilized by the CNN module which in turn reduces the training difficulty of the network. Another important parameter of the convolution block is 'zero padding' (z) which regulates the size of the input image at every level of the convolution operation. For any input image having dimensions of $P_i \times Q_i \times R_i$, where the width, height and number of input channels are represented by P_i, Q_i and R_i, respectively, the output volume denoted by $P_o \times Q_o \times R_o$ for using N_o number of filters with each of size *'$r \times r$'* is represented as:

$$P_o = \frac{P_i - r + 2z}{q} + 1 \tag{3.8}$$

$$Q_o = \frac{Q_i - r + 2z}{q} + 1 \quad (3.9)$$

Apart from this, several non-saturated activation functions such as hyperbolic tangent functions (tanh), rectified linear unit (ReLU), sigmoid etc. are also incorporated in the convolution layers to introduce no-linearity. Activation functions are a significant part of the forward propagation design of the hierarchical CNN structure, operation of which can be denoted as:

$$B_i = x(A_i) \quad (3.10)$$

Where, $A_i$and $B_i$are the feature maps produced from the i^{th} convolution operation, before and after introducing the non-linear activation function denoted by$x$ (.), respectively.

2) Pooling Layer

The pooling layers are merged in succession with the convolution layers in the hierarchical structure of a CNN model. Pooling layers serve the purpose of dimension reduction by applying non-linear down sampling on the previously obtained high dimensional feature output from the convolution layers and helps to avoid the issue of over-fitting as well. Usually, a series of non-intersecting rectangular sub-regions are formed by the obtained feature maps and from which, significant feature information is extracted with the help of several pooling operators such as global pooling, average pooling, maximum pooling etc. In this way, the spatial volume of the feature output is reduced and at the same time, the computational time is also shortened by reducing the number of network parameters. Mathematically, a pooling operation can be represented as:

$$m_{x,y,z} = pool_{(a,b)\in S_{x,y}}\left(n_{a,b,z}\right) \quad (3.11)$$

Where, $m_{x,y,z}$ represent the k^{th} feature map after the corresponding $pool(.)$ operation. Here, $S_{x,y}$denotes the pooling receptive region around the nodes at location (x, y) and $(n_{a,b,z})$ denotes the nodes at location (a, b).

3) Fully Connected Layer

Fully connected (FC) layers are placed at the end of the CNN modules which serves the purpose of flattening the 2-dimensional feature outputs from the previous convolution and pooling layers into 1-dimensional interpretable data for the classification and regression tasks. Along with that, to contend with the issue of overfitting in training of the CNN networks, dropout regularization factor is often introduced after fully connected layers. The dropout function helps to mitigate the issue of overfitting in training of the CNN modules where the weight of half of the hidden layer nodes are dropped randomly at each training step. In this way, the appearance of one neuron of a particular hidden layer does not block the activity of another neuron of the same hidden layer which alleviates the situation of two nodes of a same hidden layer appearing at the same time and hence, improves the generalization ability of the network. For classification tasks, the output layer of a CNN network utilizes softmax activation for assigning class labels to the feature attributes and predicting categories. In addition to that, to ensure reliable classification performance, it is necessary to reduce cross entropy losses, which indicates the differences between the actual and the predicted model. The formula to determine the cross-entropy losses is given by:

$$Z(z,p) = -\sum_i z_i \, log(\, p_i) \tag{3.12}$$

Here, p denotes the probability score from the output of the FC layer and z is the predicted label which can assume values 0 or 1. Here back propagation has been used to compute the cross-entropy losses. Also, using stochastic gradient descent rule, the weights and biases of the previous operating layers have been adjusted. In existing literature, several state-of-the-art CNN architectures were reported for feature extraction and classification purpose by employing different configuration of the hidden operating layers. In this study, we explore four of such classical CNN architectures using the transfer learning (TL) strategy to extract deep neural features. A brief overview of TL strategy is given below.

3.3.4 Transfer learning

Transfer learning (TL) signifies the process of streamlining information from one field to another. In context of deep learning, TL depicts the application of a finely tuned CNN architecture for feature extraction and classification purpose, which was trained earlier on a different data archive. It should be mentioned here that in practice, training a CNN architecture using TL strategy is more expedient than training it from scratch. The pre-trained CNN architecture consists of weights and biases, which characterize the features learned from the previous datasets and which again in fact can be transferred to different datasets [28]. Using TL, the last couple of hidden operating layers in the CNN architecture namely fully connected layers and the classification layers can be dissolved, and the rest of the CNN architecture can be trained on different datasets. Hence, using TL technique, a pre-trained CNN model can operate on a fresh classification task by fine-tuning its last couple hidden operating layers. In this study, TL strategy is applied to train four pre-trained CNN architectures namely AlexNet, VGGNet16, ResNet50 and GoogleNet for the purpose of automated feature extraction. A brief description of the employed pre-trained CNN models is given below, highlighting their different configurable operating layers and parameters.

3.3.5 Pre-trained CNN models

1) AlexNet

The first CNN architecture used in this study is an efficient deep learning framework namely AlexNet which has been the winner of ImageNet Large-Scale Visual Recognition Challenge (ILSVRC), 2012 [29]. The AlexNet model was trained on the ILSVRC database and contains roughly 60 million network parameters. The basic structure of AlexNet is shown in Fig. 3.2. AlexNet consists of overall 8 network layers deep with 5 convolution blocks where, the first two convolution layers make use of 96 and 256 number of filters of sizes 11×11×3 and 48×5×5, respectively. Two max pooling layers, each having filter sizes 3×3, are connected to these convolution layers. The latter three convolution layers have 384, 384, and 256 numbers of filters having sizes of 256×3×3, 192×3×3 and 192×3×3, respectively. Another max-

pooling layer of filter size 3×3 is connected at the conjunction between the last convolution layer and the succeeding two fully connected layers, both of which contain 4096 number of neurons each. The AlexNet model incorporates the ReLU activation function in its convolution blocks and the dropout regularization technique in the final classification layers.

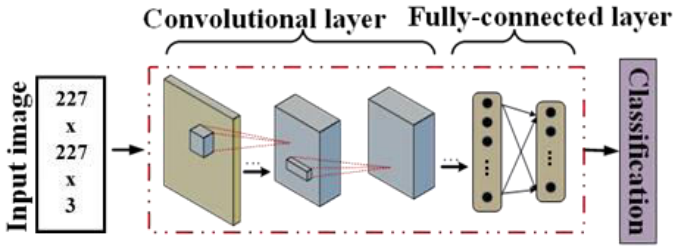

Fig. 3.2 Structure of AlexNet

2) VGGNet

VGGNet is a popular CNN architecture which was developed by the Oxford Visual Geometry Group (VGG) [30]. The structure of VGGNet is shown in Fig. 3.3. Like AlexNet model, VGGNet was also trained on the ILSVRC database, which contains over 1.2 million images of 1000 different class labels. This CNN algorithm has multiple deep variants ranging from 11 to 19 layers, out of which, we have utilized the 16 layers deep VGGNet16 model in this work. Like AlexNet, the overall VGGNet16 architecture also contains 5 convolution blocks with 3×3 convolution filters. The associated stride values are kept as 1 with filling size of 1. To reduce the spatial volume of the feature outputs, max-pooling layers of size 2×2 is used as handler in the VGGNet16 model with step length of 2. At the end of the last max-pooling layer, three fully connected layers with 4096 number of neurons are connected to integrate the deep features into the 1-D feature map. A softmax classification layer is attached at the end of the three fully connected layers for the classification purpose. The VGGNet16 architecture uses around 138 million network parameters in its deep hidden layers.

3) ResNet50

Residual networks or widely popular as ResNet is another efficient deep CNN architecture that has been proposed in [31]. The ResNet architecture incorporates a novel 'identity mapping' strategy in its hidden operating layer.

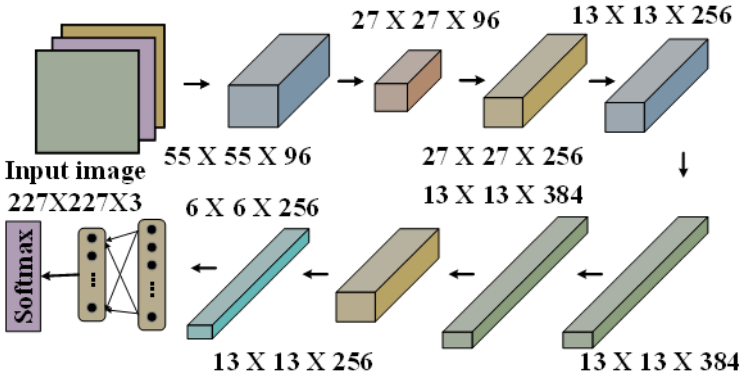

Fig. 3.3 Structure of VGGNet16

The problem of vanishing gradient is solved with the help of this identity mapping technique by providing an alternative shortcut path for the gradient to pass through. In addition, the identity mapping also helps the ResNet model to skip or bypass one or more than that weighted hidden layers if the current layers are not necessary as shown in Fig. 3.4. These skip connections aid in avoiding the possible issue of overfitting in extracting feature information from input data. It should be mentioned here that in this study, we have implemented the ResNet architecture which is 50 layers deep i.e. ResNet50 since it yielded the best performance among other ResNet models.

4) GoogleNet

GoogleNet is a widely used CNN model, which was the winner of ILSVRC, 2014 [32]. GoogleNet was trained on the ILSVRC database, which contains over 1.2 million images of 1000 different class labels. This CNN architecture implements an 'inception unit' that permits real-time processing of input data across different convolutional layers, which helps in increasing the depth of

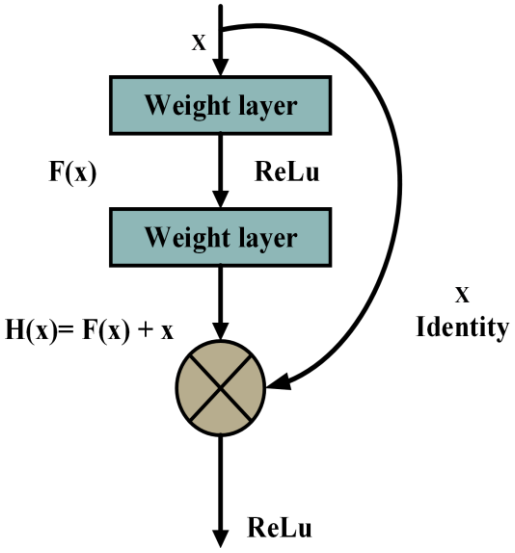

Fig. 3.4 Structure of a residual module

the architecture while eluding computation complexity. The inception units contain 2 convolutional layers, 4 convolution layers for dimension reduction and 1 max-pooling layer. GoogleNet consists of 9 such inception modules, 2 convolution layers, 1 average-pooling as well as 4 max-pooling layers and 1 classification layer with softmax activation. Interestingly, a global average-pooling layer is positioned at the bottom of the GoogleNet architecture in place of a fully connected layer to reduce the error rate. It implements ReLU activation units in the convolution layers and the dropout regularization strategy to escape overfitting in the classification layer. In this study, in order to extract deep neural features, the softmax classification layer was dissolved and the corresponding high dimensional feature vector was obtained as an output from the average-pooling layer. The structure of an inception module is shown in Fig. 3.5.

3.3.6 Machine Learning classifiers

In the present chapter, three well-known machine learning classifiers have been employed for classification of PQ signals using deep features extracted

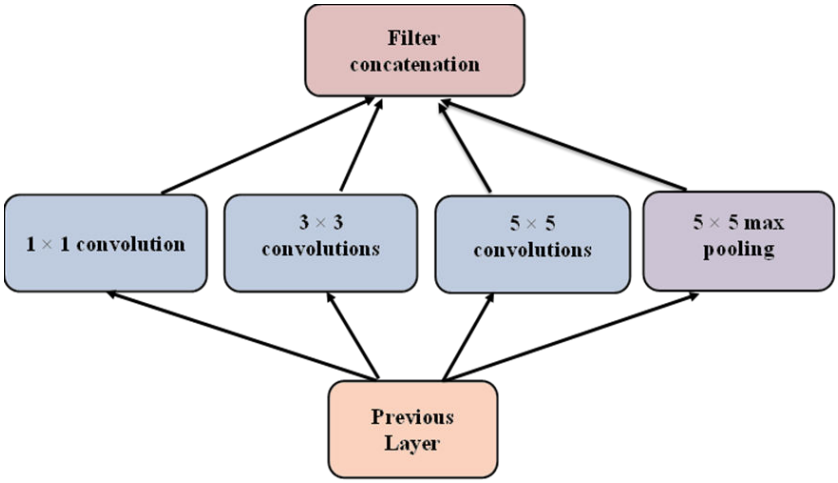

Fig. 3.5 Structure of an inception module

from pre-trained CNN models. The theoretical details of the employed ML classifiers are discussed below in brief.

1) Random Forest

Random forest (RF) is a well-known machine-learning algorithm, which consists of a group of standard decision tree classifiers. RF utilizes a novel bootstrap-bagging strategy to allocate training inputs for each of the decision tree classifiers. The number of the training inputs dispersed at the nodes of each tree classifier corresponds to square root times of the initial feature size [33]. Also, the RF classifier boasts the advantage of being robust against noise by random splitting of the training inputs between the nodes of three classifiers. The output of the RF classifier is decided by aggregating the decisions of all the tree classifiers, using a majority voting method. It is also to be mentioned here that in order to optimize the performance of the RF classifier, setting the number of decision tree classifiers is an important task. Therefore, to optimize the classification performance, the number of decision trees varied within a range of 50 to 150 and noticed that using 80 decision trees; the best classification results were obtained.

2) Support vector machines

Along with RF, another machine-learning algorithm, namely support vector machines (SVM) has been implemented in this work. Detailed description about the SVM classifier is reported in past studies [34]. SVM incorporates an optimum separating hyper-plane (OSH) to fit the input training data and the class margins between data inputs of different data labels is enhanced using the theory of structural risk minimization (SRM) [34]. Non-linear SVMs are used to map the training datasets from input space to higher dimensional feature space using kernel functions. In this work, we have used different kernel functions to determine the appropriate kernel function delivering highest classification accuracy. To determine the optimal width of the RBF kernel, the regularization parameter has been varied from 1 to 200 in steps of 0.1.

3) k-nearest neighbor (kNN)

In addition to RF and SVM, another well-known machine-learning classifier namely *k*-nearest neighbor (kNN) has been used in this study for classification of PQ signals. The kNN classifier is widely used in solving different classification problems since it is relatively simple to implement and robust towards ambiguous data samples. Based upon the recurrent class labels inside a certain dimensional cluster of training samples, kNN categorizes data labels based on majority voting technique [35]. Hence, selection of the two hyper-parameters of kNN is important to optimize the classification performance. The first one being distance parameter, which defines the class labels and the latter, is the selection of the *k*-value, which determines the dimension of the clusters being formed with training samples.

3.4 Results and Discussions

3.4.1 Analysis of PQ signals using XST

In this contribution, the PQ signals were initially transformed into time-frequency (T-F) domain using XST. For computation of cross spectrum, a sample PQ signal from each class is chosen as the reference. The cross

spectrum of the rest of the PQ signals for each class is done with their respective chosen reference signal. The single PQ signal (S_6, SNR=15dB) and corresponding time-frequency image obtained using ST and XST is depicted in Fig. 3.6 (a-c). In addition, a multiple PQ signal (S_{22}, SNR=15dB) and its corresponding T-F image obtained using XST and conventional ST is shown in Fig. 3.7 (a-c). It is evident from Fig. 3.6 (a-c) and Fig. 3.7 (a-c), that the resolution of images obtained using XST is better than the conventional ST i.e. the T-F images obtained using XST are less noisy compared to ST. As a consequence, different PQ signals can be clearly distinguished based in T-F plane using XST whereas, it is difficult to distinguish between single and multiple PQ signals from the conventional ST spectrum when the SNR is low. This is evident from Fig 3.6 (c) and Fig. 3.7 (c), where the T-F images for both single and multiple PQ signals look almost alike although they both represent different PQ signals. This inadvertently will lead to misclassification and poor detection accuracy. Thus, it is evident from the above analysis that XST proposed in this study is robust against noise which

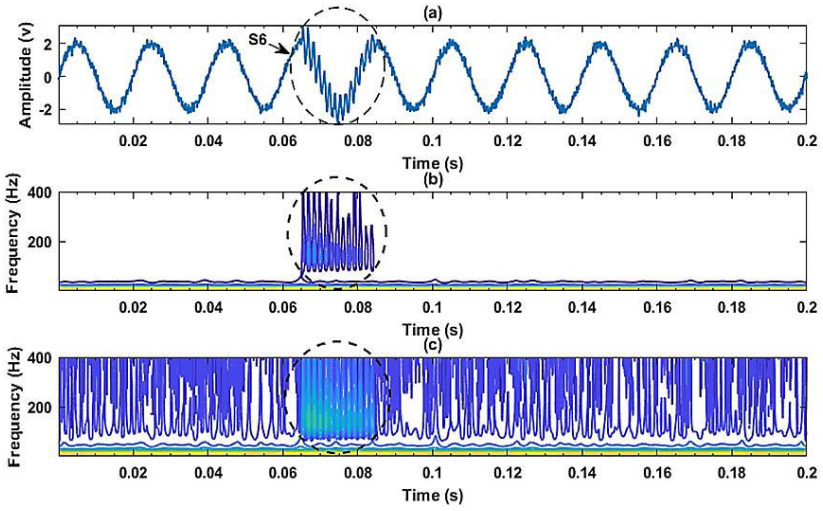

Fig. 3.6 Time domain PQ signal (a) S_6 and corresponding T-F images obtained using (b) XST (c) ST for SNR=15dB

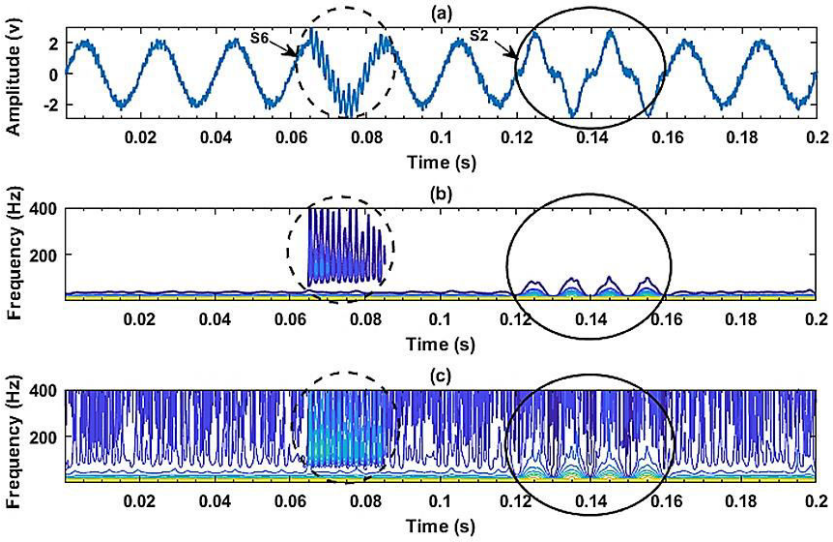

Fig. 3.7 Time domain PQ signal (a) S_{22} and corresponding T-F images obtained using (b) XST (c) ST for SNR=15 dB

can be used to classify PQ signals accurately compared to ST especially in a noisy environment. Also, it is evident from Fig. 3.6 (b) and Fig. 3.7 (b) that the T-F images of different PQ signals are different from each other. Thus, T-F images can be fed to deep neural networks for automated feature extraction.

3.4.2 Performance metrics

The T-F images obtained using XST were fed as inputs to four classical CNN architectures, from which deep features were extracted. It is to be mentioned here that in order to reduce the computational burden of the machine-learning classifiers in the subsequent classification stage, the extracted deep features were ranked according to their discriminative capability and only the top feature values having superior discriminative powers were selected in this study. For this purpose, we have used one-way analysis of variance (ANOVA) test to observe their respective discriminative powers. The ANOVA test essentially yields a probability density value, i.e., frequently

labeled as the '*p*-value', which signifies the probability of occurrence of any feature value between different classes of PQ signals. The discriminative capability of the features values is derived from the magnitude of the *p*-values. The lower magnitude of *p*-value corresponds to greater class separation of any feature value between different classes since *p*-values having lower magnitude indicates towards lower probability of the null hypothesis being rejected in the ANOVA test and vice-versa. Therefore, we have selected the p-values as a metric of distinguishability in this study. For measuring the discriminative powers of the extracted deep features, p-value having a threshold of 10^{-10} was selected in this work. In addition to the ANOVA analysis, the false discovery rate (FDR) correction test was also carried out to rule out the false positive cases in the following classification stage. Like the ANOVA analysis, a threshold value of 10^{-10} was again set for the FDR correction test. Finally, after performing the ANOVA analysis and FDR test, the top 50 highly correlated and statistically significant deep features from each deep learning network were selected as inputs to the machine-learning classifiers for classification of PQ signals. In this work, classification performance of the proposed method is assessed in terms of the following statistical parameters namely Accuracy, Recall and Specificity. These statistical parameters are calculated using the confusion matrix obtained for PQ classification using (3.13) -(3.15) as:

$$Accuracy(\%) = \left(\frac{TP+TN}{TN+FN+TP+FP}\right) \times 100 \tag{3.13}$$

$$Re\,c\,all(\%) = \left(\frac{TP}{TP+FN}\right) \times 100 \tag{3.14}$$

$$Specificity(\%) = \left(\frac{TN}{TN+FP}\right) \times 100 \tag{3.15}$$

In the abovementioned equations, the terms TP and TN correspond to the correctly classified scenarios for the respective classification problem, respectively. Similarly, FP and FN denote the corresponding falsely classified cases, respectively. It is important to mention here that in this work we have incorporated a 5-fold cross validation scheme to avoid the possible pitfall of overfitting in the classification stage. Through this scheme, the

feature inputs to the machine-learning classifiers were partitioned into the ratios of 4:1, where 4 parts of the feature data were used to train the classifiers and the single remaining part was used for validation purpose. In this way, out of 500 signals, machine learning classifiers were trained using the deep features extracted from 400 PQ signals, and the remaining 100 signals used to evaluate the performance. Apart from this, to ensure reliable classification performance, 10 consecutive iterations have been performed and finally mean along with standard deviation values have been computed, based on which the performance parameters have been reported in this work.

3.4.3 CNN training

Here, we have used the transfer learning (TL) method to train the CNN models for classification of PQ disturbances. TL symbolizes the transfer of knowledge from one field of interest to another. In reality, training a CNN network and updating the weights and biases network from scratch is lengthy task and at the same time the overfitting problem may degrade the training performance especially when the training data is limited. To overcome this problem, TL offers a unique solution through which, a CNN architecture which has been previously trained on a different but large dataset can be fine-tuned and hence can be used for a different classification problem. In a nutshell, TL allows transfer of feature mapping and embedding information of any previous source model (MS) to a new target model (MT) can be transferred by only fine-tuning the parameters of the previously trained network. It is seen that for any image classification task, the initial few convolution layers can extract common image features such as edges and curves, while the deeper layers are capable of mapping the abstract feature representations more effectively. Therefore, when TL is used for any classification task, the common practice is to tune the deeper layers so that they learn from the new dataset while the information obtained from the shallow layers can be transferred. Considering the abovementioned facts, TL strategy has been adopted in this study to extract deep features from XST images of PQ signals. It is to be mentioned here that to feed the PQ disturbance T-F images to the pre-trained CNN networks, the images were resized to the dimensions of 227×227×3 for the AlexNet model and 224×224×3 for the VGGNet16, ResNet50 and GoogleNet models,

respectively. In this study, for modification of CN models, we have used Keras library (Python) with TensorFlow running at the backend. In this work, a single fully connected layer has been retained for all the CNN models, and the number of output neurons has been set to eighteen, since the present work is an 18-class classification problem. Following the FC layer, a dropout unit is placed in series with softmax layer. The dropout rate is set to 0.5. The cross-entropy loss function is integrated inside the dropout layer. In addition to cross entropy function, this study also includes a momentum update factor of 90%. This aids in better converging of the network by taking inputs directly from the gradient of the loss function. In this study, the number of training epochs of the network has been regulated through an early stopping approach. Through this approach, the training procedure of the network is stopped if validation loss doesn't get reduced by 10^{-3} for 10 consecutive epochs. Here, the epoch weights showing minimum validation loss have been considered for evaluation. In the training phase of the CNN, a mini-batch size of 250 was chosen. The initial learning rate was set at 10^{-3}. Moreover, after every single training batch, the learning rate was reduced by a factor of 10^{-5}. Adam optimizer was utilized to scale the learning rate for each network weight. The complete classification framework was carried out using a workstation having Intel core i7, 2.2 GHz processor, with 16GB RAM and NVidia GTX 1650 graphic card.

3.4.4 Results of PQ classification

The classification performance of the proposed PQ detection framework is presented in this section. The obtained classification Accuracy, Recall and Specificity (obtained by taking mean of individual parameters from the confusion matrices) along with their standard deviation values are reported in Table 3.2 for respectively. From the classification results reported in Table 3.2, it can be observed that very high mean classification accuracies have been obtained for all the machine-learning classifiers which indicate that the proposed PQ detection scheme is highly efficient. From Table 3.2, it can also be observed that for all four deep networks, RF classifier delivered the highest classification performance for all four networks followed by the SVMand kNN classifiers. Among four deep neural networks, features extracted from ResNet50 deep learning delivered the best performance

Table 3.2 Classification performance of different classifiers

Deep Learning Network	**Classifier**	**Accuracy (mean ± std) (%)**	**Recall (mean ± std) (%)**	**Specificity (mean ± std) (%)**
AlexNet	RF	98.45 ± 0.25	98.29 ± 0.17	98.54 ± 0.16
	SVM-RBF (σ = 1.24)	97.29 ± 0.18	98.67 ± 0.08	98.91 ± 0.13
	kNN (k=5)	96.52 ± 0.22	97.89 ± 0.15	98.17 ± 0.10
VGGNet16	RF	98.10 ± 0.31	97.34 ± 0.17	96.25 ± 0.28
	SVM-Linear	97.79 ± 0.10	98.04 ± 0.38	97.20 ± 0.53
	kNN (k=3)	97.02 ± 0.24	95.24 ± 1.15	96.57 ± 0.50
ResNet50	RF	99.72 ± 0.16	100 ± 0.0	99.70 ± 0.12
	SVM-RBF (σ = 4.8)	98.79 ± 0.25	97.40 ± 1.04	97.45 ± 0.71
	kNN (k=7)	98.02 ± 0.12	96.21 ± 0.65	98.37 ± 0.51
GoogleNet	RF	98.65 ± 0.24	97.50 ± 0.14	98.28 ± 0.28
	SVM (polynomial index=3)	98.10 ± 0.16	98.47 ± 0.58	97.42 ± 0.73
	kNN (k=5)	97.82 ± 0.82	96.59 ± 1.20	97.27 1.04

among all three CNN models. The very high classification accuracies obtained in this work validate the efficacy of the proposed PQ detection model. It is to be mentioned here that the parameters of kNN and SVM yielding highest classification accuracies are indicated in parenthesis in Table 3.2. Moreover, the obtained standard deviation values are also observed to very small in magnitude which signifies that the proposed classification model has performed robustly. Therefore, it can be inferred that the performance of the proposed PQ disturbance detection model is overall satisfactory and hence, can be potentially implemented to develop an efficient PQ detection framework. For better visualization of the interclass classification accuracies, the confusion matrix showing the performance of

RF classifier achieved using deep features extracted from ResNet50 model is shown in appendix in Table A.2.

3.4.5 Comparison with different number of folds

In this section, further investigation has been carried out to detect the variation in classification performances by varying different folds (train-test ratio). Fig. 3.8 shows the variation in classification performances in terms of accuracy obtained by varying different number of folds. From Fig. 3.8, it can be observed that by increasing the number of folds, average accuracy can be increased for all classifiers, by performing multiple iterations. The best accuracy is achieved for 5-fold cross validation. In Fig. 3.8, classification performance of machine learning classifiers using deep features extracted from only ResNet50 are presented since it delivered better performance than other deep neural networks. So, the performance parameters reported in Table 3.2 are reported based on 5-fold cross validation.

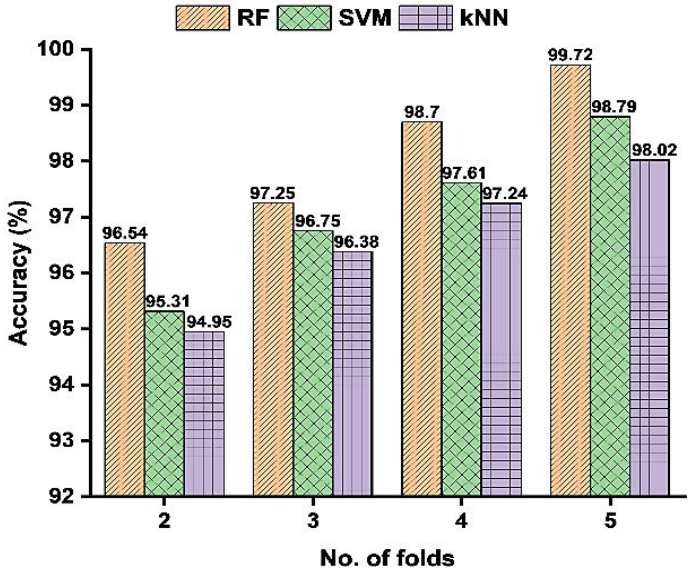

Fig. 3.8 Variation of classification accuracy with no of folds

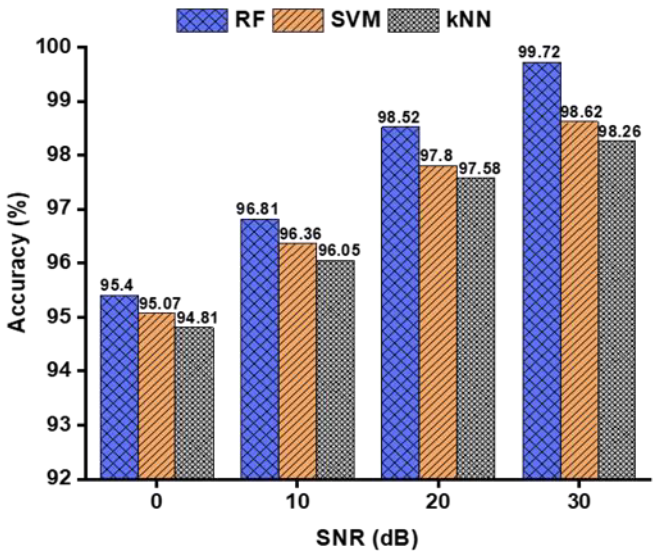

Fig. 3.9 Variation of classification accuracy with varying SNR (dB)

3.4.6 Effect of noise on classification performance

To validate the efficiency of the proposed PQ detection model, white Gaussian noise with different signal-to-noise ratios (SNR) ranging from 0-30 dB is mixed with the PQ signals. The variation of classification accuracy with SNR for RF classifier using features extracted from ResNet50 is shown in Fig. 3.9. From Fig. 3.9, slight degradation in the performance of is noticed with the decrease in SNR. Also, no significant improvement in accuracy is observed after SNR=30dB. However, it can also be observed even when the SNR value is as low as 0 dB, 95.4% detection accuracy is achieved for RF classifier. This is because the application of XST has resulted in better resolution of T-F images even in the presence of noise. In other words, application of cross spectrum has improved the noise robustness significantly. Therefore, it can be said that the proposed PQ disturbance detection scheme performs robustly in the presence of noise.

3.4.7 Effect of frequency variation on classification performance

The frequency of power grid can fluctuate over a limited range which can influence the PQ detection accuracy. To observe the effect of frequency on PQ classification, the fundamental frequency of the simulated PQ events varied from 48Hz-52Hz in steps of 0.5 Hz. For each case, the T-F images were obtained using XST and were fed to four deep networks for feature extraction and subsequent feature selection. Finally, the classification of T-F images was done using three machine learning classifiers. The variation in classification accuracies with frequency for three classifiers obtained using deep features extracted from `ResNet50 is shown in Fig. 3.10. It is imperative from Fig.3. 10 that the performance of different machine learning classifiers is almost consistent with the variation in frequency with very little fluctuations observed in performance parameters. Thus, it can be said that the performance of the proposed system is immune to the change in grid frequency fluctuations.

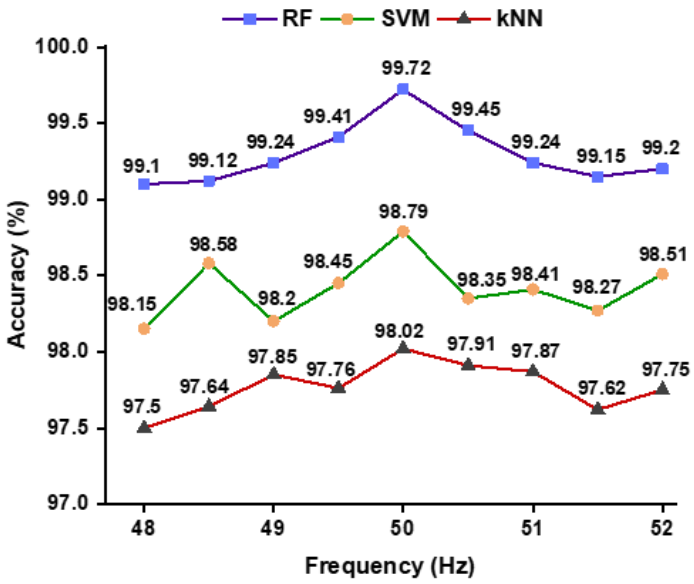

Fig. 3.10 Variation of classification accuracy with the change in frequency

3.4.8 Classification performance using other time-frequency methods

In Table3.3, the performance of the proposed XST based T-F analysis is compared with some state-of-the-art T-F methods like short time Fourier transform (STFT), continuous wavelet transform (CWT), and generalized Stockwell transform (ST). Using three well-known T-F analysis methods, the input PQ signals were converted to RGB images. For computing STFT, Hamming window with 75% overlap has been used. For computing CWT, Morlet wavelet function has been used. The RGB spectrogram images were subsequently fed to four pre-trained deep networks for feature extraction and subsequent classification. Here also, only performance of ResNet50 with RF classifier is shown, since it has delivered better results compared to other models. It can be observed from Table 3.3 that the performance of XST is better than the existing T-F methods. This improvement is due to the increased resolution of XST images in the T-F frame obtained due to cross spectrum analysis, which has resulted in better accuracy of PQ signals compared to existing T-F methods.

Table 3.3 Classification performance using other T-F methods

T-F analysis	**Accuracy (mean ± std) (%)**	**Recall (mean ± std) (%)**	**Specificity (mean ± std) (%)**
STFT	95.23 ± 0.75	94.01 ± 0.27	95.25 ± 0.36
CWT	96.51 ± 0.51	96.32 ± 0.13	95.69 ± 0.29
ST	97.25 ± 0.37	98.05 ± 0.32	96.40 ± 0.14
XST	99.56 ± 0.07	98.49 ± 0.34	98.26 ± 0.31

3.4.9 Computational Cost

The overall computation time of the proposed PQ signal detection framework is discussed in this section. The computation of XST of 18 PQ signals and subsequent deep feature extraction using AlexNet, VGGNet16, ResNet50 and GoogleNet required 542 seconds, 798 seconds, 640 seconds, and 700seconds, respectively. Classification of PQ signals using RF, SVM and kNNrequired

65.1 seconds, 57.8 seconds and 54.3 seconds, respectively. Although the classification time required for RF classifier is marginally higher than the SVM and kNN yet it delivered better results than the other two. The entire feature extraction and classification of PQ signals was done using MATLAB R2020a environment, Intel core i5 system, 2.5 GHz processor, with 8 GB RAM.

3.4.10 Validation on Real-life PQ signals

In this section, additional experiments have been carried out on real-life PQ signals to verify the practicability of the proposed method. For this purpose, real-life PQ signals were procured from several available online databases [36-38]. Fig. 3.11 shows a real-life sag PQ signal no 2911 [38] and its corresponding T-F image obtained using XST. Here also, it is observed that for a real-life PQ signal, the T-F image plot obtained using XST is less noisy than that of ST. In this context, it is to be mentioned here that for deep feature extraction from real-life PQ signals, ResNet50 is used since it delivered best performance among 4 deep networks. The performance of different machine learning classifiers in classifying real life PQ signals using features extracted from ResNet50 model is reported in Table 3.4. The parameters of machine learning classifiers are tuned using the methods as mentioned earlier. It can be observed from Table 3.4 that the performance of different machine algorithms in classifying real life PQ signals are reasonably satisfactory. The overall classification accuracy of 96.45% has been achieved which further indicates the practicability of the proposed PQ classification model.

3.4.11 Comparative study with existing literature

In Table 3.5, the performance of the proposed PQ detection framework is compared with the existing methods. It can be observed from the comparative study that the proposed framework returned comparable and even better performance than some of the existing state of the art methods. It can be observed from the comparative study that the proposed framework returned comparable and even better performance than some of the existing state-of-the-art methods. It can be observed from the comparative study that the proposed framework returned comparable and even better performance than

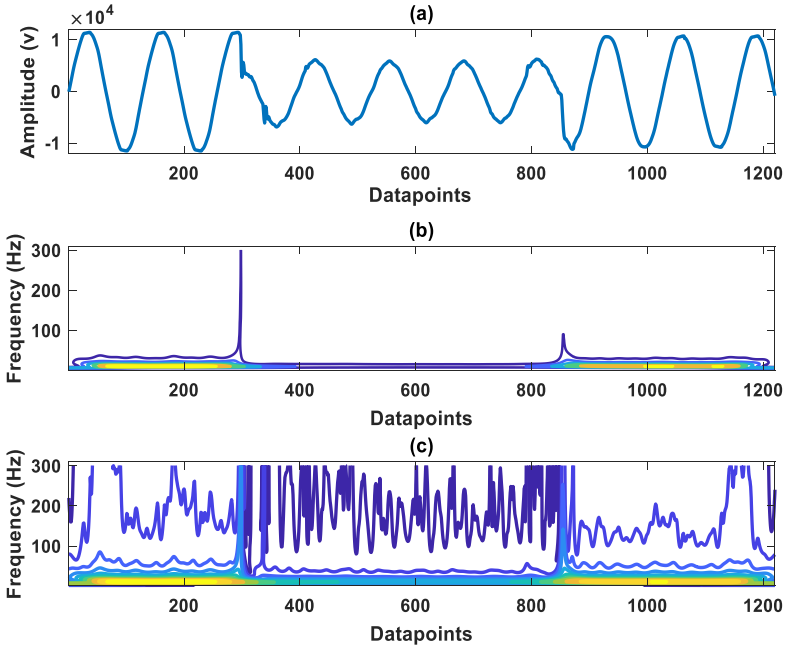

Fig. 3.11T-F image of (a) real life PQ signal obtained using (b) XST (c) ST

Table 3.4 Classification performance on real-life PQ signals

Classifier	**Accuracy (mean ± std) (%)**	**Recall (mean ± std) (%)**	**Specificity (mean ± std) (%)**
RF	96.45 ± 1.04	97.20 ± 0.83	95.10 ± 1.29
SVM-RBF (σ =2.6)	95.24 ± 1.40	96.42 ± 1.30	94.25 ± 1.80
kNN (k=5)	94.05 ± 1.05	95.50 ± 1.02	93.40 ± 2.04

most of the existing methods. Thus, the proposed method has definite edge over the existing methods in classification of synthetic as well as real PQ events. Moreover, compared to ST based methods [39-40], our proposed method is also more robust against noise.

Table 3.5 Comparison with existing methods

Reference	Number of PQ classes	Method	Accuracy (%)
[9]	14	TQWT + SVM	97.29
[39]	11	ST+ Probabilistic Neural Network (PNN)	97.40
[40]	12	ST+ Fuzzy expert system	99.20
[4]	11	Cross correlation + RST	97.10
[41]	10	EWT+ CNN	97.41
[7]	22	XWT+ SVM	99.09
[42]	13	Rule-based ST+DT	99.37
[43]	9	Undecimated wavelet transform (UWT) + CNN	99.5
[17]	13	MST+RF	99.61
[44]	9	Wigner Value Distribution + CNN	99.67
[45]	16	Multiresolution ST + DT	99.69
This work	**22 (synthetic)**	**XST+ResNet50+RF**	**99.72**
This work	**5 (Real-Life)**		**96.45**

3.5 Conclusions

In the present chapter, cross Stockwell transform aided deep learning framework for automated detection of PQ signals is proposed. The 1D PQ signals were transformed into 2D time-frequency images using XST. Four deep neural networks were trained for automated feature extraction from the T-F images of the transformed PQ signals. Finally, using ANOVA test and FDR correction, highly discriminative and statistically significant features were fed as inputs to three standard machine learning classifiers for PQ signal classification. In addition, tests have been carried out on real-life PQ data for practical verification. Investigations revealed that the proposed framework can classify PQ signals with very high accuracy. Among three deep neural networks, features extracted from ResNet50 model delivered best performance with RF classifier. Moreover, extensive analysis has been

carried out by varying different attributes of PQ signals which indicated that the performance of the proposed ResNet50 aided RF classifier is reasonably satisfactory for all cases. Finally, the proposed method has also been validated on real-life PQ signals for practical validation. It has been observed that the proposed model is capable of classifying the real-life PQ signals accurately even when the noise level is very low. Comparison with existing methods indicates that the performance of the proposed method is comparable and even better. Thus, it can be concluded the proposed framework can be used for accurate classification of PQ events in a noisy environment where conventional ST fails. Also, the proposed method is relatively simpler with no complex optimization involved. In future, the proposed model will be implemented in hardware using FPGA or low-cost micro-controller module for real-life PQ diagnosis.

References

[1] D. H. Chiam, K.H. Lim & K.H. Law, "LSTM power quality disturbance classification with wavelets and attention mechanism", Electr Eng, vol. 105, pp.259–266, 2023.

[2] S. Ekici, F. Ucar and B. Dandil, "Power quality event classification using optimized Bayesian convolutional neural networks", Electr Eng, vol. 103, pp. 67–77, 2021.

[3] F. A. S. Borges, R. A. S. Fernandes, I. N. Silva and C. B. S. Silva, "Feature Extraction and Power Quality Disturbances Classification Using Smart Meters Signals," IEEE Transactions on Industrial Informatics, vol. 12, no. 2, pp. 824-833, April 2016.

[4] A. Akbarpour, M. Nafar and M. Simab, “Multiple power quality disturbances detection and classification with fluctuations of amplitude and decision tree algorithm”. Electr Eng, vol. 104, pp. 2333–2343, 2022.

[5] T. Zhong, S. Zhang, G. Cai and N. Huang, "Power-quality disturbance recognition based on time-frequency analysis and decision tree", IET Generation, Transmission & Distribution, vol.12, no.18, pp.4153-4162, 2018.

[6] M. Masoum, S. Jamali and N. Ghaffarzadeh, "Detection and classification of power quality disturbances using discrete wavelet transform and wavelet networks", IET Sci. Meas. Technol., vol. 4, no. 4, pp. 193-205, 2010.

[7] I. S Samanta. P.K. Rout and S. Mishra, "Feature extraction and power quality event classification using curvelet transform and optimized extreme learning machine", vol.103, Electr Eng, pp. 1–16, 2021.

[8] M. Zhang, K. Li and Y. Hu, "Classification of power quality disturbances using wavelet packet energy and multiclass support vector machine", Emerald COMPEL, vol. 31, no. 2, pp. 424-442, 2012.

[9] K. Thirumala, M. S. Prasad, T. Jain and A. C. Umarikar, "Tunable-Q Wavelet Transform and Dual Multiclass SVM for Online Automatic Detection of Power Quality Disturbances," IEEE Transactions on Smart Grid, vol. 9, no. 4, pp. 3018-3028, 2018.

[10] K. Thirumala, A. C. Umarikar and T. Jain, "Estimation of Single-Phase and Three-Phase Power-Quality Indices Using Empirical Wavelet Transform," IEEE Transactions on Power Delivery, vol. 30, no. 1, pp. 445-454, 2015.

[11] M. Biswal and P. K. Dash, "Estimation of time-varying power quality indices with an adaptive window-based fast generalized S-transform", IET Sci. Meas. Technol., vol. 6, no. 4, pp. 189-197, 2012.

[12] S. He, K. Li and M. Zhang, "A real-time power quality disturbances classification using hybrid method based on S-transform and dynamics", IEEE Trans. Instrum. Meas., vol. 62, no. 9, pp. 2465-2475, 2013.

[13] C. N. Bhende, S. Mishra, and B. K. Panigrahi, “Detection and classification of power quality disturbances using S-transform and modular neural network,” Electr. Power Syst. Res., vol. 78, no. 1, pp. 122–128, 2008.

[14] S. Hasheminejad, S. Esmaeili, and S. Jazebi, “Power quality disturbance classification using S-transform and hidden Markov model,” Electrical Power Components and Systems, vol. 40, no. 10, pp. 1160–1182, 2012.

[15] C. Cui, Y. Duan, H. Hu, L. Wang and Q. Liu, "Detection and Classification of Multiple Power Quality Disturbances Using Stockwell Transform and Deep Learning," IEEE Transactions on Instrumentation and Measurement, vol. 71, pp. 1-12, 2022.

[16] S. Chatterjee, N. Ray Choudhury and R. Bose, "Detection of Epileptic Seizure and Seizure-free EEG Signals Employing Generalized S-Transform”, IET Science, Measurement & Technology, vol.11, no.7, pp. 847–855, 2017.

[17] M. V. Reddy and R. Sodhi, "A modified S-transform and Random Forests-Based Power Quality Assessment Framework", IEEE Trans. Instrum. Meas., vol. 67, no. 1, pp. 78-89, 2018.

[18] K. Nandi, A. K. Das, R. Ghosh, S. Dalai and B. Chatterjee, "Hyperbolic Window S-Transform Aided Deep Neural Network Model-Based Power Quality Monitoring Framework in Electrical Power System," IEEE Sensors Journal, vol. 21, no. 12, pp. 13695-13703, 2021.

[19] H. H. Goh, L. Liao, D. Zhang, W. Dai, C. S. Lim, T. A. Kurniawan and K.C. Goh, "An Integrated Approach Improved Fast S-transform and SVD Noise Reduction for Classification of Power Quality Disruptions in Noisy Environments", Electric Power Components and Systems, vol.50, no.14-15, pp. 868-885, 2022.

[20] M.J.B. Reddya, R. K. Raghupathya, K. P. Venkatesha and D. K. Mohanta, "Power quality analysis using Discrete Orthogonal S-transform (DOST)", Digital Signal Processing, vol. 23, no. 2, pp.616-626, 2013.

[21] S. Chatterjee, S. Dalai, S. Chakravorti and B. Chatterjee, “Use of Chirp Excitations for Frequency Domain Spectroscopy Measurement of Oil-paper Insulation,” IEEE Transactions on Dielectrics and Electrical Insulation, vol.25, no.2, pp. 1103–1111, 2018.

[22] A. K. Das, S. Chatterjee, S. Dalai and B. Chatterjee, "Cross Spectrum Aided Surface Condition Assessment of Metal Oxide Surge Arrester Employing Convolutional Neural Network", IEEE Transactions on Dielectrics and Electrical Insulation, vol.28, no.6, pp.2134-2143, 2021.

[23] S. Modak, S. S. Roy, R. Bose and S. Chatterjee, “Focal Epileptogenic Area Recognition Employing Cross EEG Rhythm Spectrum Images and Convolutional Neural Network”, IEEE Sensors Journal, vol. 21, no.20, pp.23335-23343, 2021.

[24] IEEE, 1159-2009, "IEEE Recommended Practice for Monitoring Electric Power Quality", 2009.

[25] R. G. Stockwell, L. Mansinha and R. P. Lowe, "Localization of the complex spectrum: The S transform," IEEE Transactions on Signal Processing, vol. 44, no. 4, pp. 998-1001, April 1996.

[26] A. K. Das, D. Dey, B. Chatterjee and S. Dalai, "A Transfer Learning Approach to Sense the Degree of Surface Pollution for Metal Oxide Surge Arrester Employing Infrared Thermal Imaging," IEEE Sensors Journal, vol. 21, no. 15, pp. 16961-16968, 1 Aug.1, 2021.

[27] S. Chaudhary, S. Taran, V. Bajaj and A. Sengur, "Convolutional Neural Network Based Approach Towards Motor Imagery Tasks EEG Signals Classification," IEEE Sensors Journal, vol. 19, no. 12, pp. 4494-4500, 15 June15, 2019.

[28] Y. Celika, M., Talob, O., Yildirim, M. Karabatak, et al., "Automated invasive ductal carcinoma detection based using deep transfer learning with whole-slide images", Pattern Recognition Letters, vol. 133, pp. 232-239, 2020.

[29] A. Krizhevsky, L. Sutskever and G.E. Hinton, “ImageNet classification with deep convolutional neural networks.”, NIPS, pp. 1106–1114, 2012.

[30] S. Karen and A. Zisserman. "Very deep convolutional networks for large-scale image recognition." arXiv preprint arXiv: 1409.1556, 2014.

[31] K. He et al. "Deep residual learning for image recognition." Proceedings of the IEEE Conference on Computer Vision and Pattern Recognition (CVPR), 2016.

[32] S. Christian, et al. "Going deeper with convolutions." Proceedings of the IEEE Conference on Computer Vision and Pattern Recognition (CVPR), 2015.

[33] T. Zhang, W. Chen and M. Li, "AR based quadratic feature extraction in the VMD domain for the automated seizure detection of EEG using random

forest classifier", Biomed. Signal Process. Control, vol. 31, pp. 550-559, 2017.

[34] V. N. Vapnik, "The Nature of Statistical Learning Theory", Springer, 2000.

[35] T. M. Cover, P.E. Hart, "Nearest neighbor pattern classification", IEEE Trans. Inf. Theory, vol.13, no.1, pp. 21– 27, 1967.

[36] Olivia Florencias-Oliveros, M. J. Espinosa-Gavira, Juan-José González de la Rosa, A. Agüera-Pérez, José Carlos Palomares-Salas, J. M. Sierra-Fernández, May 11, 2017, "Real-life Power Quality Sags ", IEEE Dataport, doi: https://dx.doi.org/10.21227/H2K88D.

[37] Olivia Florencias-Oliveros, M. J. Espinosa-Gavira, J. J. González-de-la-Rosa, A. Agüera-Pérez, J. C. P. Salas, J. M. Sierra-Fernández, May 11, 2017, "Real-life Power Quality Transients ", IEEE Dataport, doi: https://dx.doi.org/10.21227/H2Q30W.

[38] "DOE Disturbance Library," US Dept. Energy Electr. Power Res. Inst., Orlando, FL, USA. [Online]. Available: http://pqmon.epri.com/disturbance_ library/see_all.html.

[39] S. Mishra, C. N. Bhende, and B. K. Panigrahi, "Detection and classification of power quality disturbances using S-transform and probabilistic neural network," IEEE Trans. Power Del., vol. 23, no. 1, pp. 280–287, 2008.

[40] H. S. Behera, P. K. Dash, and B. Biswal, "Power quality time series data mining using S-transform and fuzzy expert system," Appl. Soft Comput., vol. 10, no. 3, pp. 945–955, 2010.

[41] L. Fu, K. Yan, and T. Zhu, "PowerCog: A practical method for recognizing power quality disturbances accurately in a noisy environment," IEEE Trans. Ind. Informat., vol. 18, no. 5, pp. 3105–3113, 2022.

[42] M. V. Reddy and R. Sodhi, “A rule-based S-transform and AdaBoost Based Approach for Power Quality Assessment,” Electr. Power Syst. Res., vol. 134, pp. 66–79, 2016.

[43] A. Yilmaz, A. Küçüker, G. Bayrak, D. Ertekin, M. Shafie-Khah, and J. M. Guerrero, “An improved automated PQD classification method for distributed generators with hybrid SVM-based approach using un-decimated wavelet transform,” Int. J. Electr. Power Energy Syst., vol. 136, 2022, Art. no. 107763.

[44] K. Cai, W. Cao, L. Aarniovuori, H. Pang, Y. Lin, and G. Li, “Classification of power quality disturbances using Wigner–Ville distribution and deep convolutional neural networks,” IEEE Access, vol. 7, pp. 119099–119109, 2019.

[45] T. Zhong, S. Zhang, G. Cai, Y. Li, B. Yang, and Y. Chen, “Power quality disturbance recognition based on multiresolution S-transform and decision tree,” IEEE Access, vol. 7, pp. 88380–88392, 2019.

Chapter 4

Autocorrelation Aided Islanding Detection Using Bi-directional Long Short Type Memory Network

4.1 Introduction

In recent times due to the increase of load demands there is an unguent need for finding alternate sources of power generation that can match these load demands. This is done by using distributed generation (DG) system where conventional power generation sources are connected with alternate ones like solar, wind, fuel cell, etc. Despite the clear advantages, some serious problems arise due to various transient phenomena while connecting or disconnecting the DG sources with the utility grid. Among the different transient phenomenon, islanding detection is a major issue. Islanding is the condition where a part of the system gets isolated from the rest and the loads in this part are thus fed from the power generating unit connected to this isolated branch [1]. Appropriate detection of islanding is desirable because various operational problems related to power quality, safety hazard, voltage and frequency instability and damage to the system equipment etc. arise due to islanding. Thus, accurate detection of islanding is an important problem to address [2].

Existing methods for islanding detection include active and passive methods. In active methods, small disturbances are injected into the system and islanding detection is performed by examining the change in output parameters. Some popular active islanding detection methods include active frequency drift (AFD), automatic phase shift (APS), and slip mode frequency shift (SMS) etc. [3-4]. However, with increase in reactive load these methods

show higher non-detection zone (NDZ) [5]. In passive methods, a threshold value of parameters is selected and based on the choice of threshold value, islanding is detected. However, the choice of suitable threshold is a challenge that may often lead to misinterpretation of islanding events [6]. In [7-8], rate of change of frequency (ROCOF) has been recommended as an index for detection of islanding events. However, it has been reported in [5] that in the case of real and reactive power mismatch, ROCOF leads to NDZ. Hence, to minimize NDZ, advanced signal processing techniques have been applied for accurate detection of islanding events.

In existing literature, many signal processing techniques combined with machine learning tools have been implemented. Application of wavelet packet transform and extreme machine learning for islanding detection has been reported in [9]. In [10], Hilbert-Huang transform with extreme learning machine has been used for islanding detection. In [11], wavelet transform has been used to distinguish between islanding and non-islanding conditions. Application of Stockwell (S)-transform with modular probabilistic neural network (PNN) and support vector machines (SVM) have been reported in [12] to detect and classify islanding. Application of wavelet transform and S-transform for islanding detection has been reported in [13]. In [5], use of signal processing techniques like hyperbolic S-transform, time-time (T-T) transform and mathematical morphology (MM) methods with SVM have been reported for islanding detection. Application of empirical mode decomposition and random forest classifier for islanding detection has been reported in [14]. Advanced signal decomposition technique for detection of islanding has been reported in [15]. Recently, application deep learning for islanding detection has been reported in existing literature [16-17]. Application of convolutional neural network (CNN) and continuous wavelet transform for islanding detection has been reported in [17].

In this paper, a novel technique using autocorrelation-based feature extraction technique has been proposed for detection of islanding condition. It is to be mentioned here that autocorrelation used in this work has definite advantages over other signal processing techniques. In the first case, autocorrelation operation is computationally simple compared to other signal processing techniques [18]. Moreover, unlike the wavelet transform, the performance

does not depend on the type of mother wavelet used. In comparison with EMD, autocorrelation is free from the problem of mode-mixing and end-

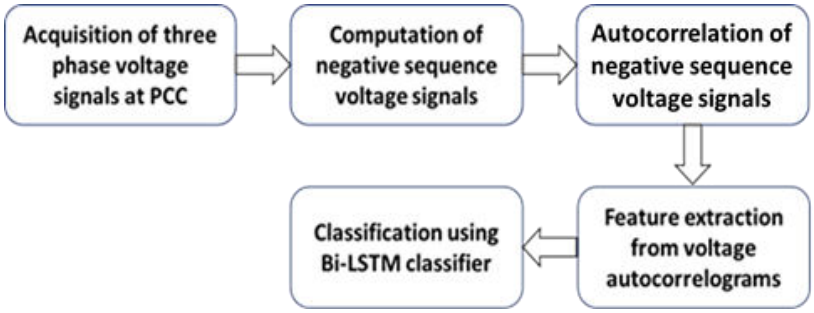

Fig. 4.1 Flow chart of proposed framework.

effect problems. Another distinct advantage of autocorrelation is that it is robust against random and uncorrelated noise present in any signal [19]. This implies that if two similar signals are contaminated with random uncorrelated noise, then the effect of that noise will not be reflected in the auto-correlogram as the correlation coefficient value for random uncorrelated noise is very small [20]. Considering the advantages as stated above, application of autocorrelation-based feature extraction has been reported in many existing literature [21-22]. In this study, we investigate the feasibility of using autocorrelation-based feature extraction for classification of islanding event in power systems.

In the present contribution, islanding as well as several real-life power system transient conditions, namely three phase faults, tripping of other DGs etc. have been simulated on a grid connected DG system. Initially, three phase voltage signals form the point of common coupling are recorded from which negative sequence voltage signals corresponding to different transient events is computed. The computed negative sequence voltage from the point of common coupling is autocorrelated for feature extraction purpose. The extracted features were fed to a Bi-LSTM classifier for classification of islanding and other transient events. It was observed that the proposed framework employing autocorrelation-based feature extraction and Bi-LSTM

classifier is capable of detecting islanding as well as non-islanding events accurately. A brief flowchart of the proposed method is given in Fig. 4.1.

4.2 System under study

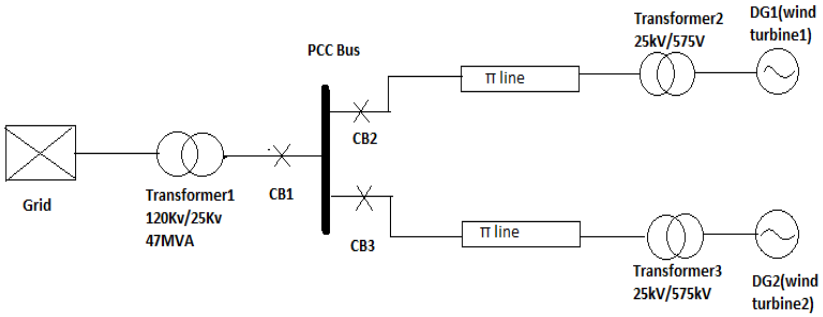

Fig. 4.2 Simulated power system model

The system under study is shown in Fig.4.2. Here a generalised DG model have been simulated having 2 DGs (wind turbines) which are connected to the grid via a point of common coupling (PCC). Each DG unit have been placed at a distance of 30 km from the PCC in a pi-section. The parameter details of the generator, transformer, distributed lines and the load is mentioned below:

- Generator: Type-swing, frequency (f) = 60Hz, V_{RMS}=120 kV and phase=0 (deg.)

- Distributed Generators (DGs): 2 wind farms consisting of 6 wind turbines are connected to a 25 kV distribution system feeding a 120 kV gird through a 30 km, 25 kV feeder.

- Transformer 1: Nominal power=47 MVA, f=60 Hz, Voltage rating=120kV/25kV, $V_{1(RMS)}$=20kV, R_1(pu)=0.08/30, L_1(pu)=0.08, $V_{2(RMS)}$=20kV, R_2(pu)=0.08/30, L_2(pu)=0.08, R_m(pu)=500, L_m(pu)=500

- Transformer 2,3: Nominal power=6×1.75MVA, f=60Hz, Voltage rating =25kV/575V, $V_{1(RMS)}$=25 kV, R_1(pu)=0.025/30, $L_{1(pu)}$=0.025, $V_{2(RMS)}$=575V, $R_{2(pu)=}$0.025/30, $L_{2(pu)}$=0.025, $R_{m(pu)}$=500, $L_{m\ (pu)}$=Infinity.

- Distribution lines: 2 pi-section 30 km lines, f=60 Hz, R_1=0.1153 Ω/km, R_0=0.413 Ohms/km, L_1=1.05 mH/km, L_0=3.32 mH/km, C_1=11.33 nF/km, C_0=5.01 nF/km

The islanding event is simulated by tripping the main circuit breaker CB1 with loads L_1 = 2MW, L_2 =2MW, 30 MVAr, respectively. At this condition, voltage readings are taken from the point of common coupling (PCC). In addition to islanding, other transient conditions like tripping of other DG's, three phase fault etc. have been simulated to distinguish between islanding and other transient phenomenon. The circuit breakers were tripped according to the various simulated conditions, by varying switching times. In addition, voltage signals under normal operating conditions were also recorded. The simulation of different transient events is performed via. MATLAB Simulink.

4.3 Methodology

4.3.1 Negative sequence computation

Negative sequence component of voltage and current is one of the primary indicators of any transients in a system [5]. So, in this paper the negative sequence voltage components have been computed on the three phase voltage signals acquired from the PCC. The mathematical expression for computation of negative sequence component from three phase voltage signals is described below:

$$V_0 = \frac{1}{3}(V_a + \lambda^2 V_b + \lambda V_c) \tag{4.1}$$

Where, V_a, V_b and V_c represents the three phase voltage signals received at the PCC and V_2 is the negative sequence voltage and $\lambda=1\angle 120^\circ$ is the complex operator. Using the above formulae, the three phase voltage signals recorded at the PCC have been converted to negative sequence voltage.

4.3.2 Autocorrelation sequence computation feature extraction

The sole objective of the present work is to detect the islanding and transient disturbances in a grid connected DG system. For this purpose, suitable signal processing tool has been applied on the computed negative sequence voltage components for categorization of each type of transients [5]. In the present chapter, autocorrelation has been used to analyze the negative sequence voltage waveforms. In digital signal processing, autocorrelation is a measure of the similarity between two alike signals. In the other words, it is the measure of self-similarity of a signal. Autocorrelation of a discrete signal $x(n)$ is calculated using the following formula:

$$\hat{S}_{xx}(m) = \begin{cases} \sum_{n=0}^{N-m-1} x_{n+m}\, x_n & m \geq 0 \\ S_{xx}(-m) & m < 0 \end{cases} \tag{4.2}$$

In (4.2), 'xx' is the autocorrelation sequence (also known as autocorrelogram) and the index 'm' indicates the lag or the time shift parameter. For a given discrete sequence with N number of sample points, autocorrelation operation gives ($2N$-1) sample points.

4.3.3 Feature extraction

Feature extraction is an important part in any classification task. Extracting meaningful features can boost the performance of the classifier. In this paper, we have extracted 36 features from the negative sequence voltage autocorrelograms. The extracted features from autocorrelation sequences are given in In Table 4.1. It is to be mentioned here that these extracted features (EF) are a combination of different statistical, Hjorth as well as non-linear features. Detailed mathematical expression of these extracted features is provided in [19]. These 36 features are fed as inputs to a Bi-LSTM classifier for classification of islanding and non-islanding events.

4.3.4 Bi-directional-long short term memory network

Bidirectional-long short term memory network (Bi-LSTM) is a deep neural network used for time series prediction as well as for classification. Bi-LSTM

is proposed as an extension of long short term memory network (LSTM), which tackles the problem of vanishing gradient suffered by the Recurrent Neural Networks (RNNs). Fig. 4.3 shows a basic RNN which looks somewhat like this from the high level. Detailed information about the RNN

Table 4.1 Extracted features

EF_1: Maximum value	EF_{19}: Margin factor
EF_2: Index of the maximum value	EF_{20}: Form factor
EF_3: Equivalent width	EF_{21}: Clearance factor
EF_4: Centroid	EF_{22}: Kurtosis factor
EF_5: Absolute centroid	EF_{23}: Waveform index
EF_6: Root mean square width	EF_{24}: Peak index
EF_7: Mean	EF_{25}: Skewness index
EF_8: Standard deviation	EF_{26}:1st Quartile
EF_9: Skewness	EF_{27}: 3rd Quartile
EF_{10}: Kurtosis	EF_{28}: Waveform length
EF_{11}: Median	EF_{29}: Wilson amplitude
EF_{12}: R.M.S value	EF_{30}: Sample Sign integral
EF_{13}: Square root of amplitude	EF_{31}: Hjorth feature mobility
EF_{14}: Peak to peak value	EF_{32}:Hjorth feature complexlity
EF_{15}: Variance	EF_{33}: Shannon Entropy
EF_{16}: Crest factor	EF_{34}: Renyi Entropy
EF_{17}: Shape factor	EF_{35}: ApproximateEntorpy
EF_{18}: Impulse factor	EF_{36}: Sample Entropy

can be found out in [23]. The Bi-LSTM uses two independent RNNs instead of a single RNN. The basic working principle behind such a network is that the input sequence in its normal order is fed to the first network while the sequence is reversed when fed to the second layer. This reversal of input sequence helps the model learn not only from the previous states but also from next states simultaneously. Fig. 4.4 shows the architecture of a bidirectional RNN (BRNN). As it's evident from Fig. 4.3 and Fig. 4.4 that the only difference between RNN and BRNN is that in BRNNs, there is an

additional independent RNN to enable the model to learn from not only the past but also the future. Otherwise, the basic working principle remains the same. The vanishing gradient problem of RNN exists here too. So, to deal with the aforesaid issue, again LSTMs come to the rescue. The structure of Bi-LSTM is shown in Fig. 4.5. From Fig. 4.5, it can be seen that in Bi-

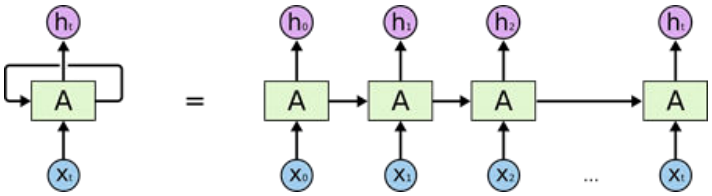

Fig. 4.3 Simplified structure of RNN.

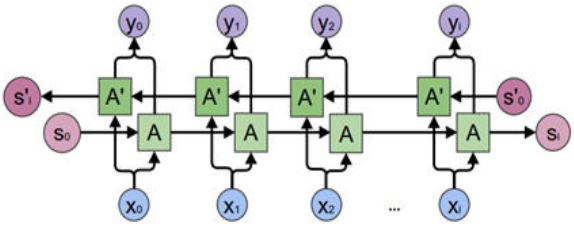

Fig. 4.4 Structure of BRNN

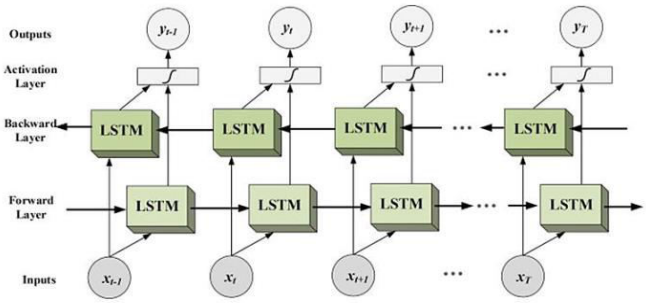

Fig. 4.5 Structure of Bi-LSTM.

LSTM, the single layered repeating module of an RNN is replaced by a four layered repeating layer, but twice here, one for the forward RNN and the other for the backward RNN. An important thing to note is that the output sequence is calculated by subjecting the RNN layers to an activation function. So, Bidirectional LSTMs are an extension of traditional LSTMs. Application of Bi-LSTM as a classifier has been reported in many recent works [24-25]. In this work we investigate the feasibility of using Bi-LSTM as a classifier for classification of islanding and other transient events using features extracted from negative sequence voltage autocorrelograms.

4.4 Results and Discussions

4.4.1 Autocorrelation of negative sequence voltage signals

Fig.4.6 (a-d) shows the time variation of negative sequence voltage signals obtained under normal operating condition, islanding condition, three phase fault and tripping of other DG, respectively. The corresponding autocorrelation sequences for the above 4 events are also shown in Fig. 4.7(a) through Fig. 4.7(d), respectively. From Fig. 4.7 (a-d) it can be observed that the negative sequence voltage autocorrelograms of different transient events are distinctly different from each other. So, it is possible to distinguish different transient events by extracting suitable features from the

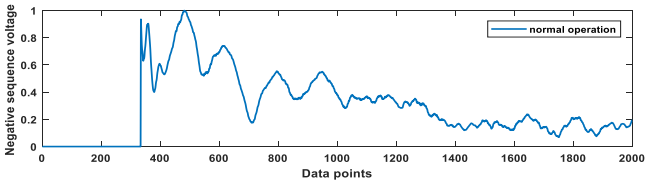

(a)

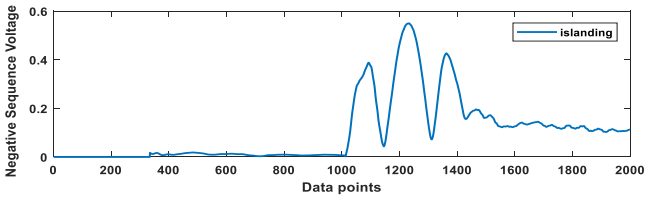

(b)

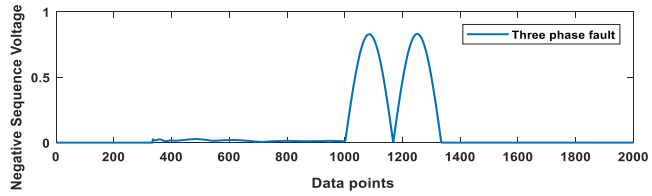

(c)

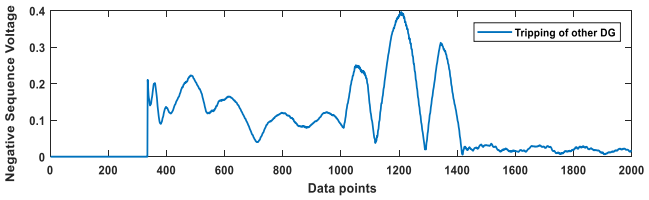

(d)

Fig. 4.6 Normalized negative sequence voltage of different transient events

autocorrelation sequences. In this study, 36 features as mentioned in Table 4.1 are extracted from the autocorrelation sequences of negative voltage sequence components for classification of islanding and non-islanding events. The training of Bi-LSTM classifier as well as the performance of the proposed model using the extracted features is discussed in the next section.

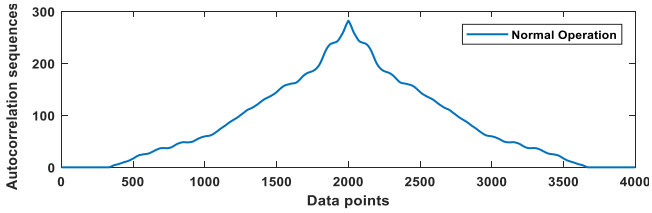

(a)

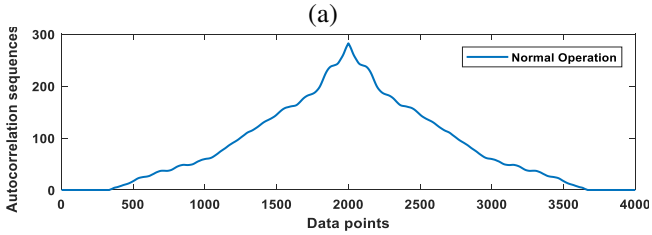

(b)

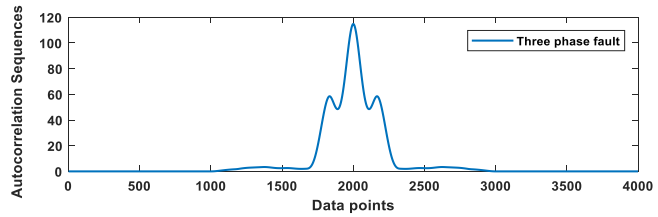

(c)

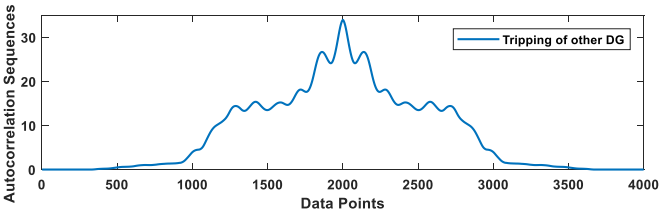

(d)

Fig. 4.7 Autocorrelation sequences of negative sequence voltages

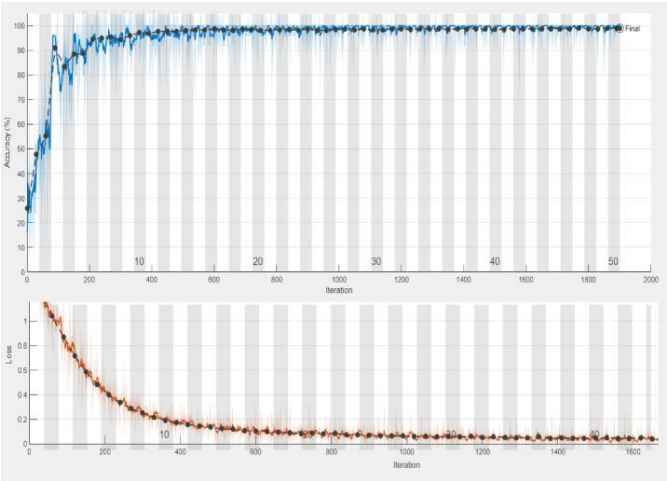

Fig. 4.8 Training of Bi-LSTM classifier

4.4.2 Training of Bi-LSTM

The Bi-LSTM proposed in this work has a hierarchical structure that consists of an initial input layer for sequence input. This is followed by one Bi-LSTM layer, one dropout layer and four fully connected layers. Finally, a classification layer with softmax as the activation function is placed at the output. The number of neurons fed to the input layer is 36. In the case of Bi-LSTM, the hidden units are selected as 100 with 50% dropout rate. The classification layer at the output is responsible for predicting the respective classes as determined by the probabilistic scores obtained from the Bi-LSTM layer. For the purpose of training, the initial learning rate was kept at 0.001 and for scaling the learning rate corresponding to each weight, Adam optimizer was selected and Cross-entropy was chosen as the loss function. The number of iterations were set to 2000 with the size of mini-batch size kept at 20 and for training the Bi-LSTM, number of epochs was set at 80. The training of the Bi-LSTM classifier is shown in Fig. 4.8. The entire training was performed on a personal computer with machine configuration as follows: Processor: Intel i5 (9th Gen), RAM: 8 GB RAM, Graphics Card: NVIDIA GTX in MATLAB 2020 (a) environment.

4.4.3 Evaluation of Bi-LSTM

In this section, the classification performance of the Bi-LSTM classifier is evaluated. In the present work, a total of 1000 negative sequence voltage signals (250 per class) were obtained. These signals were obtained by varying the parameters like varying in active and reactive power, time of occurrence etc. After autocorrelation operation, 250 autocorrelograms were obtained for each class. Now as mentioned earlier, since 36 features were extracted from each autocorrelograms, size of the input feature matrix is 250 ×36. These features were split in the ratio of 80:20 for training and testing the classifier performance. In this work, two types of (one binary and one multiclass) classification problems are presented. The description of different types of classification problems is given in Table 4.2. The purpose of the binary classification (C-I) is to distinguish only between islanding and non-islanding events including the normal operation. The multiclass classification can distinguish each type of event separately and can send the decision to the

relay to take necessary action. The performance of Bi-LSTM classifier has been evaluated in terms of the following indices namely accuracy, sensitivity and specificity, respectively. The mathematical expression of the above indices are given by (4.3)– (4.5):

$$Accuracy(\%) = \frac{TP+TN}{TP+TN+FP+FN} \times 100 \tag{4.3}$$

$$Sensitivity(\%) = \frac{TP}{TP+FN} \times 100 \tag{4.4}$$

$$Specificity(\%) = \frac{TN}{TN+FP} \times 100 \tag{4.5}$$

The parameters true positive (*TP*), true negative (*TN*), false positive (*FP*) and false negative (*FN*) were computed from the confusion matrices of C-I and C-II, respectively. The performance of the Bi-LSTM classifier is shown in Table 4.3. It can be seen from Table 4.3that Bi-LSTM has delivered very high accuracy for both C-I and C-II, respectively. The performance of C-I is marginally better than C-II. Nevertheless, for both C-I and C-II, the performance of Bi-LSTM is almost consistent with some minor deviation indicating satisfactory performance of the proposed model.

Table 4.2 Classification Problem

Classification	**Description**	**Type of problem**
C-I	Islanding vs. Non-islanding Events	Binary
C-II	Normal operation vs. Islanding vs Three phase fault vs. Tripping of other DGs	Multiclass

Table 4.3 Performance of Bi-LSTM classifier

Classification	**Accuracy (%)**	**Sensitivity (%)**	**Specificity (%)**
C-I	99.0	100.0	98.45
C-II	98.50	99.20	97.75

4.4.4 Comparison with standard machine learning algorithms

In this section, the performance of the proposed model is compared with some existing benchmark machine learning algorithms namely, support vector machines, *k*-Nearest Neighbour (kNN) and random forest (RF) classifiers. Detailed description of these classifiers can be found out in [26-28]. For SVM, kernel functions were varied and it was observed that RBF kernel has delivered best results. To determine the optimum kernel width, the regularization parameter is varied in steps of 0.1 from 1-200. For kNN, the

Table 4.4 Classification performance using other ML classifiers

Classification	**Classifier and Parameters**	**Accuracy (%)**	**Sensitivity (%)**	**Sensitivity (%)**
C-I	SVM-RBF σ=1.2	97.50	96.20	95.48
	kNN k=3, Euclidean	97.25	98.56	97.30
	RF	98.45	99.27	97.85
	Proposed Bi-LSTM	99.0	100	98.45
C-II	SVM-RBF σ=1.2	96.21	97.20	96.75
	kNN k=5, Euclidean	97.10	98.65	96.52
	RF	97.65	98.56	98.14
	Proposed Bi-LSTM	98.50	99.20	97.75

performance is evaluated by varying the distance parameter as well as the value of *k*. In the case of RF classifier, the optimal number of decision tress is kept at 50. The performance of different classifiers in islanding detection is reported in Table 4.4. It can be observed that for both C-I and C-II, the Bi-

LSTM classifier proposed in this study delivered best results compared to other classifiers. From Table 4.4, it can also be seen that the performance of RF is better than both SVM and kNN. It is interesting to note that all the classifiers have delivered reasonably accurate results which indicate the robustness of the proposed autocorrelation-based feature extraction model.

4.4.5 Performance analysis in presence of noise

The performance of the proposed model is also analyzed in the presence of noise. For this purpose, white Gaussian noise with different signal to noise ratios (SNR) are mixed with the voltage signals. The classification accuracy

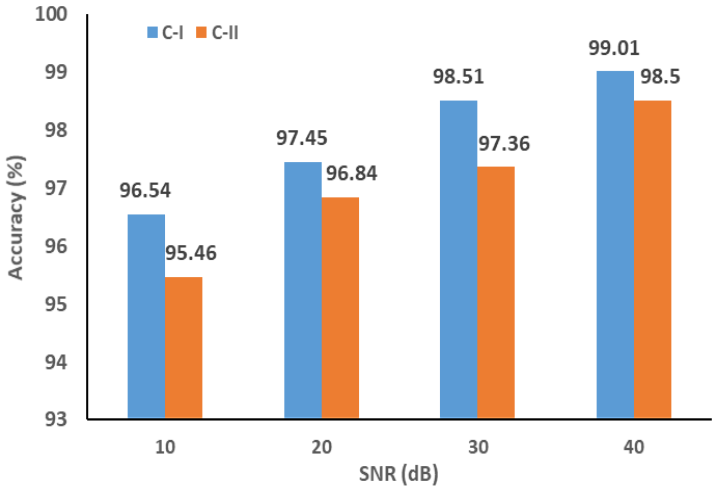

Fig. 4.9 Variation of accuracy with noise level (SNR)

of the proposed Bi-LSTM model is plotted against different signal to noise ratios (SNR) in Fig. 4.9 for both C-I and C-II, respectively. It can be observed that the classification accuracy showed not much deviation even when the SNR is as low as 10 dB. This is observed to be true for both CPs. This is because since autocorrelation-based signal analysis and feature extraction technique is robust against noise, hence the classification accuracy is almost unperturbed in presence of noise. Thus, the performance of the proposed model is robust against noise.

4.5 Conclusions

In this paper, a novel technique for classification of islanding and non-islanding events in a grid connected DG system is proposed. For this purpose, islanding and several other transient events (faults, DG trip etc.) were simulated and three phase voltage signals corresponding to each transient events have been recorded from which respective negative sequence voltage signals have extracted. Then autocorrelation is applied on the acquired negative sequence voltage signals. From the respective autocorrelograms, 36 fault features were obtained. The features were fed to Bi-LSTM classifier for classification of islanding and non-islanding events. In this study, one binary and one multiclass classification problem has been addressed. It has been observed that for both the cases, the performance of the proposed model is satisfactory. Further investigations have revealed that in comparison with the standard machine learning classifier, the performance of the proposed Bi-LSTM model is better. Besides, it has been observed that the performance of the proposed autocorrelation aided machine learning model is immune to noise. Thus, it can be concluded that the proposed autocorrelation aided Bi-LSTM-based islanding detection method can be used for accurate detection of islanding and non-islanding events in distributed generation system.

References

[1] S. Hasan and S. S. Saleh, "A new passive islanding detection technique for a microgrid based on transient energy", IET Generation, Transmission & Distribution, 2022.

[2] N. Gupta, R. Dogra, R. Garg and P. Kumar, "Review of islanding detection schemes for utility interactive solar photovoltaic systems", International Journal of Green Energy, vol.19, no.3, pp.242, 2022.

[3] F.Yu et al., "Parameter design optimization for Sandia frequency shift islanding detection method", Proceedings of IEEE International Symposium on Power Electronics for Distributed Generation Systems (PEDG), pp.182-186, 2012.

[4] T. Tang and S. Xie, "Research on 2nd harmonic impedance measurement based active islanding detection method", Proceedings of 7th International Power Electronics and Motion Control Conference, vol.3, pp.1812-1816, 2012.

[5] S. R. Mohanty et al., "Comparative Study of Advanced Signal Processing Techniques for Islanding Detection in a Hybrid Distributed Generation System," IEEE Transactions on Sustainable Energy, vol. 6, no. 1, pp. 122-131, 2015.

[6] S. Jang and K. Kim, “An islanding detection method for distributed generation algorithm using voltage unbalance and total harmonic distortion of current,” IEEE Transactions on Power Delivery., vol. 19, no. 2, pp. 745–752, 2004.

[7] H. H. Zeineldin et al., “Impact of DG interface control on islanding detection and non-detection zones,” IEEE Transactions on Power Delivery., vol. 21, no. 3, pp. 1515–1523, 2006.

[8] M. Mishra, M. Sahani and P. K. Rout, "An islanding detection algorithm for distributed generation based on Hilbert–Huang transform and extreme

learning machine." Sustainable Energy, Grids and Networks, vol. 9, pp. 13-26, 2017.

[9] H. H. Zeineldin and S. Kennedy, “Sandia frequency-shift parameter selection to eliminate non-detection zones,”. IEEE Transactions on Power Delivery, vol. 24, no. 1, pp. 486–487, 2009.

[10] M. Mishra et al., "An Islanding Detection Method Based on Wavelet Packet Transform and Extreme Learning Machine." International Journal of Renewable Energy Research, vol 6, no.3, pp.856-865, 2016.

[11] S. Reza and M. Akbari, "New islanding detection technique for DG using discrete wavelet transform." IEEE International Conference on Power and Energy, (PECON), 2010 2010.

[12] S. R. Mohanty et al., "Classification of disturbances in hybrid DG system using modular PNN and SVM”, International Journal of Electric Power and Energy systems, vol. 44, no. 1, pp.764-777, 2013.

[13] P. K. Ray et al., "Disturbance detection in grid-connected distributed generation system using wavelet and S-transform." Electric Power Systems Research, vol. 81, no. 3, pp. 805-819, 2011

[14] S. Mishra et al., "Islanding Detection of Microgrid using EMD and Random Forest Classifier," Proceedings of IEEE International Conference on Computational Intelligence for Smart Power System and Sustainable Energy (CISPSSE), 2020, pp. 1-5.

[15] B. K. Chaitanya, A. Yadav and M. Pazoki, "An Advanced Signal Decomposition Technique for Islanding Detection in DG System," IEEE Systems Journal, vol. 15, no. 3, pp. 3220-3229, 2021.

[16] C. R. Reddy, et al., "A Deep learning approach for Islanding Detection of Integrated DG with CWT and CNN," Proccedings of IEEE International Conference on Sustainable Energy and Future Electric transportation (SEFET), 2021, pp. 1-7.

[17] A. K. Ozcanli and M. Baysal, "Islanding detection in microgrid using deep learning based on 1D CNN and CNN-LSTM networks", Sustainable Energy, Grids and Networks, vol. 32, 2022

[18] K. P. S. Rana, R. Singh and K.S. Sayann, "Autocorrelation based intelligent technique for complex waveform presentation and measurement", Journal of Instrumentation, vol.4, no.5, p.05007, 2009.

[19] J.G. Proakis and D.G. Manolakis, "Digital signal processing Principles algorithms and applications", New Delhi, India: Prentice Hall, 1997.

[20] S. Biswas et al., "An approach based on rough set theory for identification of single and multiple partial discharge source," International Journal of Electric Power and Energy systems., vol. 46, pp. 163–174, Mar. 2013.

[21] A. Banik et al., "Autocorrelation aided rough set-based contamination level prediction of high voltage insulator at different environmental condition, IEEE Transactions on Dielectrics and Electrical Insulation, vol. 23, no. 5, pp. 2883-2891, 2016.

[22] M. Schuster and K. K. Paliwal, "Bidirectional recurrent neural networks," IEEE Transactions on Signal Processing, vol. 45, no. 11, pp. 2673-2681, 1997.

[23] X. Li, C. Yu, F. Su, T. Quan and X. Yang, "Novel training algorithms for long short-term memory neural network", IET Signal Process., vol. 13, no. 3, pp. 304-308, 2019.

[24] M. Geng et al., "Epileptic Seizure Detection Based on Stockwell Transform and Bidirectional Long Short-Term Memory," IEEE TNSRE, vol. 28, no. 3, pp. 573-580, March 2020.

[25] V. N Vapnik, 'The Nature of Statistical Learning Theory' Springer, ISBN0-387-94559-8, 2000.

[26] Cover, T.M., Hart, P.E.: 'Nearest neighbor pattern classification', IEEE Trans. Inf. Theory, vol.13, no.1, pp. 21– 27, 1967

Chapter 5

Time-Frequency Image Representation Aided Deep Feature Extraction-Based Grid Connected Solar PV Fault Classification Framework

5.1 Introduction

Solar photovoltaic (PV) systems are one the most popular and reliable sources of renewable energy that can cater to the ever-increasing demand of increasing demand of non-conventional energy sources all over the world. The solar PV systems can generate electricity with zero carbon-di oxide emission, thereby can reduce the detrimental effects of climate change [1]. Hence, large scale solar PV systems are being installed all over the world. Solar PV system can operate in either standalone mode or in grid connected mode. Operation of grid connected solar PV system is more challenging and requires proper monitoring to ensure the reliability of power system network. In the event of faults occurring in grid connected PV system, the power system operation gets critically affected resulting in substantial financial losses. Different types of faults can occur in a grid connected PV system [2-4]. If not detected early, these faults severely limit the operation of solar PV system. For small scale solar panels, detection and isolation of faults is generally done by skilled technicians. However, the above method is dependent on human intervention and is error prone especially for large solar panel connected to grid. Therefore, it is necessary to develop an accurate and fast fault detection methodology for maintaining safe and continuous operation of grid connected solar PV systems.

Commonly occurring faults in solar panels include hotspots, cracks, delamination, and discoloration, malfunctioning of bypass diode, internal short circuit etc. [3]. In existing literature several techniques have been proposed by the researchers for fault detection of solar PV systems. Application of imaging techniques like infrared imaging [5] for condition monitoring of solar panels have been reported in [5-6]. Although imaging techniques can be useful for remote condition monitoring of solar panels, the method fails to give reliable results during low-light conditions. Condition monitoring of PV modules using current voltage (I-V) characteristics [7] have been reported in existing literature [7-9]. Recently, advanced signal processing techniques as well as modern machine learning tools for fault detection and classification in solar panels. In [10], fault detection in solar photovoltaic array using fast Fourier transform (FFT) and total harmonic distortion (THD) has been reported. Since the current waveforms during faulty condition are significantly deviant from stationary behavior, analysis in time-frequency domain has been reported in existing literature.

In [11] feature extraction using wavelet transform multi-resolution analysis has been proposed for classification of faults in solar panels. In [12] wavelet packet transform has been applied for DC arc fault detection in solar PV systems. However, the main limitation of wavelet transform-based signal analysis technique is that it is not signal adaptive in nature as the shape of the mother wavelet remains fixed throughout the length of the signal. Application of several signal decomposition techniques has been used to diagnose faults in solar PV systems [13-14]. In [13], empirical mode decomposition (EMD) has been used for fault detection in solar PV systems. But the main limitation of EMD is that it suffers from mode mixing and end effect problems. Application of dispersion entropy and variational mode decomposition (VMD) for detection of faults in grid connected PV system has been reported in [14], However, one limitation of VMD is that iterative extraction of intrinsic mode functions (IMFs) is tedious and computationally expensive. In [15], recurrence plot has been implemented for detection of DC series fault in solar PV systems. Application of machine learning algorithms like support vector machines (SVM) [16], artificial neural network [17], k nearest neighbour [18] decision tree (DT), random forest (RF), extra trees (EXT), extreme gradient boosting machine (XGBoost) and light gradient

boosting machine (LightGBM) [19], principal component analysis (PCA) [20] etc. for fault classification in solar PV system has been reported in many existing literatures. Although satisfactory accuracy has been achieved in classifying faults in solar PV systems, from practical point of view existing methods have certain limitations.

In the first case, most of the existing methods rely upon manual feature extraction for classification of faults in solar PV systems. In any classification problem, feature extraction is an important part as the performance of the machine learning features can be extracted either manually with prior knowledge or automatically without prior knowledge. Manual feature selection always imposes the risk of selecting redundant features which may directly influence the classification results. Considering the above-said facts, this study proposes a deep feature extraction-based framework for accurate fault detection in solar PV systems. The advantage of deep learning algorithms is that it can select features automatically from a given input image and at the same time can improve classification accuracy by selecting only the relevant features and by discarding the redundant ones. Moreover, deep learning can be easily implemented in low-cost microcontroller or raspberry-pi. Considering the advantages as stated above, in this work, a stacked sparse autoencoder model is used to extract deep features from the time-frequency images of current data. SSA is a deep learning architecture which is widely used for automatic feature extraction purposes. Application of SSA-based feature extraction has been reported in various existing literature [21-22]. The main benefit of using SSA-based feature extraction technique is that the feature extraction method is fully automated without any need for manual intervention. Moreover, SSA is an unsupervised deep machine learning approach i.e., they don't need any labeled data for training [21]. In other words, SSA can train and self-learn without pre-defined class labelling which can be used for real-time PV array fault diagnosis even if prior information about the type of fault data is not present. Thus, SSA has definite advantages over supervised machine learning algorithms. Taking these benefits into account, SSA is utilized in this work to extract meaningful features from the time-frequency representation (TFR) of current signals to construct an accurate and reliable solar PV fault detection system. In this study, three phase current signals of healthy as well as three

different fault scenarios were from the point of common coupling (PCC). The acquired three phase current data were initially converted to direct (*d*-axis) and quadrature (q-axis) using extended Park's vector approach. The extended

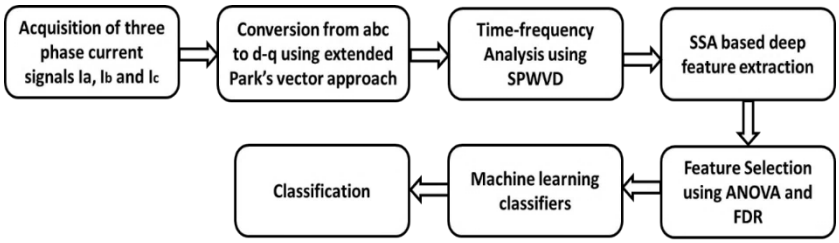

Fig.5.1 Flow chart of the proposed fault detection method

Park's vector approach has been successfully implemented for identification of faults in induction motors [23,26]. However, the aforesaid approach is not explored in power system for detection of faults. Considering the aforesaid fact, Park's vector approach has been used in this work. The novelty of the proposed work is that this is the first study where extended Park's vector approach has been used to analyze the three phase fault currents in grid connected solar PV systems. Using extended Park's vector approach, the obtained *d*axis and *q*axis currents in time–domain was transformed to time-frequency images using smoothed pseudo-Wigner-Ville distribution (SPWVD). A distinct advantage of using SPWVD over other time-frequency methods for e.g., continuous wavelet transform (CWT) is that the former does not depend on the nature of the choice of mother wavelet [24]. Moreover, unlike short time Fourier transform, the time- frequency analysis does not depend on the overlap and the type of window. Also, SPWVD is free from the mode-mixing and end-effect problems as suffered by EMD. Therefore, SPWVD is used in this work to analyze the current data in time-frequency (T-F) frame. A flowchart of the proposed fault detection framework is portrayed in Fig. 5.1. The main contributions of the present work are as follows:

(i) A novel technique using extended Park's vector approach is proposed for fault detection of grid connected solar PV systems. The transformed current

components (I_d and I_q) obtained from Park's vector were analyzed in time-frequency domain using smoothed pseudo-Wigner-Ville distribution (SPWVD).

(ii) A stacked sparse autoencoder (SSA)-based deep learning framework is proposed for automated feature extraction from TF images of current data.

(iii) Using analysis of variance (ANOVA) and false discovery rate (FDR) correction, most discriminative deep features were selected.

(iv) Classification of faults is done using selected deep features and four popular machine learning algorithms.

5.2 Acquisition of Fault data

In the present work, three phase current signals have been obtained a real-life grid connected solar PV experimental dataset to develop the fault classification model. The experimental setup consisted of a grid connected solar PV system operated under maximum power point tracking (MPPT) and limited power point tracking (LPPT) mode. The detailed description of the experimental set-up can be found in [25]. The schematic of the grid connected PV system is given in Fig. 5.2(a). The actual photograph of the experimental set-up is shown in Fig. 5.2(b). The fault dataset has a total of 16 data files with each file containing information about each type of event. These files were labelled as 0-7, with 0 being fault free and 1-7 representing different faults simulated under both MMPT and LPPT mode of operation. The different types of fault cases investigated include PV array mismatch, faults in inverters, anomalous grid operation, faults in feedback sensors and faults in MPPT controller with varying severity etc. It is to be mentioned here that in the present work, PV array mismatch caused due to 10% to 20% nonhomogeneous partial shading is used. Since PV array mismatches are challenging to detect in real-life due to the large variability in sensor data at the DC-side, therefore it is selected to verify the efficacy of the proposed method. The percentage of PV array mismatch has been determined using the method mentioned in [26]. In addition, each file contains information about the following parameters: (i) sampling time ($\sim 10\mu s$) (ii) I_{pv}: current

measurement from PV array (iii) V_{pv}: voltage measurement from PV array (iv) V_{dc}: measurement of DC voltage (v) measurement of three phase currents (I_a, $I_b$andI_c) (vi), Measurement of three phase voltages V_a, V_b and V_c (vii)

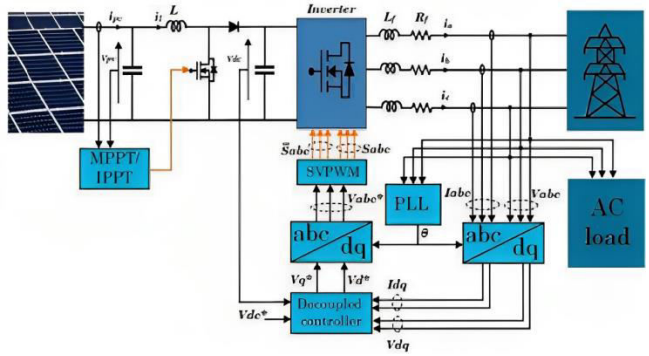

(a)

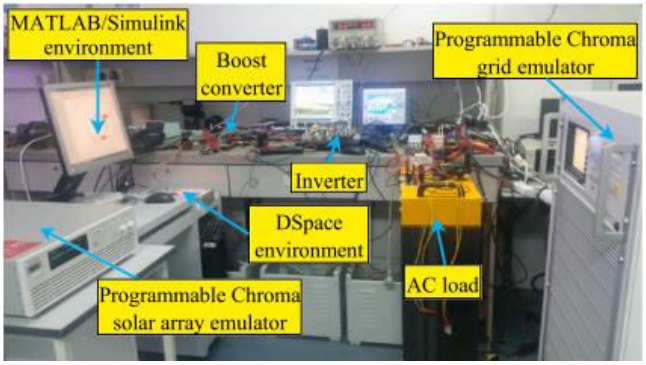

(b)

Fig.5.2 Schematic of (a) Experimental set-up (b) Actual photograph [25]

magnitude of current I_{abc} (viii) frequency of current (ix) magnitude of voltage V_{abc} (x) frequency of voltage V_f. In this work, the three phase current data (I_a , I_b and I_c) has been used for classification of faults in grid connected PV system. Also, in this study, out of 16, 4 data files, (three files representing different types of faults and one fault-free condition) have been used to develop the fault classification model for grid connected PV system operating under MPPT mode. The different class labels with their detailed description

used in this work are given in Table 5.1. The time variation of single cycle (0.02 s) three phase current signals for different classes (mentioned in Table 5.1) are shown in Fig. 5.3(a-d), respectively. It can be seen from the time

Table 5.1 Fault classes and their description

Class Label	**Type of Fault**	**Description**
C_0	No fault	Healthy condition
C_1	Feedback Sensor fault	One phase sensor fault 20%
C_2	PV array mismatch	10 to 20% non-homogeneous partial shading
C_3	Boost converter controller fault	+20% in time constant parameter of PI controller in MPPT controller of the boost converter

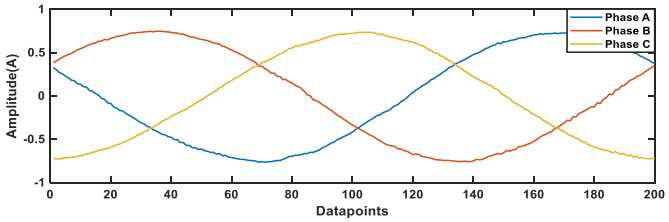

(a)

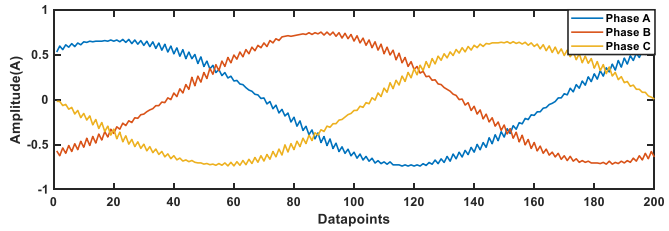

(b)

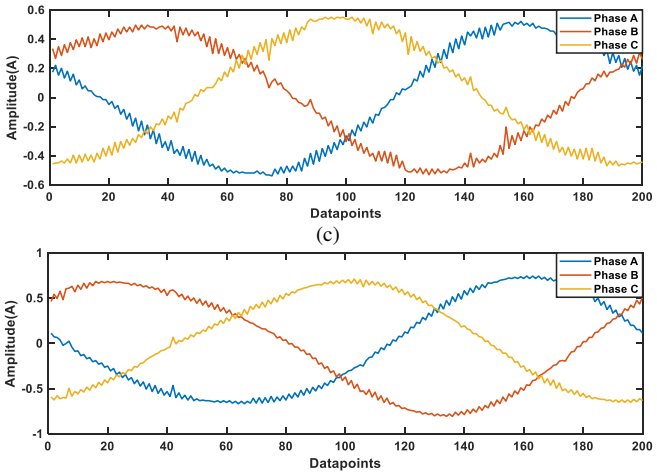

Fig. 5.3 Single cycle fault current signals for (a) C_0 (b) C_1(c) C_2 and (d) C_3

variation of single cycle three phase current waveforms shown in Fig. 5.3(a-d), it is difficult to discriminate between no-fault and fault current waveforms as the current waveforms look almost alike. Hence, extended Park's vector approach is applied on current waveforms to transform the current data to *d* axis and *q* axis, respectively.

5.3 Methodology

5.3.1 Extended Park's Vector approach

The extended Park's vector approach is a popular method of mapping three phase voltage or current signals into direct (d) and quadrature (q) axis. The mapping allows visualization of three-phase quantities into d and $q$axis. The mathematical formulae that relate d-axis (I_d) and q-axis (I_q) current components with three phase quantities (I_a, I_b and I_c) is given by [27]:

$$I_d = \sqrt{\frac{2}{3}} I_a - \frac{1}{\sqrt{6}} I_b - \frac{1}{\sqrt{6}} I_c \tag{5.1}$$

$$I_q = \frac{1}{\sqrt{2}} I_b - \frac{1}{\sqrt{2}} I_c \tag{5.2}$$

Using the above formulae, single cycle three phase current signals (I_a, I_b and I_c) shown in Fig. 5.3(a-d) acquired from PCC were converted to d-axis and q-axis components, respectively. The time variation of I_d and I_q components for no fault as well as for different types of fault classes are shown in Fig. 5.4(a-d) and Fig. 5.5 (a-d), respectively. It is evident from Fig. 5.4 (a-d) and Fig.5.5 (a-d), that significant differences in d-axis and q-axis currents are observed for both no-fault as well as for different fault classes. Such variations were absent if only three phase current signals were considered as

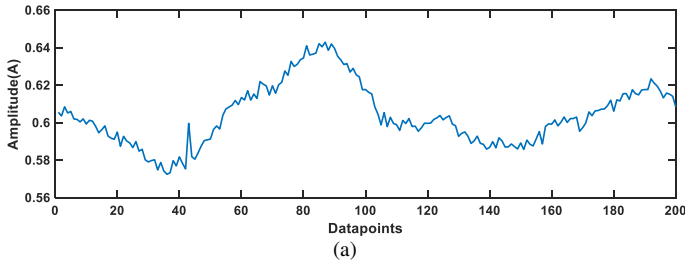

(a)

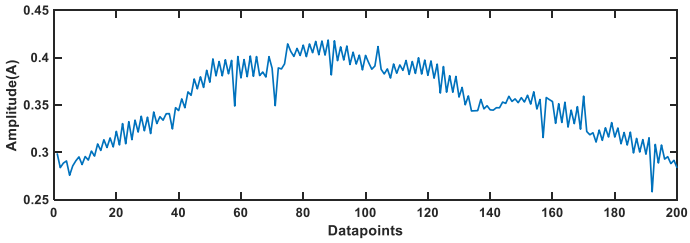

(b)

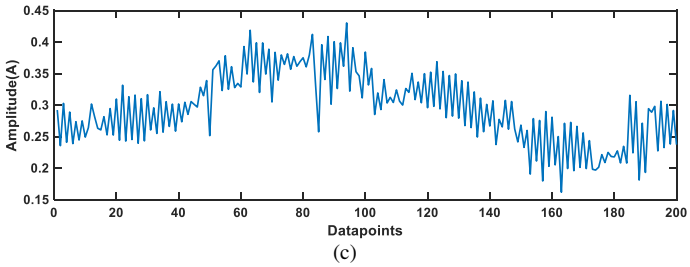

(c)

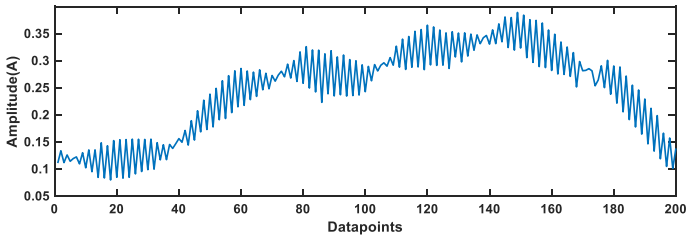

(d)

Fig. 5.4 Direct (d)-axis current signals (I_d) for (a) C_0 (b) C_1(c) C_2 and (d) C_3

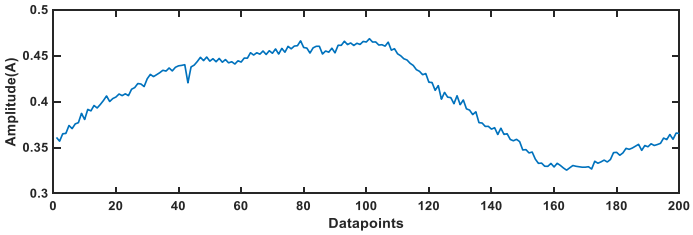

(a)

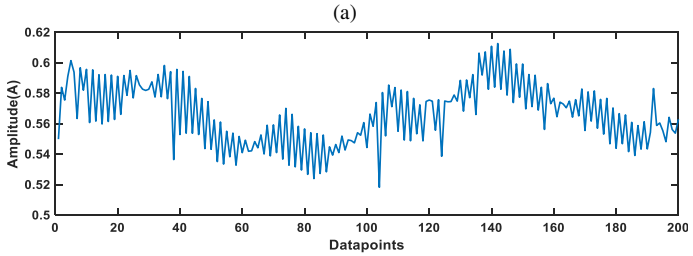

(b)

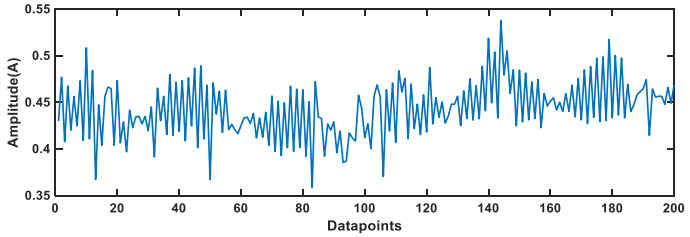

(c)

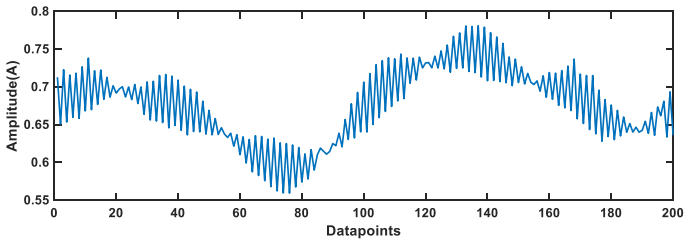

(d)

Fig. 5.5 Quadrature (q)-axis current signals (I_q) for (a) C_0 (b) C_1(c) C_2 and (d) C_3

shown in Fig. 5.3(a-d). Thus, it is evident that segregation of three phase current signals into d-axis and q-axis components can aid in better discrimination of faults. Additionally, it is evident from Fig, 5.4(a-d) and Fig. 5(a-d) that both d-axis and q-axis currents are non-stationary in nature. Hence, analysis in joint T-F plane will deliver fruitful results. Considering the aforesaid fact, in this study, smoothed Wigner-Ville distribution (SPWVD) is employed in this work. Brief mathematical details of SPWVD are given in the next subsection.

5.3.2 Smoothed pseudo-Wigner-Ville distribution

As mentioned earlier, I_d and I_q current data shown in Fig. 5.4 and Fig. 5.5, reveals that the signals of healthy as well as different fault classes are having non-stationary characteristics. Due to such non-stationary behaviour of current data, analysis in joint T-F plane can be suitable to investigate the non-linear dynamics of current signals to diagnose faults in PV systems. In existing literature, several methods like, Wigner-Ville distribution (WVD) [28] and smoothed pseudo-Wigner-Ville distribution" (SPWVD) [29-30] etc. are available to analyze EEG time-series in joint time-frequency plane. According to [29], resolution in TF image plot obtained from STFT, CWT and WVD is poor due to cross-terms of both time and frequency. In this study, this problem is overcome by using smoothed pseudo-Wigner-Ville distribution (SPWVD) which yields excellent time-frequency resolution due to introduction of cross-term reducing windows in time and frequency domain simultaneously. Additionally, the type and length of the "cross-term

reducing window" can be selected independently. Due to these advantages, SPWVD is more suitable to bring out hidden features from the time-frequency images of current data compared to traditional time-frequency analysis like short time Fourier transform (STFT), continuous wavelet transform (CWT), etc. The mathematical formulation of the smoothed pseudo-Wigner-Ville distribution of any current signal l(t) can be represented as [29]:

$$SPWVD(t,f) = \int_{-\infty}^{\infty} u\left(\frac{\tau}{2}\right) u^*\left(-\frac{\tau}{2}\right) \int_{-\infty}^{\infty} v(t-t') \dots \dots l\left(t'+\frac{\tau}{2}\right) l^*\left(t'-\frac{\tau}{2}\right) dt' e^{-j2\pi f t} d\tau \quad (5.3)$$

In the above equation, $u(t)$ denotes a window that reduces cross-terms in time domain whereas $v(t)$ signifies a window that reduces cross-terms in frequency domain. It is worthwhile to mention that $v(t)$ can be selected independently.

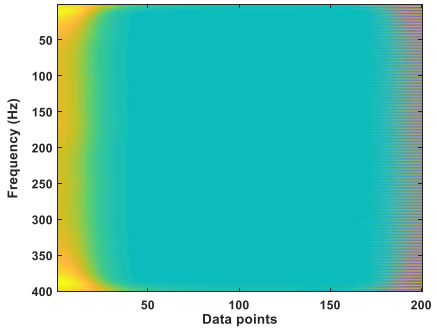

(a)

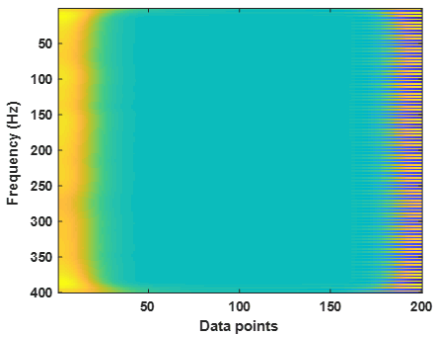

(b)

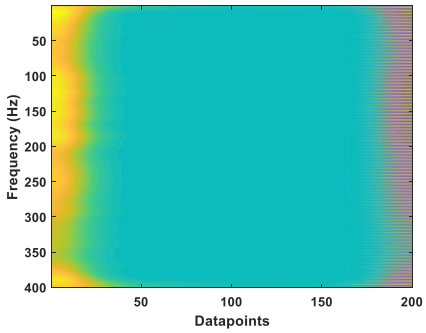

(c)

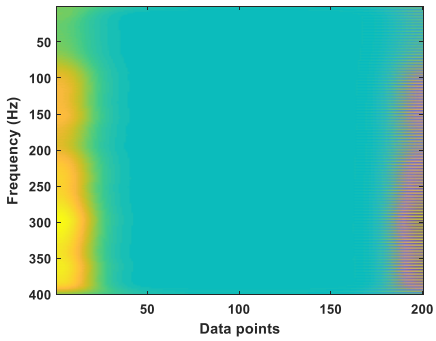

(d)

Fig. 5.6 Time-frequency representation of *d*-axis current signals obtained using SPWVD for class (a) C_0 (b) C_1 (c) C_2 and (d) C_3

Time-frequency analysis of I_d and I_q current signals yields complex time-frequency (T-F) matrices. The T-F images were obtained by taking the magnitude of the respective T-F matrices. The T-F plots of *d*-axis and *q*-axis current signals (I_d) and (I_q) for fault free as well as faulty signals analyzed using SPWVD have been shown in Fig. 5.6 (a-d), and 5.7 (a-d), respectively. In Fig. 5.6 and Fig. 5.7,*y*-axis denotes the frequency and *x*-axis denotes the time (data points). It is worth mentioning here that image plot of the magnitude of the T-F matrices i.e., time-frequency representation (TFR) plots can be used as inputs to the deep learning network for automated feature extraction [30].

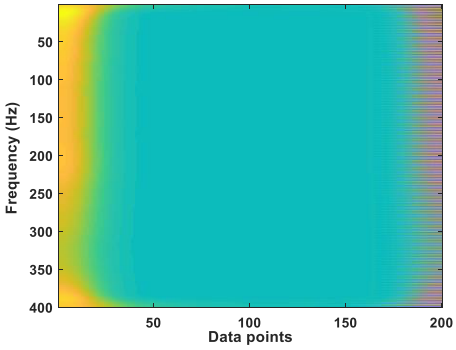
Frequency (Hz)
50
100
150
200
250
300
350
400
50
100
150
200
Data points

(a)

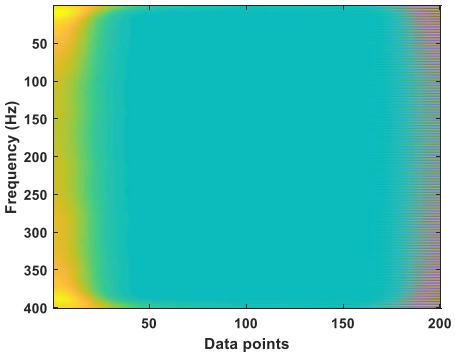
Frequency (Hz)
50
100
150
200
250
300
350
400
50
100
150
200
Data points

(b)

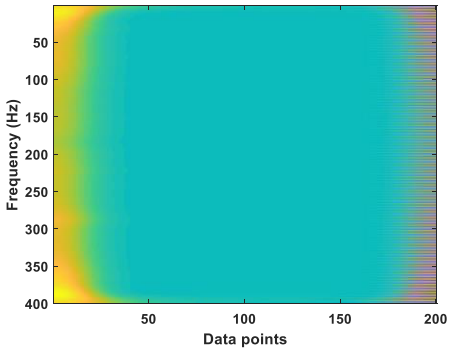
Frequency (Hz)
50
100
150
200
250
300
350
400
50
100
150
200
Data points

(c)

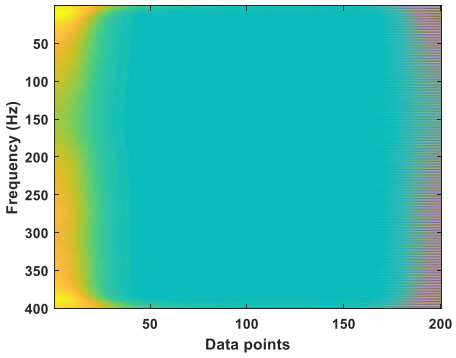

(d)

Fig. 5.7 Time-frequency representation of *d*-axis current signal obtained using SPWVD for class (a) C_0 (b) C_1 (c) C_2 and (d) C_3

5.3.3 Stacked sparse auto encoder

Feature extraction is an important part of any classification. Feature extraction is an important part of any classification task. Manual selection of features is unsophisticated and unreliable. Also, it may lead to misclassification because of the selection of insignificant and redundant features. In this work, a deep learning framework known as stacked sparse autoencoder (SSA) based automated feature extraction and reduction process has been proposed to obtain significant features from the time-frequency (T-F) matrix of different current signals obtained after applying SPWVD. Brief theoretical background of SSA is given below.

An autoencoder is an unsupervised machine learning algorithm consisting of two fundamental parts of an autoencoder and a decoder. A SSA model consists of two sparse autoencoder, connected in cascade. The encoder part of the first model extracts deep features from the input data and the encoder part of the second model eliminates the redundant features, extracted by first model, and reduces the dimension of the feature set [31]. In Fig. 5.8, a schematic diagram of stacked autoencoder architecture is shown. The encoder part encodes the input data x in terms of meaningful features F and

the decoder reconstructs the input data as outputx' in terms of approximation of x from the encoded features by using (5.4) and (5.5) as:

$$F = h(Wx + B) \tag{5.4}$$

$$x' = g(W'F + B') \tag{5.5}$$

Here, h and g are the activation functions of the hidden layers of encoder and decoder respectively and W, W', B and B' are the weight matrices and bias vectors of encoder and decoder, respectively. In SSA, several parameters control and prevent the learning and model overfitting. For example, sparsity regularizer of an autoencoder model enforces a constraint on the sparsity of the output from the hidden layers. This regularizer is a function of the average output activation value of a hidden neuron, $\hat{\rho}_i$defined as:

$$\hat{\rho}_i = \frac{1}{n}\sum_{j=1}^{n} F_i(x_j) \tag{5.6}$$

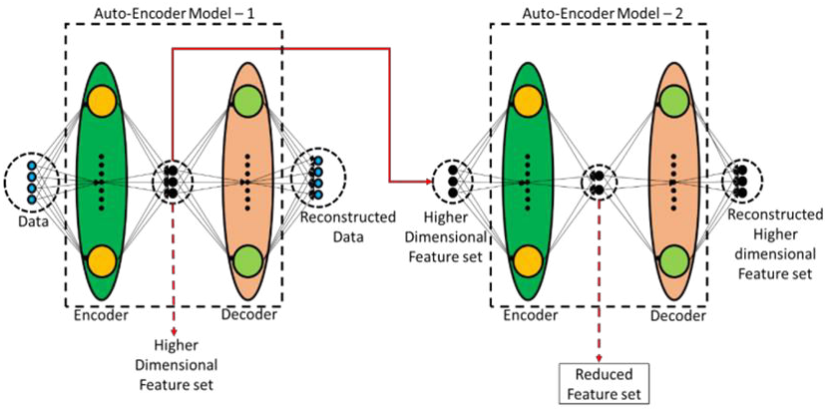

Fig. 5.8 Structure of stacked sparse autoencoder

Where, i, n, and j indicates the i^{th} neuron, total number of training data and j^{th} training sample respectively. The sparsity of the autoencoder model, $\xi_{sparsity}$ has been determined by using Kullback-Leibler divergence theorem which is given by:

$$\xi_{sparsity} = \sum_{i=1}^{D} \rho \, log(\frac{\rho}{\hat{\rho}_i}) + (1-\rho) \, log(\frac{1-\rho}{1-\hat{\rho}_i}) \tag{5.7}$$

Two parameters 'sparsity regularization' and 'sparsity proportion' control the impact of sparsity regularizer and the average activation value. Different regularization techniques are present to control the overfitting of the autoencoder model during the training process [31]. Here, L_2 regularization method is utilized to train the model. The L_2 regularized weight matrices is given by:

$$\xi_{weights} = \frac{1}{2} \sum_{l}^{L} \sum_{j}^{n} \sum_{i}^{k} (w_{ji}^{(l)})^2 \tag{5.8}$$

The cost function used by the algorithm for approximation of input data as the output is expressed as:

$$C = \frac{1}{N} \sum_{n=1}^{N} \sum_{k=1}^{K} (x_{kn} - \hat{x}_{kn})^2 + \theta \times \xi_{weights} \delta \times \xi_{sparsity} \tag{5.9}$$

In (5.9), the first term denotes the mean squared error between input and output for k^{th} neuron, θ and δ are the L_2 regularization coefficient and sparsity regularization coefficient of the autoencoder model. The term $\xi_{sparsity}$ is the sparsity regularizer which is determined by Kullback-Leibler divergence this present work. In this contribution, sparsity regularization parameters, sparsity proportion, L_2 weight regularization parameter and maximum training epochs are set as 4, 0.05, 0.001 and 100 respectively. To obtain the encoded features at the end of the training process, a decoder layer has been removed from the model at the final training iteration.

5.3.4 Machine learning classifiers

In this present chapter, the extracted deep features are classified using random forest (RF), multiclass support vector machines (SVM), *k*-nearest neighbour (kNN) and naïve Bayesian (NB) classifiers. Since, theory of these aforementioned machine learning classifiers is well known, hence detailed mathematical description is not reported here. However, details of RF, SVM, kNN and NB classifiers can be found out in [32-34].

5.4 Results and Discussions

5.4.1 Performance analysis of Stacked sparse auto encoder (SSA)

The T-F images of I_d and I_q signals for four classes obtained using SPWVD had initial dimensions of 415 × 526 × 3. The T-F images were then converted to grayscale and were further resized into 224 × 224, before being served as inputs to the stacked sparse autoencoder model for deep feature extraction. The SSA performance in feature reconstruction form the input images by training the hidden layers is shown in Fig. 5.9. It can be seen from Fig. 5.9 that the best training performance is obtained when epoch value reaches 100. So, 100 epochs were used in this work to train the autoencoder model. In this present contribution, the number of hidden layers for the first autoencoder model has been set to 50, from where 50 highly correlated deep features have been obtained initially. The feature set was given as input to the second autoencoder model whose number of hidden layers have been set to 25 and from the output terminal of the encoder layer, a feature set comprising 25 deep features have been obtained.

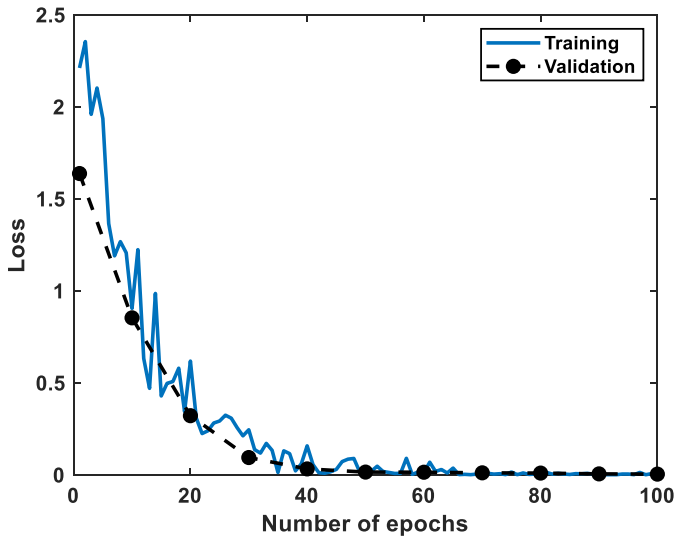

Fig. 5.9 Training of sparse autoencoder

The statistical significance of these features was examined utilizing analysis of variance (ANOVA test) were found to be statistically significant with *p*-value less than 0.001. Finally, using the 25 extracted deep features, classification of faults was done for both fan and drive end signals. In this paper, 5-fold cross validation with train-test ratio of 80%-20% has been used to evaluate the classifiers performance. Classification performance has been observed in terms of four statistical parameters, which are Accuracy, Sensitivity, Specificity and Precision. The mathematical expressions corresponding to these measuring indices (expressed in percentage) are given by (5.10) -(5.13):

$$Accuracy(ACC) = \frac{TP+TN}{TP+FP+TN+FN} \times 100 \tag{5.10}$$

$$Sensitivity(SEN) = \frac{TP}{TP+FN} \times 100 \tag{5.11}$$

$$Specificity(SPE) = \frac{TN}{TN+FP} \times 100 \tag{5.12}$$

$$Pr\,e\,cision(PRC) = \frac{TP}{TP+FP} \times 100 \tag{5.13}$$

Where *TP*, *TN*, *FP* and *FN* symbolize true positive, true negative, false positive and false negative respectively. Table 5.2 and Table 5.3 show different classifiers' performances evaluated in terms of the aforesaid measuring indices for both I_d and I_q current signals respectively. It is to be mentioned here that in Table 5.2 and Table 5.3, the optimal number of trees for the RF classifier were selected as 50 and 60, respectively. In the case of SVM, grid search algorithm was used to determine the regularization parameter by varying from 1-500 in steps of 0.1. The optimum kernel width in Table 5.2 and Table 5.3 was set at 2.4 and 3.6, respectively. For kNN, Euclidean distance has been used with the optimum value of *k* set at *k*=3 and *k*=5, for Table 5.2 and Table 5.3, respectively. From Tables 5.2 and 5.3, it can be observed that most of the classifiers delivered reasonably high accuracy, sensitivity, specificity, and precision for both I_d and I_q current signals. However, the performance of different classifiers is found to be slightly better for the I_d compared to I_q signals. Among different classifiers, kNN returned highest classification accuracies than the other classifiers. The performance of NB classifier is found to be inferior for both the cases.

Nevertheless, the performance of different classifiers is satisfactory for both I_d and I_q signals. In addition, the standard deviation values indicated in parenthesis are reasonably low for the kNN classifier indicating that the proposed model is robust.

Table 5.2 Classification performance of quadrature axis (I_q) current data

Classifier	ACC (%)	SEN (%)	SPE (%)	PRC (%)
RF	93.88±4.1	94.22±3.7	92.72±4.2	92.61±7.0
SVM	91.40±5.4	89.89±9.1	92.16±6.6	86.14±9.8
kNN	**98.79±1.0**	**96.00±2.4**	**95.38±3.6**	**96.80±1.2**
NB	89.96±2.4	95.50±1.2	92.11±1.7	88.17±2.3

Table 5.3 Classification performance of quadrature axis (I_q) current data

Classifier	ACC (%)	SEN (%)	SPE (%)	PRC (%)
RF	92.56±3.8	93.10±3.5	91.45±4.0	92.10±6.5
SVM	90.25±4.5	87.49±8.1	91.20±5.8	87.24±9.1
kNN	**97.56±1.8**	**95.20±2.5**	**94.80±3.8**	**94.05±1.8**
NB	88.86±2.5	94.45±1.3	91.05±2.8	87.15±4.1

5.4.2 Statistical test of different classifiers

In Fig 5.10, statistical analysis using one-way analysis of variance (ANOVA) test and post-hoc Tukey Kramer test has been reported. This is done to get better insight into the classification performances of different machine learning classifiers employed in this study. Using the ANOVA test, an overall significance with $p < 0.05$ has been obtained. From the post-hoc analysis signals, both RF and kNN deliver higher statistical significances with NB. Also, between RF and SVM, lower statistical significance is observed for both I_d and I_q current signals. Nevertheless, the performance of classifiers for both datasets is observed to be reasonably satisfactory, indicating the robust performance of the proposed model.

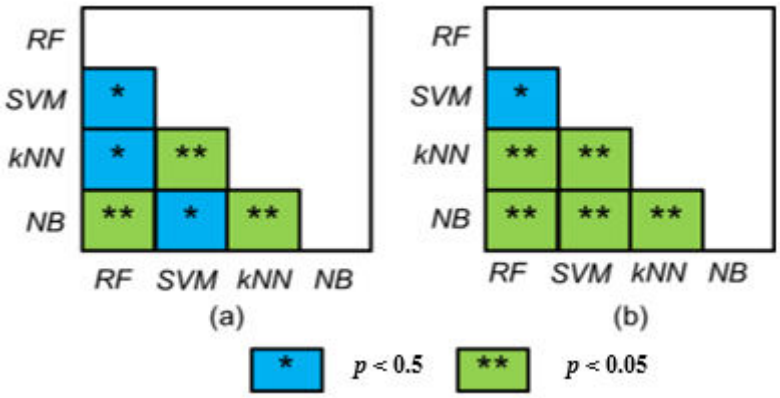

Fig. 5.10 Post-hoc statistical test (Tukey Kramer) between all the classifiers

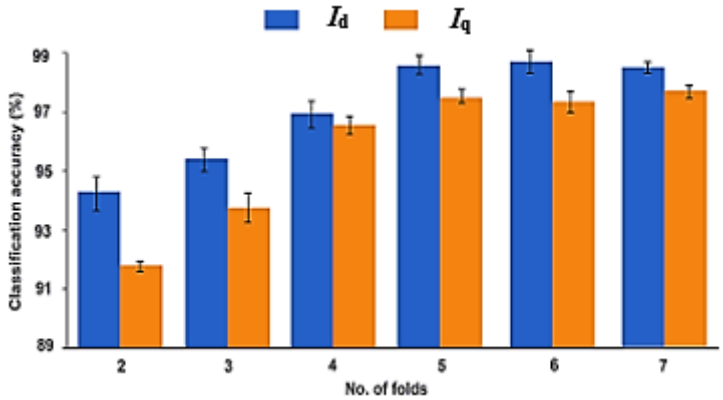

Fig 5.11. Variation in classification accuracies with varying number of folds

5.4.3 Comparison by varying number of folds

The classification performance of the proposed model is further verified by implementing different number of folds in the cross-validation process. It is to be mentioned here in this section, classification accuracy only kNN classifier is being reported since it delivered best performance compared to the other classifiers as reported in Table 5.2 and Table 5.3. The variation in the obtained classification accuracies with different number of folds ranging

from 2-7 is presented in Fig. 5.11, for both I_d and I_q fault signals respectively. From Fig. 5.11, it can be seen that initially, the classification accuracies increase with increase in number of folds. The increasing trend in the obtained classification accuracies plateaus after 5 folds and thereafter, no significant rise is observed. Considering this observation, a 5-fold cross-validation technique has been adopted in this study for classification of PV array faults.

5.4.4 Comparison using different methods.

In this section, the performance of proposed SPWVD aided TFR-based fault classification framework and kNN classifier is compared with some existing methods like short time Fourier transform (STFT). Wigner-Ville distribution (WVD) as well as Hilbert transform (HT). The accuracy of fault classification obtained using different classifiers is shown in Table 5.4. For each of the above-mentioned methods, the deep features were extracted using SAE for both I_d and I_q transformed current data. It can be observed that among different methods, SPWVD delivered better performance than the other T-F methods which indicates the superiority of the proposed SPWVD method. This observation was found to be true for both I_d and I_q current signals. Also, compared to WVD, SPWVD returned better performance. This is because, application of SPWVD reduces cross-terms in time domain which is reflected in the TF representation. Hence, SPWVD based T-F representation can be considered as a superior time-frequency image representation method for classification of grid connected solar PV systems. In addition, the overall computation time (which includes signal to image conversion using SPWVD, deep feature extraction using SAE and

Table 5.4 Comparison using different methods

Method	Classifier	I_d	I_q	Computational time (minutes)
STFT	kNN	93.45±3.3	92.76±4.0	14.56
WVD		95.46±2.1	94.50±3.2	11.52
HT		96.14±1.4	95.35±2.6	12.50
SPWVD		**98.79±1.0**	**97.56±2.1**	**10.45**

classification using kNN) indicated in Table 5.4 indicates that the proposed SPWVD method takes minimum time compared to other methods. The computational time is calculated using a system with 32GB RAM, Intel core i5 64-bit processor and central processing unit (CPU) clocked at 3.6 GHz with one NVIDIA graphics processing unit (GPU) and using MATLAB 2020 a environment.

5.4.5 Comparison with other T-F methods

In Table 5.5, performance of the proposed fault detection scheme is compared with some of the existing methods which have been reported earlier using the same dataset. In Table 5.5, the comparative study was carried out considering only those literatures where similar dataset has been used for fault classification in grid connected PV systems. It can be noticed from Table 5.5 that the proposed fault detection scheme has performed better compared to the existing literature. In addition, it should also be noticed that most of the existing studies were carried out using conventional machine learning methods, which is dependent on manual mode of feature extraction. In this study, the fault classification performance has been reported using deep feature extraction from current signals which signify the superiority of the proposed bearing fault detection scheme.

Table 5.5 Comparison with existing literature

Reference	**Method**	**ACC (%)**
[2]	Adaptive Neuro-Fuzzy interface System	95.4
[35]	PCA + kNN	97.9
[36]	PCA+ kNN	97.36
[36]	PCA+RF	97.78
This study (I_d)	SPWVD + SSA-based deep features + machine-learning classifiers	98.79
This study (I_q)	SPWVD + SSA-based deep features + machine-learning classifiers	97.56

5.5 Conclusions

In the present chapter, a novel framework using SPWVD based time-frequency analysis and SSA based deep feature extraction is proposed for automated detection of faults using single cycle fault current signature analysis. The proposed method is validated on fault current data obtained from real life grid connected PV system. Instead of considering the three phase current waveforms, the proposed method makes use of extended Park's vector approach to convert the single cycle three phase current signals to *d*-axis and *q*-axis components to improve the fault detection accuracy. The obtained I_d and I_q currents in time domain were transformed into time-frequency plane using SPWVD. It has been observed that the time-frequency images of healthy as well as faulty current data showed distinct differences among each other. The RGB time-frequency images were converted to grayscale and were subjected to deep feature extraction using SSA. Then, ANOVA test followed by FDR correction were used for selection of meaningful deep features. The selected relevant deep features were then fed to four benchmark machine learning classifiers for classification of current signals. It has been observed that among different classifiers, kNN delivered better classification performance compared to other machine learning classifiers. Comparative study with existing studies revealed that the performance of the proposed method is comparable and even better. Thus, it can be concluded that the proposed method can be implemented to develop an efficient fault detection system for grid connected solar PV systems. In the present work, only three fault cases have been investigated. In future, more fault scenarios will be investigated to develop a robust fault classification model. In addition, the proposed deep learning aided fault classification method will be validated in hardware using low-cost microcontroller or FPGA module.

References

[1] A. Rafique, A. Ulasyar, H.S. Zad, et al, “Real Time Detection of Partial Shading in the Photovoltaic Systems Using New F uzzy Logic Technique”, Appl. Sol. Energy 58, pp. 631–642, 2022.

[2] P. Kayal and T.V. Abdul Vasih, “Fault Detection in Photovoltaic Systems Using Optimized Neural Network”, Appl. Sol. Energy 59, pp. 269–282, 2023.

[3] P. Jenitha and I. Selvakumar, “A. Fault detection in PV systems”. Appl. Sol. Energy 53, pp. 229–237, 2017.

[4] Y.Y. Hong, R. A. Pula, "Methods of photovoltaic fault detection and classification: A review", Energy Reports, vol. 8, pp. 5898-5929, 2022.

[5] K. A. K. Niazi, W. Akhtar, H. A. Khan, Y. Yang and S. Athar, "Hotspot diagnosis for solar photovoltaic modules using a Naive Bayes classifier”, Solar Energy, vol.190, pp.34-43, 2019.

[6] N. V. Sridharan & V. Sugumaran, "Visual fault detection in photovoltaic modules using decision tree algorithms with deep learning features", Energy Sources, Part A: Recovery, Utilization, and Environmental Effects, pp. 1-17, 2021.

[7] Z. Chen, L. Wu, S. Cheng, P. Lin, Y. Wu and W. Lin, "Intelligent fault diagnosis of photovoltaic arrays based on optimized kernel extreme learning machine and I-V characteristics", Appl. Energy, vol.204, pp. 912-931, 2017.

[8] A. Eskandari, J. Milimonfared and M. Aghaei, “Line-line fault detection and classification for photovoltaic systems using ensemble learning model based on I-V characteristics”, Sol. Energy, vol. 211, pp. 354-365, 2020.

[9] S. Fadhel, C. Delpha, D. Diallo, I. Bahri, A. Migan, M. Trabelsi and M.F. Mimouni, "PV shading fault detection and classification based on I-V curve

using principal component analysis: Application to isolated PV system", Sol. Energy, vol.179, pp. 1-10, 2019.

[10] T. K. Das, S. Chattopadhyay & A. Das, "String Fault Detection in Solar Photo Voltaic Arrays", IETE Journal of Research, vol.69, no.5, pp. 2670-2682, 2021.

[11] Z. Yi and A. H. Etemadi, "Fault Detection for Photovoltaic Systems Based on Multi-Resolution Signal Decomposition and Fuzzy Inference Systems," IEEE Transactions on Smart Grid, vol. 8, no. 3, pp. 1274-1283, 2017.

[12] M. Ahmadipour, M. M. Othman, M. Alrifaey, R. Bo and C. K. Ang, "Classification of faults in grid-connected photovoltaic system based on wavelet packet transform and an equilibrium optimization algorithm-extreme learning machine", Measurement, vol.197, pp.111338, 2022.

[13] W. Miao, Q. Xu, K. H. Lam, P. W. T. Pong and H. V. Poor, "DC Arc-Fault Detection Based on Empirical Mode Decomposition of Arc Signatures and Support Vector Machine," IEEE Sensors Journal, vol. 21, no. 5, pp. 7024-7033, 2021.

[14] C. Lebreton, F. Kbidi, A, Graillet, T. Jegado, F. Alicalapa, M. Benne, C. Damour, “PV System Failures Diagnosis Based on Multiscale Dispersion Entropy”, Entropy. vol. 24, no.9, pp.1311, 2022.

[15] A. Amiri, H. Samet and T. Ghanbari, "Recurrence Plots Based Method for Detecting Series Arc Faults in Photovoltaic Systems," IEEE Transactions on Industrial Electronics, vol. 69, no. 6, pp. 6308-6315, June 2022.

[16] J. Wang, D. Gao, S. Zhu, S. Wang &H.Liu, "Fault diagnosis method of photovoltaic array based on support vector machine", Energy Sources, Part A: Recovery, Utilization, and Environmental Effects, 2019.DOI: 10.1080/15567036.2019.1671557.

[17] F. Harrou, B. Taghezouit and Y. Sun, "Improved k NN-Based Monitoring Schemes for Detecting Faults in PV Systems," in IEEE Journal of Photovoltaics, vol. 9, no. 3, pp. 811-821, May 2019.

[18] M. Hussain, M. Dhimish, S. Titarenko and P. Mather, "Artificial neural network based photovoltaic fault detection algorithm integrating two bi-directional input parameters", Renew. Energy, vol. 155, pp. 1272-1292, 2020.

[19] D. Adhya, S. Chatterjee & A. K. Chakraborty, " Stacking ensemble-based fault diagnosis approach for improved operation of photovoltaic arrays", Energy Sources, Part A: Recovery, Utilization, and Environmental Effects, 44:2, 5421-5439, 2022.

[20] A. Bakdi, W. Bounoua, A. Guichi and S. Mekhilef, “Real-time fault detection in PV systems under MPPT using PMU and high-frequency multi-sensor data through online PCA-KDE-based multivariate KL divergence”, International Journal of Electrical Power & Energy Systems, vol. 125, 2021.

[21] K. Samanta, S. Chatterjee and R. Bose, "Cross-Subject Motor Imagery Tasks EEG Signal Classification Employing Multiplex Weighted Visibility Graph and Deep Feature Extraction," IEEE Sensors Letters, vol. 4, no. 1, pp. 1-4, 2020.

[22] A.K. Das, S. Dalai and B. Chatterjee, "Deep learning–based surface contamination severity prediction of metal oxide surge arrester in power system", IET Science, Measurement & Technology, vol.15, no.4, pp.376, 2021.

[23] A. K. Das, S. Das, A. K. Pradhan, B. Chatterjee and S. Dalai, "RPCNNet: A Deep Learning Approach to Sense Minor Stator Winding Interturn Fault Severity in Induction Motor Under Variable Load Condition," IEEE Sensors Journal, vol. 23, no. 4, pp. 3965-3972, 2023.

[24] S. Modak, S. Singha Roy, R. Bose and S. Chatterjee, "Focal Epileptic Area Recognition Employing Cross EEG Rhythm Spectrum Images and

Convolutional Neural Network," IEEE Sensors Journal, vol. 21, no. 20, pp. 23335-23343, 2021.

[25] A. Bakdi, A. Guichi, M. Saad and W. Bounoua, “GPVS-Faults: Experimental Data for fault scenarios in grid-connected PV systems under MPPT and IPPT modes”, Mendeley Data, 2020.

[26] J. Ma, X. Pan, K. L. Man, X. Li, H. Wen, and T. On Ting, “Detection and assessment of partial shading scenarios on photovoltaic strings,” IEEE Trans. Ind. Appl., vol. 54, no. 6, pp. 6279–6289, Nov 2018.

[27] S. Das, P. Purkait, D. Dey and S. Chakravorti, "Monitoring of inter-turn insulation failure in induction motor using advanced signal and data processing tools," IEEE Transactions on Dielectrics and Electrical Insulation, vol. 18, no. 5, pp. 1599-1608, 2011.

[28] N. Bahador and J. Kortelainen, “Deep learning-based classification of multichannel bio-signals using directedness transfer learning”, Biomedical Signal Processing and Control, vol. 72, Part A, 2022, 103300.

[29] S. K. Khare, V. Bajaj and U. R. Acharya, "SPWVD-CNN for Automated Detection of Schizophrenia Patients Using EEG Signals," IEEE Transactions on Instrumentation and Measurement, vol. 70, pp. 1-9, 2021.

[30] S. K. Khare, V. Bajaj and U. Rajendra Acharya, "PDCNNet: An automatic framework for the detection of Parkinson’s disease using EEG signals," IEEE Sensors Journal, vol. 21, no. 15, pp. 17017-17024, 2021.

[31] C. Zhang, X. Cheng, J. Liu, J. He and G. Liu, “Deep sparse autoencoder for feature extraction and diagnosis of locomotive adhesion status”, J. Control Sci. Eng. pp. 1–9, 2018.

[32] C. Cortes, V. Vapnik ‘Support vector networks’, Machine Learning, vol. 20, no. 3, pp. 273–295, 1995.

[33] R. Bose, K. Samanta, S. Modak and S. Chatterjee, "Augmenting Neuromuscular Disease Detection Using Optimally Parameterized Weighted Visibility Graph," IEEE Journal of Biomedical and Health Informatics, vol. 25, no. 3, pp. 685-692, 2021.

[34] I. Banerjee, S. S. Mullick, and S. Das, “On Convergence of the Class Membership Estimator in Fuzzy k-Nearest Neighbor Classifier,” IEEE Trans. Fuzzy Syst., vol. 27, no. 6, pp. 1226–1236, 2018.

[35] M. Hajji, M.F. Harkat, A. Kouadri, K. Abodayeh, M. Mansouri, H. Nounou and M. Nounou, “Multivariate feature extraction based supervised machine learning for fault detection and diagnosis in photovoltaic systems”, European Journal of Control, vol. 59, pp.313–32, 2021.

[36] B. Chokr, N.Chatti, A. Charki, T. Lemenand, and M. Hammoud, “Feature extraction-reduction and machine learning for fault diagnosis in PV panels”, Solar Energy, vol.262, no.111918, pp.1-12, 2023.

Chapter 6

Conclusions and Future Work

6.1 Conclusions

In the present thesis, several advanced signal processing and machine learning techniques have been proposed for detection and classification of transient disturbances in power systems. The outcomes of the present thesis work are briefly summarized as follows:

In ***chapter 2***, multi-resolution analysis of two very frequently occurring power system transients namely oscillatory and impulsive transients are done using discrete wavelet transform (DWT). Next, the envelope spectrum of the first four detail coefficients is obtained using Hilbert transform and several features are extracted from the selected envelope spectrums of both class of transient signals. Using ANOVA test, statistical analysis of the extracted features has been done to investigate the discrimination capability of the selected features which are finally used as inputs to a support vector machines (SVM) classifier for classification of power system transients. It has been observed that based on DWT envelope analysis and employing SVM classifier 100% classification accuracy is obtained in detection of different types of power system transients. Using the proposed method, it is possible to detect and classify switching transients occurring in power systems with very high accuracy. However, in this chapter, only switching transients are considered. In real-life power systems, apart from switching transients, power quality disturbances (PQ) are a common problem and detection of PQ disturbance is a challenging issue. In the next chapter, this problem is addressed and a method for accurate detection of PQ disturbances is proposed.

In ***chapter 3***, automated and accurate detection of single as well as power quality (PQ) events is important from the point of view of safety as well as maintaining the reliability of the power transmission and distribution network. However, detection of multiple PQ events in a noisy environment is a challenging task. Another important issue is the choice of meaningful features that can directly influence the accuracy of PQ detection. Considering these two aforesaid facts, this paper presents a novel framework for automated classification of PQ signals in a noisy environment employing cross Stockwell Transform (XST). The XST proposed in this paper has better noise suppression capability compared to conventional Stockwell Transform. Here, XST was used to convert 1D PQ signals to 2D time–frequency (T–F) images. To improve the accuracy of PQ detection, an automated feature extraction method employing deep learning is implemented in this work. The noise free T–F images obtained using XST were fed as inputs to several pre-trained convolutional neural networks (CNNs) for deep feature extraction. Transfer learning technique was implemented to reduce the computational cost. The extracted deep features were further undergone selection using one-way analysis of variance test followed by false discovery rate correction. The statistically significant deep features were subsequently fed to three benchmark machine learning classifiers for classification of PQ signals. In addition, tests were also carried out on real-life PQ signals to verify the practicability of the proposed framework. Investigations revealed that the proposed method returned mean accuracy of 99.72% and 96.45% for classification of simulated and real-life PQ signals, respectively. Although the proposed method is capable of detecting PQ disturbances with very high accuracy, in this chapter, the detection of islanding events in presence of grid connected renewable energy sources is not considered. Islanding detection in grid connected systems is a major issue and considering this fact in the next chapter a method for islanding detection is proposed.

In ***chapter 4***, an autocorrelation aided deep learning framework for islanding detection in grid connected distributed generation (DG) system is proposed. For this purpose, islanding along with other transient events were simulated on a grid connected power system network with DG penetration. Each case's

negative sequence voltage signals obtained at the point of common connection were used to determine the sequence components of the autocorrelation function. From the autocorrelation sequences representing each type of transient event, 36 features were extracted. The obtained feature vectors were fed as inputs to a bi-directional long-short type memory network (Bi-LSTM) classifier for classification of islanding and other events. It has been examined that the suggested methodology has resulted in 99.01% accuracy in discriminating islanding from non-islanding events. Besides, for the multiclass classification, a mean accuracy of 98.50% is obtained. Comparative studies with machine learning classifiers indicated that the result of the suggested methodology is better. The proposed model can be used for accurate prediction and classification of islanding and other transient events in power system network. Although the method proposed in this chapter can detect islanding and non-islanding events accurately, detection of faults in grid connected renewable energy systems is a challenging issue. Considering the aforesaid fact, in the next chapter, a novel method for detection and classification of faults in grid connected solar PV systems is proposed.

In ***chapter 5***, a smoothed pseudo-Wigner-Ville distribution (SPWVD) and stacked sparse autoencoder (SSA) based automated feature extraction technique is proposed for accurate detection of faults in grid connected solar PV systems. To this end, three phase current data of normal as well as different fault scenarios obtained from point of common coupling (PCC) were converted into direct (d) and quadrature (q) axis using extended Park's vector approach. Then, the obtained d-axis (I_d) and q-axis (I_q) currents were converted to 2D time-frequency images using SPWVD. The converted time-frequency spectrum of the normal as well as faulty current data were used as inputs to the proposed SSA model for deep feature extraction. After extraction of deep features using SSA, analysis of variance (ANOVA) test and false discovery rate (FDR) correction was employed to select the most discriminative features. The feature selection was followed by classification using machine learning classifiers. It has been observed that the proposed technique achieved mean fault recognition accuracy of 98.79% and 97.56%

for *d*-axis and *q*-axis currents respectively, respectively. The present approach can be used for accurate diagnosis of faults in grid connected solar PV systems.

Thus, it can be concluded that in the present thesis work several new techniques for detection and classification of transient events in power systems is proposed. Prospective extensions of the proposed thesis as future work are discussed in the following subsection.

6.2 Future Works

The proposed methodologies in this thesis are aimed at the development of efficient detection and classification frameworks for transient detection in power systems. The methods proposed in this thesis can be extended in future in different directions, some of which are mentioned below.

1. In the present thesis work, manual feature extraction method has been implemented for classification of switching transients. In future, deep learning methods could be implemented for detection and classification of switching transients in power systems. Moreover, in future, hardware set-up will be fabricated for generation of switching events in laboratory and classification of switching transients will be done using signals captured from hardware for detection of transient events.

2. For PQ transient event detection, cross time-frequency analysis employing cross Stockwell transform (XST) and automated feature extraction framework employing benchmark deep learning models have been proposed. In future, other cross spectrum analysis methods like transform like cross hyperbolic Stockwell transform (XHST), cross Hilbert transform etc. could be implemented for analysis of PQ signals in time-frequency frame. Moreover, apart from using benchmark deep learning models, a customized deep

learning model could be designed for more accurate detection of PQ signals.

3. In the context of islanding detection, autocorrelation-based feature extraction method has been used in grid connected renewable energy systems. In future, deep feature extraction using deep learning models could be implemented to improve the islanding detection scheme. Also, in future the proposed islanding detection model could be implemented in hardware in loop to validate the practicability of the proposed method.

4. For automated fault classification method in grid connected solar PV systems, a method employing smoothed-pseudo-Wigner Ville distribution method is proposed. In future, other time-frequency analysis methods could be explored for improved fault classification in grid connected PV systems. Moreover, only three faults and one fault-free case have been considered here. In future, additional fault cases will be investigated to improve the resiliency of the proposed fault detection scheme.

Appendix

A.1 Mathematical Model of PQ disturbances

In Table A.1 the mathematical model of PQ disturbances is given. In Table A.2, the confusion matrix for PQ disturbances classification is shown.

Table A.1: Mathematical model of PQ disturbances

PQ signals	Numerical model	Parameters
Flicker	$V_F = [1 + A\sin(2\pi f_F t + \theta_F)]\sin(2\pi f t + \theta)$	f= fundamental frequency $f_F \leq 10Hz, A \leq 0.03$ θ = phase angle
Harmonics	$V_H = \sin(2\pi f t + \theta) + [\sum a_k \sin(2\pi f_k t + \theta_k)]$	f_k=frequency of k^{th} order harmonic, a_k= magnitude of k^{th} order harmonic, $k > 1$
Notch	$V_N = \sin(2\pi f t + \theta) + [n_d \times V_{os} \times f_p \times V_n]$	n_d=notch depth function V_{os} = oscillation function f_p = polarity mask function V_n =notch function
Sag	$V_{sg} = [1 - m\{u_1(1 - e^{-\alpha t_1}) + u_1(m_r \sin(\omega t_1)e^{-\gamma t_1}) - u_2(1 - e^{-\beta t_1})\}]\sin(2\pi f t + \theta)$ $V_{sg} = [1 - m\{u_1(1 - e^{-\alpha t_1})\}]\sin(2\pi f t + \theta)$ $V_{sg} = [1 - m(u_1 - u_2)]\sin(2\pi f t + \theta)$	u_1, u_2 = unit step functions α=sag decay rate β= sag recovery rate $0.1 \leq m \leq 0.9$ γ= transient settling time
Swell	$V_{sw} = [1 + m(u_1 - u_2)]\sin(2\pi f t + \theta)$	$0 < \theta < 360°$ $1.1 \leq m \leq 1.8$
Oscillatory Transient	$V_{os} = \sin(2\pi f t + \theta) + [u_1 \times m \times \sin(2\pi f_{os} t_1)e^{\gamma t_1}]$ $V_{os} = \sin(2\pi f t + \theta) + [u_1 \times m \times e^{\gamma t_1}]$ $V_{os} = u_1 \sin(2\pi f t + \theta) + [u_1 \times m \times \sin(2\pi f_{os} t_1)e^{\gamma t_1}]$	$m \leq 4$ $f_{os} \leq 5$ kHz γ= transient settling time
Noise	$V_{no} = \sin(2\pi f t + \theta) + [p_{no} \times wG(t)]$	p_{No} = noise level (%) $wG(t)$ = white Gaussian noise

A.2 Confusion Matrix of PQ classification

Table A2: Confusion matrix of power quality classification

Signal	Predicted class																					
	S_1	S_2	S_3	S_4	S_5	S_6	S_7	S_8	S_9	S_{10}	S_{11}	S_{12}	S_{13}	S_{14}	S_{15}	S_{16}	S_{17}	S_{18}	S_{19}	S_{20}	S_{21}	S_{22}
True class																						
S_1	100																					
S_2		100																				
S_3			100						1													
S_4				100						1												
S_5					100									1								
S_6						100										1						
S_7							100					1										
S_8								100														
S_9									99													
S_{10}										99												
S_{11}											100											
S_{12}												99										
S_{13}													100									
S_{14}														99								
S_{15}															100							
S_{16}																99						
S_{17}																	100					
S_{18}																		100				
S_{19}																			100			
S_{20}																				100		
S_{21}																					100	
S_{22}																						100
Overall Accuracy = 99.72%																						